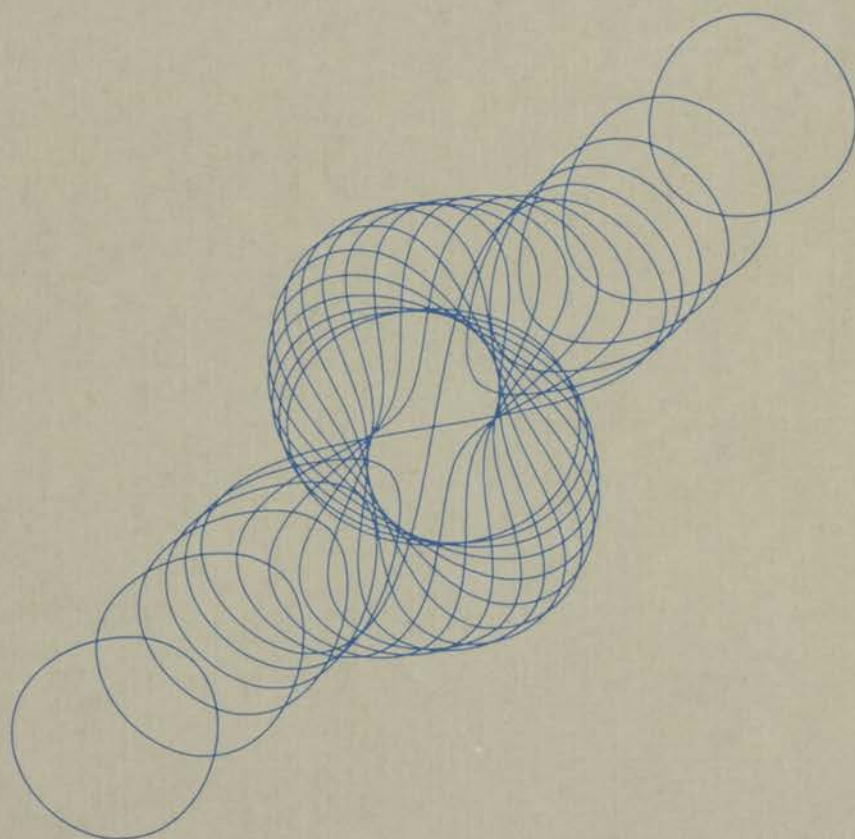


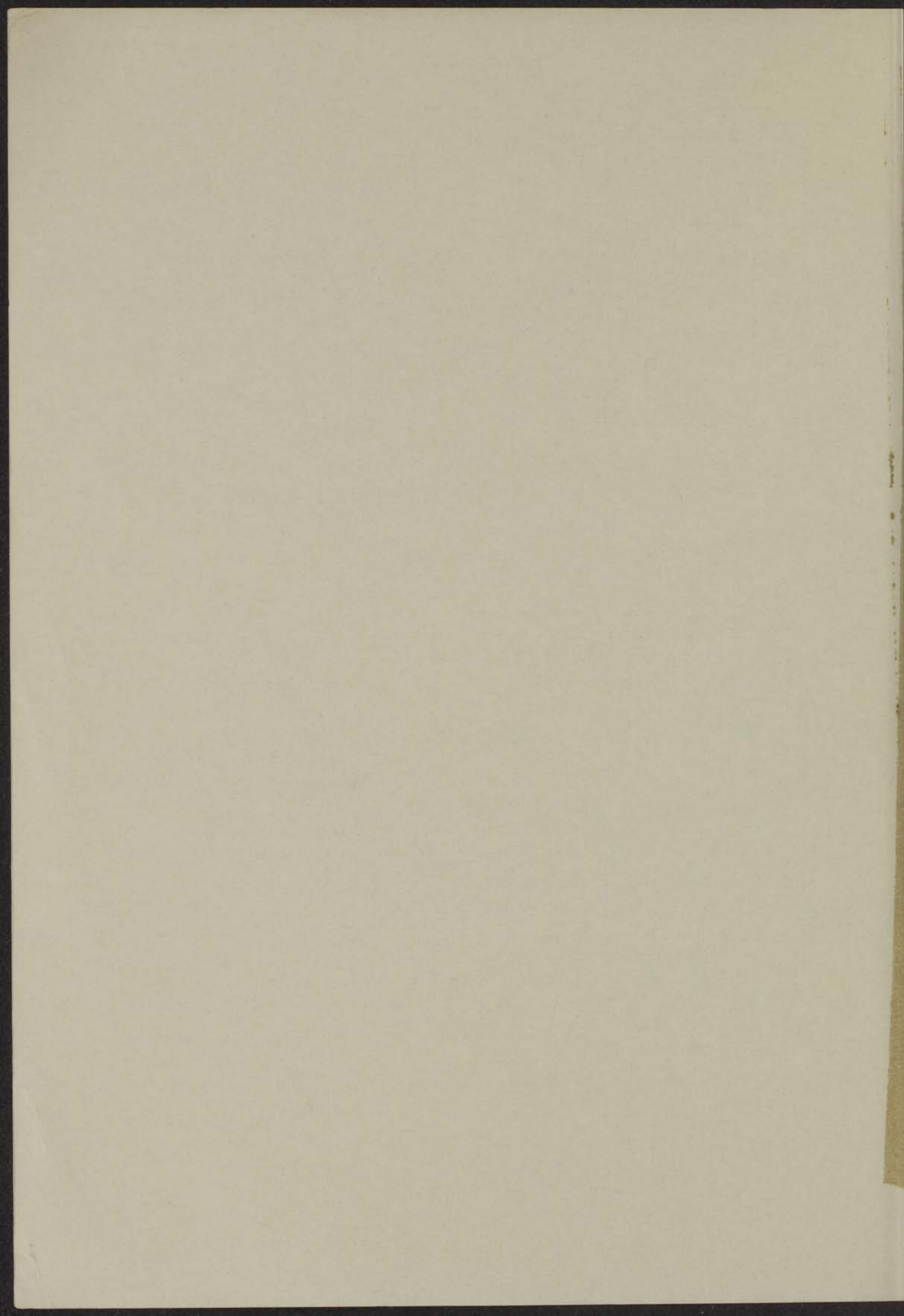
8 JUN 1971

FISSION OF ALIGNED NUCLEI BY LOW ENERGY NEUTRONS

INSTITUUT-LORENTZ
voor theoretische natuurkunde
Nieuwsteeg 18-Leiden-Nederland



R. KUIKEN



1971

FISSION OF ALIGNED NUCLEI BY LOW ENERGY NEUTRONS

PROEFSCHRIFT

TER VERKRIJGING VAN DE GRAAD VAN DOCTOR IN
DE WISKUNDE EN NATUURWETENSCHAPPEN AAN
DE RIJKSUNIVERSITEIT TE LEIDEN, OP GEZAG VAN
DE RECTOR MAGNIFICUS DR. C. SOETEMAN,
HOGLERAAR IN DE FACULTEIT DER LETTEREN,
TEN OVERSTAAN VAN EEN COMMISSIE UIT DE SENAAT
TE VERDEDIGEN OP DINSDAG 15 JUNI 1971
TE KLOKKE 15.15 UUR

DOOR

RENZE KUIKEN

GEBOREN TE HET BILDT (FR.) IN 1946

INSTITUUT-LORENTZ
voor theoretische natuurkunde
Nieuwsteeg 18-Leiden-Nederland

kast dissertaties

PROMOTOREN: Prof. Dr. J.A. Goedkoop

Prof. Dr. C.J. Gorter

Dit proefschrift is bewerkt onder leiding van

Dr. H. Postma.

1	1.1. Theoretical background of the research	1
2	1.2. Objectives of the research	2
3	1.3. Methodology	3
4	1.4. Data collection	4
5	1.5. Data analysis	5
6	1.6. Results and discussion	6
7	1.7. Conclusions	7
8	1.8. References	8
9	1.9. Appendix	9
10	1.10. Bibliography	10
11	1.11. Summary	11
12	1.12. Acknowledgements	12
13	1.13. Declaration of interest	13
14	1.14. Conflict of interest	14
15	1.15. Funding	15
16	1.16. Author contributions	16
17	1.17. Correspondence	17
18	1.18. Additional information	18
19	1.19. Supplementary material	19
20	1.20. References	20
21	1.21. Appendix	21
22	1.22. Bibliography	22
23	1.23. Summary	23
24	1.24. Acknowledgements	24
25	1.25. Declaration of interest	25
26	1.26. Conflict of interest	26
27	1.27. Funding	27
28	1.28. Author contributions	28
29	1.29. Correspondence	29
30	1.30. Additional information	30
31	1.31. Supplementary material	31
32	1.32. References	32
33	1.33. Appendix	33
34	1.34. Bibliography	34
35	1.35. Summary	35
36	1.36. Acknowledgements	36
37	1.37. Declaration of interest	37
38	1.38. Conflict of interest	38
39	1.39. Funding	39
40	1.40. Author contributions	40
41	1.41. Correspondence	41
42	1.42. Additional information	42
43	1.43. Supplementary material	43
44	1.44. References	44
45	1.45. Appendix	45
46	1.46. Bibliography	46
47	1.47. Summary	47
48	1.48. Acknowledgements	48
49	1.49. Declaration of interest	49
50	1.50. Conflict of interest	50
51	1.51. Funding	51
52	1.52. Author contributions	52
53	1.53. Correspondence	53
54	1.54. Additional information	54
55	1.55. Supplementary material	55
56	1.56. References	56
57	1.57. Appendix	57
58	1.58. Bibliography	58
59	1.59. Summary	59
60	1.60. Acknowledgements	60
61	1.61. Declaration of interest	61
62	1.62. Conflict of interest	62
63	1.63. Funding	63
64	1.64. Author contributions	64
65	1.65. Correspondence	65
66	1.66. Additional information	66
67	1.67. Supplementary material	67
68	1.68. References	68
69	1.69. Appendix	69
70	1.70. Bibliography	70
71	1.71. Summary	71
72	1.72. Acknowledgements	72
73	1.73. Declaration of interest	73
74	1.74. Conflict of interest	74
75	1.75. Funding	75
76	1.76. Author contributions	76
77	1.77. Correspondence	77
78	1.78. Additional information	78
79	1.79. Supplementary material	79
80	1.80. References	80
81	1.81. Appendix	81
82	1.82. Bibliography	82
83	1.83. Summary	83
84	1.84. Acknowledgements	84
85	1.85. Declaration of interest	85
86	1.86. Conflict of interest	86
87	1.87. Funding	87
88	1.88. Author contributions	88
89	1.89. Correspondence	89
90	1.90. Additional information	90
91	1.91. Supplementary material	91
92	1.92. References	92
93	1.93. Appendix	93
94	1.94. Bibliography	94
95	1.95. Summary	95
96	1.96. Acknowledgements	96
97	1.97. Declaration of interest	97
98	1.98. Conflict of interest	98
99	1.99. Funding	99
100	1.100. Author contributions	100

Aan mijn ouders

CONTENTS

	page
INTRODUCTION	1
References	5
 Chapter I	
THEORY AND EVALUATIONS	
1.1. Angular distribution of fission fragments and α -particles from aligned nuclei	6
1.1.1. Fission fragments	6
1.1.2. Alpha-particles	13
1.1.3. Nuclear orientation	15
References	19
1.2. Resonance theory of neutron-induced fission	20
1.2.1. Fissile nuclei; transition states and distribution of fission widths	20
1.2.2. Fission cross section and resonance spin determination	26
1.2.3. Non-fissile nuclei	28
References	34
1.3. The hyperfine splitting of heavy actinide nuclei in the RUN-compound	35
1.3.1. ^{233}U and ^{235}U	35
1.3.2. ^{237}Np	40
References	43
1.4. Absorption and scattering of fission fragments	45
References	53
 Chapter II	
EXPERIMENTAL ARRANGEMENT AND CALCULATIONS	
2.1. Experimental geometry	54
2.2. Samples for alignment of ^{235}U , ^{233}U and ^{237}Np	58
2.3. Cryostat and thermometry	62
2.4. Diffused-junction semi-conductor detectors	71
2.5. Time-of-flight technique	76
2.6. Electronics and data-handling	86
References	94

	page
Chapter III ANISOTROPY OF α -EMISSION AND OF FISSION BY THERMAL NEUTRONS	
3.1. Introductory remarks	96
3.2. ^{237}Np	97
3.3. ^{235}U	103
3.4. ^{233}U	109
References	116
Chapter IV ANISOTROPY IN THE ANGULAR DISTRIBUTION OF FISSION FRAGMENTS OF ORIENTED ^{233}U BY LOW-ENERGY NEUTRONS	
4.1. Introduction	117
4.2. Data-taking, calculations and results	119
4.3. Discussions and interpretation	128
References	136
Chapter V ANGULAR DISTRIBUTION OF FISSION FRAGMENTS FROM SUBTHRESHOLD FISSION OF ALIGNED ^{237}Np	
5.1. Theoretical considerations	137
5.2. Data collection, calculations and results	140
5.3. Discussion and interpretation	146
References	153
Chapter VI ANALYSIS OF THE ANISOTROPY IN THE ANGULAR DISTRIBUTION OF FISSION FRAGMENTS FROM ^{233}U USING A MULTILEVEL-FIT PROCEDURE	
6.1. Introduction; multilevel-fit formalism	154
6.2. The fission cross section of ^{233}U	157
6.3. Calculations and results	161
6.4. Discussion of the results and the method	164
References	167
SUMMARY	168
SAMENVATTING	170
CURRICULUM VITAE	172
NAWOORD	173

INTRODUCTION

The fission process of heavy nuclei and its related phenomena have been interpreted by various theoretical models. Since the discovery of nuclear fission it was of primary importance to formulate the energy balance of fission. The semi-empirical formula by Weiszäcker ¹⁾ for the nuclear ground-state energies provided useful estimates of the energy released in fission, primarily in the form of kinetic energy of the fragments, by a combination of several terms : binding energy of the nucleons, surface tension, electrostatic repulsion, neutron-proton symmetry and energy deficit due to unpaired nucleons. The main factors accounting for the fissility of heavy nuclei are a relative decrease in surface tension as the nuclear volume increases and a simultaneous increase in electrostatic repulsion between the protons.

For the description of the fission process the liquid drop model (LDM) was applied by N. Bohr and Wheeler in 1939 ²⁾. In this model the potential energy of the nucleus can be calculated as a function of the deformation. The nuclear potential energy as a function of the two main parameters describing nuclear deformation shows a saddle point which is a relative maximum for the elongation parameter of the nucleus. Fission can occur if the excitation of a compound nucleus is sufficient to pass this deformation saddle point. Since the excess of energy at the saddle point is rather small for a compound nucleus produced by capture of low-energy neutrons, the number of nuclear levels which the nucleus can occupy in its saddle point configuration is expected to be low. These levels at the deformation barrier through which fission can proceed are called the transition states. The reaction rate for fission can be related to the number N of transition states by a simple formula:

$$\frac{\langle \Gamma_f \rangle}{\langle D \rangle} = \frac{N}{2\pi}$$

in which $\langle \Gamma_f \rangle$ is the average fission width and $\langle D \rangle$ the average spacing of transition states. The number of transition states can be written as the sum of transmission factor for the subsequent states according to the Hill-Wheeler barrier penetration formula ³⁾.

The concept of transition states, defined in neutron resonance theory as the fission channels, provided a useful basis for the interpretation of fission, but a more advanced description was required in order to explain all the detailed properties of fission. The collective model is based on the general assumption, that an excess of energy, for instance induced by capture of a low-energy neutron, is spread over many nucleons. A collective motion of the nucleus such as deformation to the saddle-point configuration is then followed adiabatically by the intrinsic motion of the nucleons. This is possible owing to a small but essentially non-zero interaction between intrinsic and collective modes of the nucleus.

It has been pointed out by A. Bohr ⁴⁾ that when the deformation has proceeded to the saddle-point configuration the nuclear matter can be described as cold and for the even-even compound nuclei the intrinsic mode is the ground state. The excitations at the deformation barrier have a collective character and the wave functions can be written as products of vibrational and rotational modes. Wheeler ⁵⁾ classified the various collective modes and constructed a transition-state spectrum for the even-even compound nuclei. For odd-mass and odd-odd nuclei the single-particle excitations have lower energies than the vibrational modes. Thus, the transition-state spectrum for these nuclei will be characterized by rotational bands superimposed on the particle levels.

A correction on the potential energy of deformation had to be included for residual shell-structure effects. Detailed calculations by Strutinsky over an extended deformation range showed that the deformation barrier split up into two barriers which, for suitable heights of the two respective barriers, might give rise to a second potential well at higher deformations in which the nucleus can occupy levels. Many isomers of heavy nuclei have been observed with very short decay times for spontaneous fission that can be ascribed to a decay from the ground state in the second minimum of the Strutinsky potential. Also the group structure of resonances in the subthreshold fission cross sections of ^{240}Pu and ^{237}Np could be interpreted by the double-humped deformation barrier. For the double-humped deformation barrier the transition states will correspond to the nuclear states above the second barrier.

For the transition states the projection K of the nuclear spin J on the symmetry axis is a well defined quantum number because of the collective character of the nuclear motion during the passage of the deformation barrier. Assuming that the deformation of the nucleus after having passed the transition state is a rapid process, the value of K will be conserved and as a result of this assumption the emission of the fission fragments relative to the nuclear spin J will have an angular distribution according to the particular K -value. Therefore, if the nuclear spin is oriented in space a measurement of the angular distribution of fission fragments is a purely geometrical method for the determination of K -values of the transition states. The angular distribution of fission fragments can be expanded in Legendre polynomials:

$$W(\theta) = 1 + \sum_k A_k f_k P_k(\cos\theta) \quad .$$

For reasons of symmetry, only even k -values contribute to the angular distribution; f_k are the orientation parameters for the target nuclei and the factors A_k depend on the values of K and J of the transition states of the compound nucleus.

The emission of α -particles from heavy nuclei is often anisotropic owing to the fact that these nuclei in their ground states have a certain deformation. For a prolate ellipsoidal nuclear shape it was predicted by Hill and Wheeler that the barrier for the α -decay would be thinner at the poles than at the equator of the deformed nucleus. The angular distribution for α -emission also can be described by the formula given above.

Measurements of α -particle and fission-fragment anisotropies were first carried out by Dabbs et al ⁷⁾, orienting heavy target nuclei at low temperatures in crystals of $\text{RbUO}_2(\text{NO}_3)_3$ by the electric-quadrupole coupling method which was pointed out by Pound ⁸⁾. In those experiments the anisotropies in the α -particle and fission-fragment emission were measured at temperatures in the order of 1 K at which the hyperfine splitting in RbUO_2 -crystals already gave a considerable nuclear orientation.

The methods used in the series of experiments reported in this dissertation are basically the same as those used by Dabbs. The necessary nuclear orientation has been obtained by cooling the target material, also consisting of RUN-crystals, to temperatures in the order of 0.1 K. The target nuclei ^{235}U , ^{233}U and ^{237}Np could be aligned in the RUN-compound, owing to reasonably large quadrupole moments for these nuclei and a moderate heat development due to dissipation of α -particles. The anisotropy in the α -emission has been measured for the nuclei ^{233}U and ^{237}Np . The anisotropy in the angular distribution of fragments from neutron-induced fission has been measured as a function of neutron energy in the region from 0 to 2000 eV for all three nuclei. At neutron energies below approximately 60 eV the individual resonances in the fission cross sections could be observed. The measurements of the anisotropies in fission-fragment emission from ^{235}U have been reported by Pattenden and Postma⁹⁾.

In order to rule out a few experimental uncertainties concerning the degree of nuclear orientation and scattering of fission fragments, measurements on α -particle and fission-fragment emission have been done with small and thin samples for which the cooling of the target nuclei is more effective and disturbances in the angular distribution of fission fragments due to large-angle deflections of the fragments are negligible.

References

1. C.F. Weiszäcker, Zeitschr. für Phys. 96 (1935) 431.
2. N. Bohr and J.A. Wheeler, Phys. Rev. 56 (1939) 246.
3. D.L. Hill and J.A. Wheeler, Phys. Rev. 89 (1953) 1102
4. A. Bohr, Proc. Int. Conf. on Peaceful Uses Atom. Energy (Geneva, 1955) Vol.2, 220.
5. J.A. Wheeler, Fast Neutron Physics, Part II, ed. J.L. Fowler and J.B. Marion (John Wiley and Sons, New York, 1963) 2051.
6. V.M. Strutinsky, Nucl. Phys. A 95 (1967) 420.
7. J.W.T. Dabbs, Phys. Ann. Progr. Report (1960) ORNL-2910, 56, 60.
8. V.F. Pound, Phys. Rev. 79 (1950) 685.
9. N.J. Pattenden and H. Postma, submitted to Nucl. Phys.

Chapter I

THEORY AND EVALUATIONS

1.1. Angular distribution of fission fragments and α -particles from aligned nuclei

1.1.1. Fission fragments

In the fission process of heavy nuclei induced by low-energy neutrons the emission of the fission fragments as the final stage of the process, is generally assumed to occur in the direction of the nuclear symmetry axis, on the basis of energy considerations for the deforming nucleus ¹). The angular distribution of the emitted fragments depends on the orientation of the nuclear symmetry axis. The heavy nuclei investigated have a prolate ellipsoidal shape in their ground state. The spatial orientation of the symmetry axis of a compound nucleus can be described by the spin J , the projection M on an axis in a laboratory coordinate system (z -axis) and the projection K of J on the nuclear symmetry axis, however, not by the parity of the nuclear states. The orientation of the ellipsoidal nucleus and the nuclear spin with respect to the z -axis is shown in fig. 1.1.

The oriented compound nucleus is formed by s -wave capture in oriented target nuclei which limits the possible values of J to $I + \frac{1}{2}$ and $I - \frac{1}{2}$, where I is the spin of the target nucleus. The compound nucleus can be described in terms of products of an intrinsic wave function $\phi_{\tau K}$ and a symmetric-top wave function $D_{MK}^J(\phi, \theta, \chi)$ in which χ denotes the rotation of the nucleus about this symmetry axis and θ and ϕ are the polar angles defining the symmetry axis of the nucleus with respect to the reference coordinate system:

$$\Psi_M^J = \sum_K \left\{ D_{MK}^J \phi_{\tau K} + (-)^J D_{M-K}^J \phi_{\tau-K} \right\} .$$

The symmetric-top wave functions can be factorized according to its variables:

$$D_{MK}^J(\phi, \theta, \chi) = d_{MK}^J(\theta) e^{iM\phi} e^{iK\chi} .$$

section 1.1.

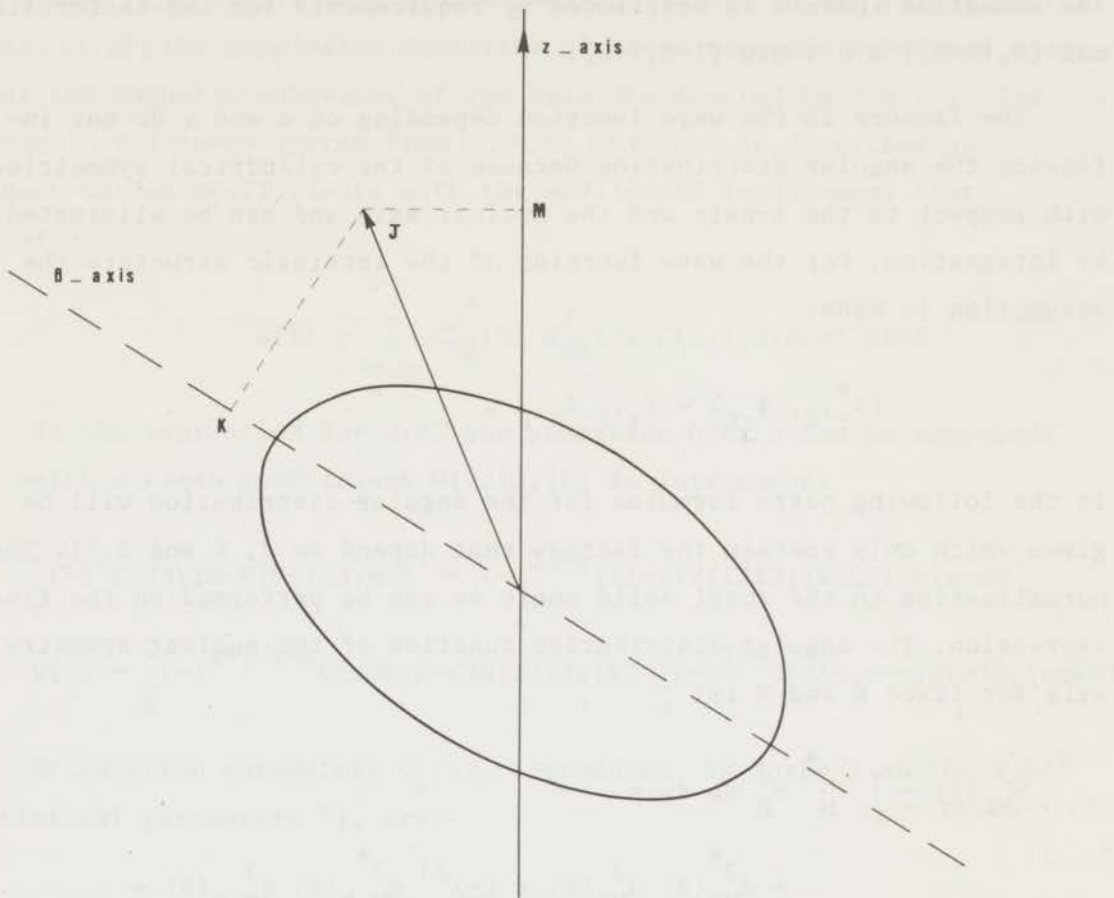


Fig. 1.1.

Orientation of a deformed nucleus with spin J . M is the projection of J on the z -axis and K is the projection of J on the nuclear deformation axis.

The differential equation for the first factor is:

$$\sin\theta \frac{d}{d\theta} \left\{ \sin\theta \frac{d}{d\theta} d_{MK}^J(\theta) \right\} + \{ J(J+1)\sin^2\theta - M^2 - K^2 + 2MK\cos\theta \} d_{MK}^J(\theta) = 0 .$$

The general solution is:

$$d_{MK}^J(\theta) = \sum_n \frac{(-)^n \{ (J+K)! (J-K)! (J+M)! (J-M)! \}^{\frac{1}{2}}}{(J-M-n)! (J+K-n)! n! (n+M-K)!} \cos^{2J+K-M-2n} \left(\frac{\theta}{2} \right) \sin^{2n+M-K} \left(\frac{\theta}{2} \right) .$$

The summation index n is restricted by requirements for the factorials:
 $\max(0, |K-M|) \leq n \leq \min(I-M, I+K)$.

The factors in the wave function depending on ϕ and χ do not influence the angular distribution because of the cylindrical symmetries with respect to the z -axis and the nuclear axis and can be eliminated by integration. For the wave function of the intrinsic structure the assumption is made:

$$(\phi_{\tau}^*, \phi_{\tau K}) = \delta_{\tau, \tau} \delta_{K, K}.$$

In the following parts formulae for the angular distribution will be given which only contain the factors that depend on J , K and θ ³⁾. The normalization to the total solid angle 4π can be performed on the final expression. The angular distribution function of the nuclear symmetry axis for fixed K and M is:

$$\begin{aligned} W_{MK}^J(\theta) &\doteq \int \psi_M^{J*} \psi_M^J d\phi d\chi = \\ &= d_{MK}^{J*}(\theta) d_{MK}^J(\theta) + (-)^{2J} d_{M-K}^{J*}(\theta) d_{M-K}^J(\theta) = \\ &= \sum_k (-)^{M-K} (1+(-)^k) C(JJk; M-M) C(JJk; K-K) P_k(\cos\theta), \end{aligned}$$

in which $P_k(\cos\theta)$ are the Legendre polynomials. It can be seen that only even k -values occur. For this expression the Clebsch-Gordan series had been used:

$$\begin{aligned} d_{MK}^{J*}(\theta) d_{MK}^J(\theta) &= (-)^{M-K} d_{MK}^J(\theta) d_{-M-K}^J(\theta) = \\ &= \sum_k (-)^{M-K} C(JJk; M-M) C(JJk; K-K) P_k(\cos\theta). \end{aligned}$$

The angular distribution of the symmetry axis and therefore also of the direction of emission of the fission fragments can be obtained by multiplying $W_{MK}^J(\theta)$ with the population densities $P(M)$ and summing over the substates M .

$$W(\theta) = \sum_M W_{MK}^J(\theta) P(M) \doteq \sum_M d_{MK}^{J*}(\theta) d_{MK}^J(\theta) P(M).$$

section 1.1.

The states (J,M) result from s-wave neutron capture in the target nuclear states (I,m); the population densities of these magnetic substates m are p(m); the magnetic substates of the spin are denoted by $\sigma = \pm \frac{1}{2}$. The change in reference system from (J,M) to (I,m) can be described by Clebsch-Gordan coefficients with the additional requirement that $M = m + \sigma$:

$$W(\theta) = \sum_{m, \sigma} d_{MK}^{J*}(\theta) d_{MK}^J(\theta) C(I, \frac{1}{2}, J; m, \sigma)^2 p(m) .$$

In the expression for W(θ) the summation over σ can be executed, for which a Racah coefficient $W(IJ I J; \frac{1}{2} k)$ is introduced:

$$\sum_{\sigma} (-)^{\sigma} C(JJk; M-M) C(I \frac{1}{2} J; m \sigma)^2 = (-)^{2I + \frac{1}{2}} (2I+1) W(IJ I J; \frac{1}{2} k) C(I I k; m-m) ;$$

$$W(\theta) = \sum_k (-)^{I + \frac{1}{2} - K - k} C(JJk; K-K) W(IJ I J; \frac{1}{2} k) \sum_m (-)^{I-m} C(I I k; m-m) p(m) P_k(\cos \theta) .$$

Orientation parameters $G_k(I)$, introduced by Rose ²⁾ as the Fano statistical parameters ⁴⁾, are:

$$G_k(I) = \sum_m (-)^{I-m} C(I I k; m-m) p(m) .$$

Using the explicit expressions for Clebsch-Gordan coefficients and Racah coefficients the following expression has been obtained ⁵⁾:

$$W(\theta) = 1 + \sum_k \frac{\sqrt{2k+1} k!}{2^k \{(\frac{1}{2}k)!\}^2} \left[\frac{(2I+k+1)(2I+k-1) \dots (2I-k+1)}{(2I+k)(2I+k-2) \dots (2I-k+2)} \right]^{\frac{1}{2}}$$

$$\times F_k(J; K) G_k(I) P_k(\cos \theta) \quad (k \text{ even}) .$$

In this expression for W(θ) a useful separation of variables has been obtained. The Legendre polynomials $P_k(\cos \theta)$ only contain the angle θ of the angular distribution.

The Legendre-polynomials are:

$$P_2(\cos\theta) = \frac{3}{2} (\cos^2\theta - \frac{1}{3})$$

$$P_4(\cos\theta) = \frac{35}{8} (\cos^4\theta - \frac{6}{7} \cos^2\theta + \frac{3}{35})$$

$$P_6(\cos\theta) = \frac{231}{16} (\cos^6\theta - \frac{15}{11} \cos^4\theta + \frac{5}{11} \cos^2\theta - \frac{5}{231}).$$

For $\theta = 0$, $P_k(\cos\theta) = 1$ for any k .

The influence of J and K is determined entirely by the expressions for $F_k(J;K)$. The explicit formulae for the factors $F_k(J;K)$ are:

$$F_2(J;K) = \frac{3K^2}{J(J+1)} - 1$$

$$F_4(J;K) = \frac{35K^4 - 5(6J^2 + 6J - 5)K^2}{3(J-1)J(J+1)(J+2)} + 1$$

$$F_6(J;K) = \frac{462K^6 - 210(3J^2 + 3J - 7)K^4 + 21(10J^4 + 20J^3 - 40J^2 - 50J + 28)K^2}{10(J-2)(J-1)J(J+1)(J+2)(J+3)} - 1.$$

The orientation of target nuclei is fully described by the parameters $G_k(I)$. Cox and Tolhoek ⁶⁾ introduced different orientation parameters f_k , of which the explicit formulae in terms of population densities $p(m)$ are:

$$f_2 = \frac{1}{I^2} \left\{ \sum_m m^2 p(m) - \frac{1}{3} I(I+1) \right\}$$

$$f_4 = \frac{1}{I^4} \left\{ \sum_m m^4 p(m) - \frac{1}{7} (6I^2 + 6I - 5) \sum_m m^2 p(m) + \frac{3}{35} (I-1)I(I+1)(I+2) \right\}$$

$$f_6 = \frac{1}{I^6} \left\{ \sum_m m^6 p(m) - \frac{5}{11} (3I^2 + 3I - 7) \sum_m m^4 p(m) + \frac{1}{11} (5I^4 + 10I^3 - 20I^2 - 25I + 14) \sum_m m^2 p(m) - \frac{5}{231} (I-2)(I-1)(I)(I+1)(I+2)(I+3) \right\}$$

$$\sum_m p(m) = 1.$$

section 1.1.

The relation between the parameters $f_k(I)$ and $G_k(I)$ is:

$$\frac{f_k(I)}{G_k(I)} = \binom{2k}{k}^{-1} I^{-k} \left[\frac{(2I+k+1)!}{(2k+1)!(2I-k)!} \right]^{\frac{1}{2}}.$$

The angular distribution then can be written as:

$$W(\theta) = 1 + \sum_k \frac{(2k+1)!}{2^k k! \{(\frac{1}{2}k)!\}^2} I^k \left[(2I+k)(2I+k-2)\dots(2I-k+2) \right]^{-1} F_k(J;K) f_k(I) P_k(\cos\theta).$$

The formula for the angular distribution contains only terms with even k , so odd orientation parameters are inconsequential to the angular distribution of fission fragments. Therefore, from a target in which the target nuclei are polarized and for which thus the orientation is described by the parameter f_1 only, no anisotropy will be observed in the angular distribution of fission fragments. Since in general only odd mass heavy nuclei are fissile by low-energy neutrons those with a spin $I \geq \frac{3}{2}$ will be of interest for the orientation experiments presently described.

For analysis and interpretation a general formula is used:

$$W(\theta) = 1 + \sum_k A_k f_k P_k(\cos\theta) \quad (k \text{ even}),$$

in which the constant A_k can be defined by:

$$A_k = C_k(I) F_k(J;K).$$

The numerical values of the non-trivial parameters A_k have been given in table 1.1 for target nuclei with spins $I = \frac{5}{2}$ and $I = \frac{7}{2}$.

Table 1.1.
 A_k -values for target spin $I = \frac{5}{2}$

K \ J	2	3	k
0	-2.679 +9.765	-2.679 +9.765	2 4
1	-1.339 -6.510	-2.009 +1.628	2 4
2	+2.679 +1.628	0.000 -11.393	2 4
3		+3.348 +4.883	2 4

A_k -values for target spin $I = \frac{7}{2}$

K \ J	3	4	k
0	-2.917 +10.232 -51.063	-2.917 +10.232 -51.063	2 4 6
1	-2.188 +1.705 +38.297	-2.479 +5.116 +2.553	2 4 6
2	0.000 -11.937 -15.319	-1.167 -6.253 +56.169	2 4 6
3	+3.646 +5.116 +2.553	+1.021 -11.937 -43.403	2 4 6
4		+4.083 +7.958 +10.213	2 4 6

section 1.1.

1.1.2. Alpha-particles

The angular distribution for the emission of α -particles from aligned nuclei has been developed by Rose ²⁾ and by Brussaard ⁶⁾. Owing to the fact that α -particles have spin zero, there will be no polarization effects, but the angular distribution may show an anisotropy effect, depending on the spin I of the α -emitter, the angular momentum L of the α -particle and the spin J of the final state of the nucleus daughter. If the parities of initial and final nuclear states are equal then only even values for L are possible. Expressions for the angular distribution of α -emission were derived from the transition probabilities from state (I, m_I) to state (J, m_J) :

$$W_{LM}(\theta) \doteq \sum_{m_I m_J} p(m_I) \langle J m_J | H_\alpha(L m_L; \theta) | I m_I \rangle^2$$

with $m_L = m_I - m_J$.

Assuming α -emission with only one L -value, the final expression, after having developed the matrix elements for $H_\alpha(L m_L)$, becomes:

$$W(\theta) = (-)^{I-J} (2I+1)(2L+1) \sum_k C(LLk; 00) W(IILL; kJ) G_k(I) P_k(\cos\theta)$$

and for the case that there is admixing of several L -values:

$$W(\theta) = \frac{(2I+1)(-)^{I-J}}{\sum_L a_{LL}^2} \sum_{kLL'} a_{LL'} \{ (2L+1)(2L'+1) \}^{\frac{1}{2}} \\ \times (-)^{-\frac{1}{2}(L'-L)} \sum_k C(LL'k; 00) W(IILL'; kJ) G_k(I) P_k(\cos\theta).$$

For the relative amplitudes $a_{LL'}$, a definition can be given in terms of absolute amplitudes and relative phases δ_L ; the total contribution of the various L -waves is normalized to 1.

$$a_{LL'} = \pm (a_L a_{L'})^{\frac{1}{2}} \cos(\delta_L - \delta_{L'}) \quad (L \neq L')$$

$$a_{LL} = a_L \quad (L = L')$$

$$\sum_L a_L^2 = 1.$$

For non-deformed nuclei the phase shift δ_L can be given, according to Rose ²⁾:

$$\delta_L = \frac{1}{2}L\pi + \arg \Gamma \left[L+1 + \frac{2(Z-2)e^2}{hv_\alpha} \right]$$

where Z is the atomic number of the α -emitter and v_α the velocity of the α -particle.

Explicit formulae for various transitions that are of interest, can be given ⁷⁾; in all cases the parity is taken to be the same for initial and final nuclear state so that only $L = 0, 2, 4$ is possible. The notation of the various symbols is the same as given by de Groot et al. ⁸⁾.

$$J = I-2; \quad L = 2$$

$$W(\theta) = 1 - \frac{30}{7} N_2 f_2 P_2(\cos\theta) + \frac{15}{2} N_4 f_4 P_4(\cos\theta)$$

$$J = I-1; \quad L = 2$$

$$W(\theta) = 1 + \frac{15}{7} N_2 f_2 P_2(\cos\theta) - 15 \frac{2I-3}{I+1} N_4 f_4 P_4(\cos\theta)$$

$$J = I; \quad L = 0, 2$$

$$W(\theta) = 1 + \left[- a_0 a_2 \cos(\delta_0 - \delta_2) 6\sqrt{5} \left\{ \frac{I(I+1)}{(2I-1)(2I+3)} \right\}^{\frac{1}{2}} + a_2^2 \frac{15}{7} \frac{(2I-3)(2I+5)}{(2I-1)(2I+3)} \right] K_2 f_2 P_2(\cos\theta) + a_2^2 \frac{45}{(2I-1)(2I+3)} K_4 f_4 P_4(\cos\theta)$$

$$J = I+1; \quad L = 2$$

$$W(\theta) = 1 + \frac{15}{7} \frac{I+6}{I} M_2 f_2 P_2(\cos\theta) - 15 \frac{2I+5}{I} M_4 f_4 P_4(\cos\theta)$$

section 1.1.

$$J = I+2; \quad L = 2$$

$$W(\theta) = 1 - \frac{30}{7} M_2 f_2 P_2(\cos\theta) + \frac{15}{4} M_4 f_4 P_4(\cos\theta) .$$

For these formulae the following quantities have been introduced:

$$N_2 = \frac{I}{2I-1} \qquad N_4 = \frac{I^3}{(I-1)(2I-1)(2I-3)}$$

$$K_2 = \frac{I}{I+1} \qquad K_4 = \frac{I^3}{I+1}$$

$$M_2 = \frac{I^2}{(2I+1)(2I+3)} \qquad M_4 = \frac{I^4}{(I+1)(I+2)(2I+3)(2I+5)} .$$

1.1.3. Nuclear orientation

The orientation of the target nuclei can be obtained by:

- a) the interaction of nuclear magnetic-dipole moments with magnetic fields;
- b) the interaction of nuclear electric-quadrupole moments with electric field gradients.

A magnetic hyperfine field can be generated by unpaired electrons. The interaction may be represented by the effective-spin Hamiltonian which in its general form is given by:

$$H = g_{//} \mu_B S_z H_z + g_{\perp} \mu_B \{ H_x S_x + H_y S_y \} + \\ + A I_z S_z + B (I_x S_x + I_y S_y) + P \{ I_z^2 - \frac{1}{3} I(I+1) \} .$$

In many cases the effective spin S is $\frac{1}{2}$. The first two terms represent the Zeeman splitting, $g_{//}$ and g_{\perp} are the gyromagnetic ratios of the electronic states and H is an external magnetic field. The terms with A and B represent magnetic-dipole coupling and the last term with P gives the electric-quadrupole coupling.

The method of obtaining alignment by the electric-quadrupole interaction was pointed out by Pound⁹). Only nuclei from the rare-earth region and the actinide elements which are strongly deformed in the ground state have quadrupole moments which are large enough to be suitable for alignment by Pound's method.

Developing an expression for the quadrupole coupling constant P, the Hamiltonian for pure quadrupole interaction is^{10,11}):

$$H = \frac{1}{2} \sum_{ij} Q_{ij} V_{ij} \quad ,$$

$$V_{ij} = \frac{\delta^2 V}{\delta x_i \delta x_j} \quad (x_i, x_j) = (x, y, z) .$$

V is the electric potential in the neighbourhood of the nucleus. Assuming at first a symmetric field gradient the only term of the tensor V different from zero is V_{zz} which is written as: $V_{zz} = eq$; the non-vanishing matrix elements of the spin Hamiltonian will be:

$$\langle m | H | m' \rangle = P \left\{ m^2 - \frac{1}{3} I(I+1) \right\}$$

where:
$$P = - \frac{3e^2 q Q}{4I(2I-1)} .$$

The quantity q which is characteristic for the electronic structure in the vicinity of the nucleus is given by the expression:

$$eq = \sum_j e_j (3\cos\theta_j - 1) r_j^{-3} \quad ;$$

the summation j is over all electrons.

Q is the observable electric-quadrupole moment of the nucleus as defined by:

$$eQ = \int \rho_i r_i^2 (3\cos^2\theta_i - 1) d\tau_i \quad ,$$

where ρ_i is the charge density in a small volume element $d\tau_i$ inside the nucleus at a distance r_i from the centre and θ_i is the angle of the radius vector r_i with the nuclear spin axis.

section 1.1.

Q is related to the intrinsic electric-quadrupole moment Q_0 by:

$$Q = \frac{3K^2 - I(I+1)}{(I+1)(2I+3)} Q_0 .$$

If there is an asymmetry in the field-gradient tensor the reference coordinate system x, y, z can be transformed to the principal axes X, Y, Z so that V_{XX} , V_{YY} and V_{ZZ} are the non-vanishing elements of the tensor. An asymmetry parameter η is defined as:

$$\eta = \frac{V_{XX} - V_{YY}}{V_{ZZ}} .$$

The effective-spin Hamiltonian will now contain off-diagonal matrix elements ^{10,11}):

$$\langle m | H | m' \rangle = \frac{1}{2} P \eta (I \pm m) (I \mp m + 1) (I \mp m + 1) (I \pm m + 2) \delta_{m', m \pm 2}$$

which will cause admixing of magnetic substates having a difference of 2 in the magnetic quantum numbers. Some predictions can be made on the relative influence of a small asymmetry term ($\eta = 0.1$) on the orientation parameters f_2 and f_4 for a nucleus with spin $I = \frac{5}{2}$. The effect appears to be practically negligible (less than 1%).

The alignment parameter f_2 can easily be calculated from the energy levels which are the resulting eigen-values of the spin Hamiltonian for pure electric-quadrupole coupling. The energies are represented by:

$$E_m = P m^2 .$$

The population densities are proportional to the Boltzmann factors of the energy levels:

$$p(m) \doteq \exp \left(- \frac{E_m}{kT} \right) = \exp \left(- \frac{Pm^2}{kT} \right)$$

$$f_2 = \frac{1}{I^2} \left[\sum_m m^2 \exp \left(- \frac{Pm^2}{kT} \right) / \sum_m \exp \left(- \frac{Pm^2}{kT} \right) - \frac{1}{3} I(I+1) \right] .$$

The high-temperature approximation for f_2 can be obtained by developing the exponentials to first order in $\frac{P}{kT}$:

$$f_2 \approx \frac{1}{I^2} \left[\frac{\sum_m m^2 \left(1 - \frac{Pm^2}{kT}\right)}{\sum_m \left(1 - \frac{Pm^2}{kT}\right)} - \frac{1}{3} I(I+1) \right]$$

$$\approx \frac{1}{I^2} \left[\frac{\sum m^2}{(2I+1)} - \frac{P}{kT} \left[\frac{(\sum m^2)^2 - (2I+1) \cdot \sum m^4}{(2I+1)^2} \right] - \frac{1}{3} I(I+1) \right]$$

$$= - \frac{1}{I^2(2I+1)} \frac{P}{kT} \left[(\sum m^2)^2 - (2I+1) \cdot \sum m^4 \right].$$

The summations of powers $\sum_{m=-I}^{m=+I} m^n$ are calculated by recurrence technique and resultingly, for high temperatures the approximation for f_2 is:

$$T \gg \frac{P}{k} : f_2 \approx - \frac{(I+1)(2I-1)(2I+3)}{45I} \frac{P}{kT} .$$

From this expression it can be seen that for positive values of P f_2 will be negative and reversely. In case of pure magnetic dipole interaction, the Boltzmann exponentials have to be developed to the second-order terms which are proportional to $\left(\frac{A}{kT}\right)^2$. The explicit expression is then:

$$T \gg \frac{A}{k} : f_2 \approx \frac{(I+1)(2I-1)(2I+3)}{360I} \left(\frac{A}{kT}\right)^2 .$$

References

References

1. A. Bohr, Proc. Internat. Conf. Peaceful Uses Atomic Energy (Geneva, 1955) Vol. 2, 151.
2. M.E. Rose, Elementary Theory of Angular Momentum (Wiley, New York, 1957).
3. L.D. Roberts, J.W.T. Dabbs, G.W. Parker, report ORNL-2430 (1957) 51.
4. U. Fano, Nat. Bur. Standards Washington D.C., report no. 1214 (1951).
5. H. Postma, private communications.
6. H.A. Tolhoek and J.A.M. Cox, Physica 19 (1953) 101.
7. P.J. Brussaard and H.A. Tolhoek, Physica 24 (1958) 233, 263.
8. S.R. de Groot, H.A. Tolhoek and W.J. Huiskamp, Orientation of Nuclei at Low Temperatures, Alpha-, Beta-, and Gamma-Ray Spectroscopy (ed. K. Siegbahn, North-Holland Publ. Cy., 1965) Vol. II, 1199.
9. R.V. Pound, Phys. Rev. 79 (1950) 685.
10. M.H. Cohen and F. Reif, Solid State Physics 5 (1957) 321.
11. T.P. Das and E.L. Hahn, Solid State Physics, Suppl. 1 (1958).

1.2. Resonance theory of neutron-induced fission

1.2.1. Fissile nuclei; transition states and distribution of fission widths

In nuclear resonance theory the process of fission of a heavy nucleus, which is excited by neutron capture, is a reaction which is competitive to other reactions, of which the most important one is gamma-ray emission. The first part of both reactions - the formation of a compound nucleus from the capture of a neutron in a target nucleus - is entirely equivalent. The process of fission as a special mode of deexcitation is governed by a collective behaviour of the nuclear matter after formation of the compound nucleus.

The collective theory of fission as developed by Bohr and Wheeler¹⁻³⁾ appropriately describes the properties of the transition states of the fissioning nucleus at the deformation barrier. Beyond this barrier the process of deformation towards the scission point is assumed to be essentially non-collective.

The deformation potential can be described as a function of two deformation parameters β and γ . The parameter β corresponds to the deformation of the nucleus in the direction of the nuclear symmetry axis, whereas γ describes deformation in directions perpendicular to this axis. The transition states of the fissioning nucleus correspond to a saddle-point configuration in the deformation potential. This saddle point is a relative maximum for β -deformation and a minimum for γ -deformation.

Neutron capture in a heavy nucleus will result in a compound nucleus with considerable excitation. The density of nuclear energy levels, corresponding to the neutron resonances, is high. As the compound nucleus deforms the individual nucleonic motion will be transformed into collective modes. At the deformation saddle point this transformation from internal energy to deformation energy has proceeded to a situation where the nuclear matter can be described as cold and the nuclear level density at this deformation has decreased to such a value that only a few levels will be available to the fission process.

section 1.2.

These levels represent the fission channels, which the nuclear system passes in its deformation process towards scission.

The transition-state spectrum can be calculated as the intrinsic nuclear states at saddle-point deformation, on each of which a vibrational and a rotational band is superimposed. For even-even compound nuclei the pairing gap is usually greater than the excess of energy above the transition ground state for excitation by low-energy neutrons. This simplifies the transition-state spectrum considerably, since in that case only levels associated with combinations of vibrational and rotational modes are involved. Each level is characterized by the nuclear spin (J), parity (π) and the projection (K) of the spin on the nuclear symmetry axis, which is the main axis of deformation.

For even-even nuclei the transition ground state has $(J^\pi, K) = (0^+, 0)$. The rotational band associated with the ground state is:

$$J^\pi = 0^+, 2^+, 4^+, 6^+, \dots$$

$$E_J = E_0 + \frac{\hbar^2}{2I_\perp} J(J+1) \quad ,$$

in which I_\perp is the moment of inertia for rotations about an axis perpendicular to the nuclear symmetry axis and E_0 is the energy of the ground state at saddle-point deformation. At somewhat higher energies, in the order of 500 keV, vibrational levels appear, on each of which a rotational band is superimposed. The rotational energy of a given level (J^π, K) is:

$$E_{(J,K)} = \frac{\hbar^2}{2I_\perp} [J(J+1) - K^2] + \frac{\hbar^2}{2I_{//}} K^2 \quad (I_{//} \ll I_\perp) \quad .$$

Since $I_{//} \ll I_\perp$, this formula suggests that the lowest transition states are characterized predominantly by low K -values.

From the experimental evidence for fission thresholds in several nuclear reactions and especially from measurements of the angular distribution of fission fragments in reactions with $l \neq 0$, Hill and Wheeler

constructed a provisional spectrum of transition states for even-even compound nuclei, not including intrinsic modes. The vibrational states are classified by the phonons of elementary vibrational modes.

The β -mode is a vibration along the nuclear symmetry axis; it represents at the deformation saddle point the fission mode itself. The γ -vibration is describing the deformations in directions perpendicular to this symmetry axis. The lowest level of γ -vibration has $(J^\pi, K) = (2^+, 2)$ and the associated rotational band is $J^\pi = 2^+, 3^+, 4^+, \dots$. Octupole deformation corresponds to the mass-asymmetry vibrational (or sloshing) mode with $(J^\pi, K) = (1^-, 0)$ and a rotational band $J^\pi = 1^-, 3^-, 5^-, \dots$. The last classified fundamental mode is the bending mode, $(J^\pi, K) = (1^-, 1)$ to which a rotational band $J^\pi = 1^-, 2^-, 3^-, \dots$ corresponds. The transition-state spectrum as presented by Lynn ⁴⁾ is shown in table 1.2.

Table 1.2.

Transition-state spectrum for even-even compound nuclei.

Energy (MeV)	K	J^π	classification of collective vibrational mode
0	0	$0^+, 2^+, 4^+, \dots$	transition ground state
~ 0.5	0	$1^-, 3^-, 5^-, \dots$	mass-asymmetry vibration
~ 0.7	2	$2^+, 3^+, 4^+, \dots$	γ -vibration
~ 0.9	1	$1^-, 2^-, 3^-, \dots$	bending vibration
~ 1.2	2	$2^-, 3^-, 4^-, \dots$	mass-asymmetry plus γ -vibration
~ 1.4	1	$1^+, 2^+, 3^+, \dots$	mass-asymmetry plus bending vibration
~ 1.6	0	$0^+, 2^+, 4^+, \dots$	γ -vibration (2 quanta)
~ 1.7	1 3	$1^-, 2^-, 3^-, \dots$ $3^-, 4^-, 5^-, \dots$	{ γ -vibration plus bending vibration

section 1.2.

In the measurement of the angular distribution of fission fragments from aligned nuclei, the anisotropy in the distribution will reflect the situation of the fissioning nucleus in the transition state at the deformation saddle point. The assumption that K remains a good quantum number from the transition states onwards is a reasonable one, owing to the fact that the deformation of the fissioning nucleus into two separate nuclei from the transition state onwards is very rapid compared to the passage of the nucleus through the deformation saddle point. However, one cannot expect to measure a purely integral K -value for a particular s -wave resonance, since for each resonance there are more transition states available which in general have different K -values. Hence, an experimental value for the anisotropy in the angular distribution will result from the relative contributions to fission of the various transition states, each of which has a well defined theoretical anisotropy value, corresponding to its quantum number K . The distribution of these relative contributions can be predicted from the theoretical distributions of fission widths for the various channels ⁴).

The definition of the transition states as fission channels, contrary to the original definition of a channel as referring to a specific pair of reaction products, can be postulated considering the distribution of fission widths for a particular transition state. Since the reduced-width amplitudes for the true channels as they depend on a specific compound state are randomly distributed about zero mean, the mean square value of the amplitudes depends only on the coupling strength of compound and transition state.

For more fission channels the reduced-width amplitude of a compound level indicated by λ , for channel c , is a linear sum over the available transition states f ⁴):

$$\gamma_{\lambda(c)} = \sum_f b_{fc} y_{\lambda f}$$

where $y_{\lambda f}$ is the amplitude of the transition state f for compound level λ and b_{fc} gives the dependence of the wave function on the transition state at the channel entrance. Actually, this formation of $\gamma_{\lambda(c)}$ is made possible by the split-up of the formal channel into two un-

correlated parts.

The fission width for the compound level λ is obtained in R-matrix theory by summation over all channels c . The partial fission width of λ for channel c for one transition state f is:

$$\Gamma_{\lambda(f,c)} = 2P_c b_{fc}^2 y_{\lambda f}^2$$

where P_c is the penetration factor for channel c . For more transition states f , the fission width becomes:

$$\Gamma_{\lambda(F)} = \sum_c 2P_c \gamma_{\lambda(c)}^2 =$$

$$\sum_f y_{\lambda f}^2 \sum_c 2P_c b_{fc}^2 + \sum_{f \neq f'} y_{\lambda f} y_{\lambda f'} \sum_c 2P_c b_{fc} b_{f'c} .$$

If the signs of the factors b_{fc} have a random sign distribution and the number of channels is large, then the second term will become negligible and the expression reduces to the linear sum of contributions from the individual transition states. By normalizing $\sum_c 2P_c b_{fc}^2$ to unity the result for the fission width is a sum of partial widths:

$$\Gamma_{\lambda(F)} = \sum_f y_{\lambda f}^2 .$$

For one transition state the amplitudes $y_{\lambda f}$ are normally distributed with zero mean. The distribution of fission widths in that case will be a Porter-Thomas distribution, which is a χ^2 -distribution with one degree of freedom.

$$P(\Gamma_{\lambda(F)}) = (2\pi \langle \Gamma_{\lambda(F)} \rangle)^{-\frac{1}{2}} \exp \left(- \frac{\Gamma_{\lambda(F)}}{2 \langle \Gamma_{\lambda(F)} \rangle} \right) .$$

For a number of transition states N the fission-width distribution will be a χ^2 -distribution with N degrees of freedom.

section 1.2.

The average total fission width $\langle \Gamma_{(F)} \rangle$ has been related by Bohr and Wheeler ⁵⁾ to the total number N and average spacing $\langle D \rangle$ of transition states as:

$$\frac{\langle \Gamma_{(F)} \rangle}{\langle D \rangle} = \frac{N}{2\pi} .$$

N can be regarded as a sum of transmission factors T_f for the transition states, of which the energies are indicated by E_f :

$$N = \sum_f T_f = \sum_f \left[1 + \exp \left\{ - \frac{2\pi(E - E_f)}{\hbar\omega_f} \right\} \right]^{-1} .$$

A particular transmission factor T_f represents the degree of openness of the fission channel f . It is given in the form of the Hill-Wheeler barrier penetration formula and evidently, the range of T_f is from zero to one.

The theory presented above is very incomplete and some of the more fundamental aspects of resonance theory have been omitted. Nevertheless, it provides a framework for an interpretation of the angular distribution of fission fragments proceeding from low-energy neutron capture in fissile nuclei. Since the total fission width is the sum of partial fission widths, $\Gamma_f = y_{\lambda f}^2$, all of which have a Porter-Thomas distribution, the anisotropy parameter A_2 which results from the mixing of several transition states with theoretical A_{2f} -values according to the defined K -values, is the normalized average of the individual components, where the relative contributions of the subsequent channels are expressed in the respective transmission factors:

$$A_2 = \frac{\sum_f A_{2f} T_f \Gamma_f}{\sum_f T_f \Gamma_f} .$$

With theoretical distributions of this kind an experimental distribution of A_2 -values of resonances may now be fitted by adjustment of the various transmission factors.

1.2.2. Fission cross section and resonance spin determination

Nuclear resonance theory has encountered some difficulties in trying to explain the complex structure of the fission cross sections of fissionable nuclei. At low neutron energies only s-wave capture occurs, giving rise to resonances of spin $J = I + \frac{1}{2}$ and $J = I - \frac{1}{2}$. For the situation where there is no interference between resonances, the fission cross section can be described by a linear sum of contributions from independent resonances, as expressed by the Breit-Wigner formula:

$$\sigma_{nf} = \sum_i \pi \chi^2 g_J \frac{\Gamma_{ni} \Gamma_{fi}}{(E - E_{oi})^2 + (\frac{1}{2}\Gamma_i)^2}$$

$$\Gamma_i = \Gamma_{ni} + \sum_r \Gamma_{ri}$$

$$\chi = \frac{\lambda}{2\pi} \quad (\lambda : \text{De Broglie wave length})$$

$$g_J = \frac{2J+1}{2(2I+1)} \quad (\text{statistical spin factor})$$

E_{oi} : energy of resonance i

Γ_{ni} : neutron width of resonance i

Γ_{fi} : fission width of resonance i

Γ_i : total width of resonance i.

The summation with index i is over all the resonances, which are representing the compound nuclear levels; the summation indicated by r is over all reactions following neutron capture. For the fissionable nuclei the mean level spacing is of the same order as the average total widths of the resonances. The interference between resonances with equal spins results to asymmetric peaks in the fission cross section. Therefore, the description of the fission cross section in terms of single-level Breit-Wigner formulae is no longer adequate. The interference between resonances requires multilevel formulae.

section 1.2.

The application of multilevel formulae to the measured fission cross section requires advanced numerical methods and the results in terms of resonance parameters are not unambiguous. A difficulty in employing multilevel methods is that the number of fission channels is not known a priori. This number is an additional variable and has to be estimated from a first-order approximation. In the case where only two levels are involved the interference can be described by explicit formulae, but if more levels have to be taken into account such formulae are not available. An extensive review of the subject has been given by Lynn⁴); (see also chapter VI).

An attempt to resolve the resonance interaction in a more experimental approach is to assign the spins of the resonances. This would make it feasible to make a useful division of the levels into two groups, where interference is only possible between resonances of one group. Yet another aid is the analysis of the statistical behaviour of resonance parameters from the various cross sections: total, capture, fission and scattering cross section. In order to rule out systematic errors, it is often necessary to measure more cross sections simultaneously.

There are various methods for determination of resonance spins, which can be divided into two categories. In the first category the spins can be assigned directly, owing to a geometrical spin dependence in the experiment.

1. Transmission of polarized neutrons through a polarized sample of target nuclei.
2. Scattering of neutrons.

The second category consists of more indirect methods, that endeavour to make use of certain measurable quantities, which may be different for the two spin values.

1. Multiplicity of γ -rays following neutron capture.
2. Intensities of primary γ -ray transitions from the compound state to states with defined spins, or intensities of suitable secondary transitions.

3. Neutron yield accompanying fission.
4. Peak-to-valley ratio in the yield of fission fragments as a function of fragment mass.
5. Kinetic energies of fission fragments.

Method 1 and 2 in the latter category are experimentally very difficult for fissionable nuclei because of the intense γ -ray spectrum accompanying fission. The three methods (3,4,5) trying to make use of fission properties have a common feature with the angular distribution of fission fragments that for a certain compound nuclear level the admixing contributions of several fission channels may reduce sharp variations in certain quantities to smoothly varying functions. As a result the split-up of experimental values between the two groups of resonance spins will be diminished.

Finally, it has been tried to establish the resonance spins in a reversed way, by the analysis of the interference between resonances from the measured cross sections. For reasons mentioned above this method is unreliable (see also chapter VI).

All methods have been tried for the spin assignment of the resonances of ^{235}U in the neutron energy region up to 60 eV, but the total result is rather unreliable. There are only few resonances for which all assignments by different methods are equal. Unfortunately, for the resonances of ^{233}U hardly any spin assignments have been made, except for the results of a few tentative multilevel analyses. The results from experimental methods were unsatisfactory and did not allow any spin determinations.

1.2.3. Non-fissile nuclei

The general properties of the fission cross sections of fissile heavy nuclei can be explained satisfactorily by the unified collective model. However, for the interpretation of other aspects in nuclear fission refinements of the existing theories were necessary. For instance, asymmetric fission was in no way proved to result from the collective model and notably, the group structure of resonances in

section 1.2.

the subthreshold energy region of the non-fissile nuclei required more advanced theoretical treatment.

The corrections for possible influence from the pairing gap on the Nilsson calculations ⁶⁻⁸⁾ of single particle states in deformed nuclei were initiated by Szymanski ⁹⁾. More detailed and extensive studies of the deformation potential calculated also for highly deformed nuclei were performed by Strutinsky ¹⁰⁾.

The calculated deformation potential ¹⁰⁾ appeared to have a double-humped barrier with correspondingly two saddle-point configurations, instead of one only, as it was predicted by the liquid drop model. The correction on potential energy of deformation has an oscillating behaviour due to a thinning out and compression of nuclear levels at the Fermi energy. This oscillation has the effect of creating a second minimum in the potential at a much higher deformation than the equilibrium deformation for the nuclear ground state, which will become influential in the actinide region. The surface tension decreases for higher mass number and hence the saddle-point barrier would tend to become lower, but the stability of those nuclei is now guaranteed by shell effects which raise the saddle-point barrier against such a decrease in surface tension. Although the barrier will not become lower, it becomes narrower instead, which gives a higher penetrability for fission by tunneling through the barrier. An application of Strutinsky's model to nuclear resonance theory was made by Lynn ¹¹⁾ and Weigmann ¹²⁾.

A typical situation of the deformation potential is shown in fig. 1.2. Analogous to the first deformation minimum (I), nuclear states can be constructed in the second minimum (II). At a certain excitation energy E_c the average spacing of compound nuclear levels, D_I , will be much higher than the spacing of nuclear levels in the intermediate well, D_{II} . At excitation energies corresponding to an intermediate level a certain coupling strength between several compound levels and this intermediate level, in combination with a high fission probability for nuclear configurations described by

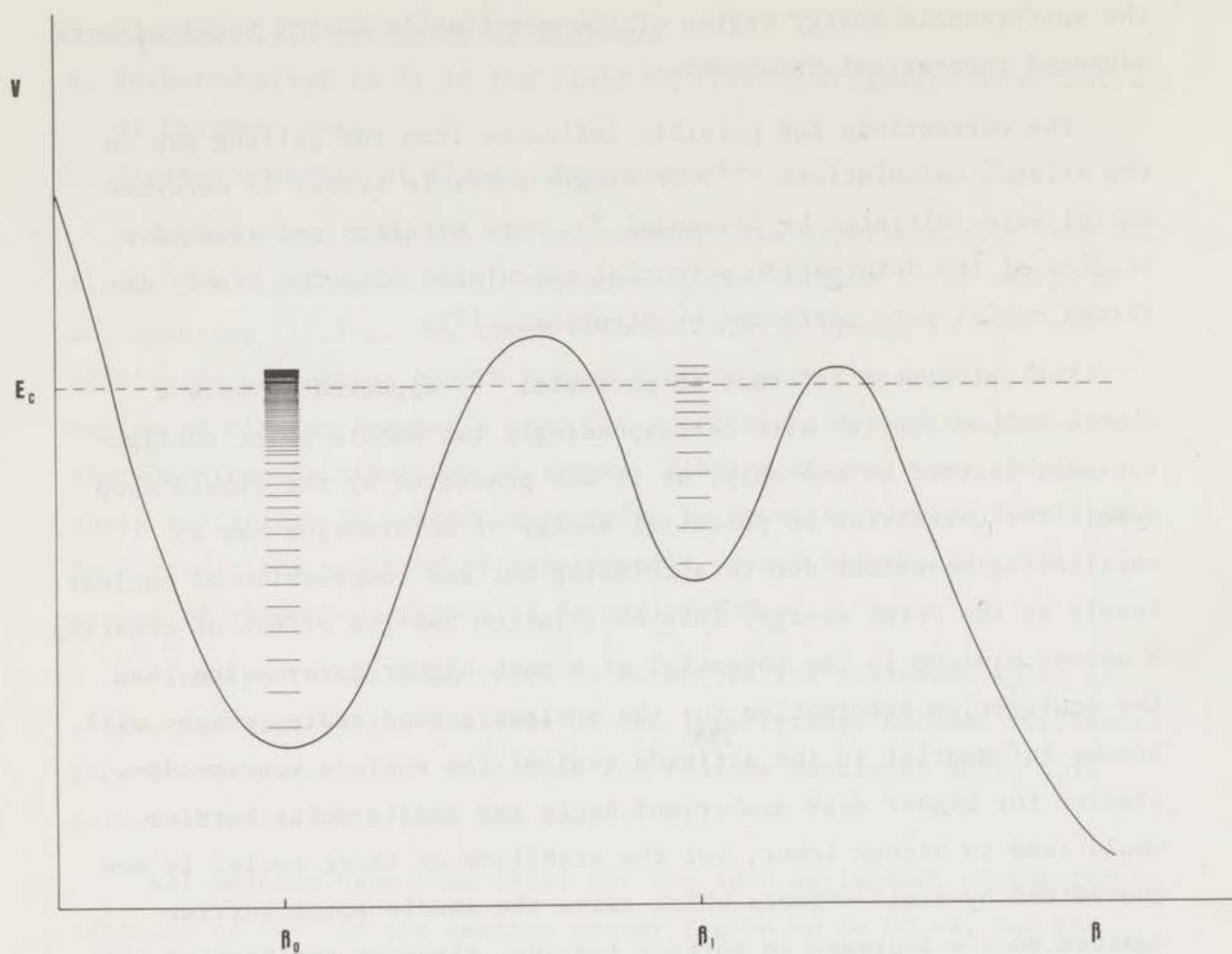


Fig. 1.2.

Double-humped deformation barrier according to the Strutinsky theory; at an energy E_c of the compound nucleus the density of levels in the first vibrational well (β_0) is much greater than the level density in the intermediate well.

intermediate states, may result into a certain group structure in the fission cross section of resonances having a considerably higher fission width than at excitation energies where the coupling between compound and intermediate levels is essentially zero.

The coupling of the compound nuclear levels and intermediate levels is due to the interaction between the β -vibrational mode and the various other modes. The interaction is denoted by a Hamiltonian

section 1.2.

H^i . The result of the coupling are class-I and class-II states, which describe nuclear states which have a total amplitude almost in one potential well, however, with a fractional admixing into the other well. Class-I states are mainly coupled to the neutron entrance channels. On the other hand, class-II states have a much larger fission width. Fission is now feasible by a transition from class-I states to a class-II state where the transition probability is proportional to the admixing of the class-I and class-II states in the neighbouring potential well.

The strength of coupling H^i between compound and intermediate levels can be classified by various conditions.

1. Very weak coupling: $|H^i| \ll D_I$

This case can be treated by ordinary perturbation theory. There will be one resonance which is strongly predominant among its neighbours in the fission cross section. If the fission widths of the unperturbed class-I states ($\Gamma_{\lambda(F)}^I$) are assumed to be negligible in comparison with those of the unperturbed class-II states ($\Gamma_{\mu(F)}^{II}$), then the observed fission widths can be calculated: $\Gamma_{\lambda(F)}$, $\Gamma_{\mu(F)}$; the indices λ and μ refer to compound and intermediate levels respectively.

$$\Gamma_{\lambda(F)} \approx \frac{\langle X_{\lambda}^I | H^i | X_{\lambda}^{II} \rangle^2}{(E_{\lambda}^I - E_{\mu}^{II})^2} \Gamma_{\mu(F)}^{II} \quad (E_{\lambda} \neq E_{\mu}).$$

$$\Gamma_{\mu(F)} \approx \left[1 - \sum_{\lambda \neq \mu} \frac{\langle X_{\lambda}^I | H^i | X_{\mu}^{II} \rangle^2}{(E_{\lambda}^I - E_{\mu}^{II})^2} \right] \Gamma_{\mu(F)}^{II}$$

$$\approx \Gamma_{\mu(F)}^{II} - \sum_{\lambda \neq \mu} \Gamma_{\lambda(F)}$$

$$\Gamma_{\mu(F)}^{II} \approx \sum_{\lambda \neq \mu} \Gamma_{\lambda(F)} + \Gamma_{\mu(F)}$$

2. Weak coupling: $D_I < |H^i| \ll D_{II}$

The fission cross section will now show a group of resonances with large fission widths. The sum of fission widths of the favoured resonances is equal to the fission width of the class-II state. This relation is exactly the same as for the very weak coupling.

The energy dependency of the fission widths for the group of predominant resonances has a behaviour which resembles a Lorentzian distribution. Assuming equally spaced resonances and a uniform coupling H^i for all class-I levels, the pattern of fission widths becomes purely Lorentzian:

$$\Gamma_{\lambda(F)} = \frac{|H^i|^2}{(E_{\mu} - E_{\lambda})^2 + \pi |H^i|^4 / D_I^2}$$

This packet of resonances has a half width:

$$W = \frac{\pi |H^i|^2}{D_I}$$

3. Moderate coupling: $\frac{\pi |H^i|^2}{D_I} \approx D_{II}$

In this situation a clear structure of Lorentzian resonance groups in the fission cross section will not be evident. However, a difference with the situation that compound and intermediate levels are totally coupled, when class-I and class-II states have become identical, can be detected from the statistical distribution of fission widths and from the disturbance of long-range correlations in level spacings.

These deductions for the fission widths in subthreshold fission have been based on the assumption that the fission and neutron widths are considerably smaller than the average level spacings. The spread of the intermediate state over the resonances is then exclusively governed by the coupling strength. When the fission widths of either class-I or class-II states become comparable to the respective level spacings the resonance pattern will change due to resonance interference.

section 1.2.

The situation might arise where the second hump in the deformation is well below the intermediate maximum. At energies just below the second maximum the fission widths for intermediate levels will exceed the average compound level spacing. Very weak coupling between compound and intermediate levels will result in the appearance of quasi-resonances in the fission cross section. This structure is characterized by sharp peaks superimposed on a broad low background hump. Since the latter is experimentally not easily perceived, interference can lead to underestimating the ratio:

$$\frac{2\pi \langle \Gamma_f \rangle}{\langle D \rangle} ,$$

which is the effective number of fission channels.

References

1. A. Bohr, Proc. of 1st Conf. on Peaceful Uses Atomic Energy (Geneva, 1955) 151.
2. D.L. Hill and J.A. Wheeler, Phys. Rev. 89 (1953) 1102.
3. J.A. Wheeler, Fast Neutron Physics, Part II, ed. J.B. Marion and J.L. Fowler (John Wiley and Sons, New York, 1963) 2051.
4. J.E. Lynn, Theory of Neutron Resonance Reactions (Clarendon Press, Oxford, 1968).
5. N. Bohr and J.A. Wheeler, Phys. Rev. 56 (1939) 426.
6. S.G. Nilsson, Mat. Fys. Medd. Dan. Vidensk. Selskab, Bind 29, nr. 16 (1955).
7. B.R. Mottelson and S.G. Nilsson, Mat. Fys. Skr. Dan. Vidensk. Selskab, Vol. 1, nr. 8 (1959).
8. S.A.E. Johansson, Nucl. Phys. 12 (1959) 449.
9. Z. Szymanski, Nucl. Phys. 28 (1961) 63.
10. V.M. Strutinsky, Nucl. Phys. A95 (1967) 420.
11. J.E. Lynn, Structure in Sub-Threshold Fission Modes, report AERE-R 5891 (1968).
12. H. Weigmann, Zeitschr. für Phys. 214 (1968) 7.

section 1.3.

1.3. The hyperfine splitting of heavy actinide nuclei in the RUN-
compound

1.3.1. ^{233}U and ^{235}U

The hyperfine interactions of these two nuclei in the chemical compound $\text{RbUO}_2(\text{NO}_3)_3$ is rather uncertain not only in the values of the parameters describing the interaction, but also in the type of interaction involved. There are a few discrepancies in the published data on the hyperfine splitting in RUN. By most investigators the interaction is assumed to be pure electric-quadrupole coupling with cylindrical symmetry. An evaluation of the available information will be given below. Summarizing this information, it seems very worthwhile to obtain results from independent methods for the determination of the values of the hyperfine-splitting constants.

In the rhombohedral crystal structure of RUN the uranyl-groups (UO_2^{++}) are all parallel to the c-axis of the crystal. Studies were done on X-ray structure determinations and infrared spectroscopy of several chemical compounds containing uranyl-like groups (XO_2^{++}) from the series of actinide elements ^{1,2,3}). It was concluded that the XO_2 -groups were essentially linear, although experimental evidence was not entirely decisive ⁴). Measurements of the bond length ^{5,6}) in the XO_2 -groups led to the assumption that the bond should be covalent ⁴).

In the periodic system the electrons commence to occupy the 5f-shell in the neighbourhood of uranium, which makes the electron structure considerably more complicated. The 5f-shell is shielded less than other shells. Small energy differences with the other shells give an uncertainty in occupation of the available states. Eisenstein and Pryce ⁴) regard a simple model for the construction of a ground state of the UO_2^{++} -ion. Since in this uranyl-ion there are no unpaired electrons its behaviour will be either diamagnetic or feebly paramagnetic. Therefore magnetic-dipole coupling will be a negligible term in the spin Hamiltonian. As to electric-quadrupole coupling the quantity q , defined in section 1.1.3 as the expectation value of $P_2(\cos\theta)r^{-3}$ for the electrons, is tentatively estimated to be positive,

considering the relatively large contribution of 6d-orbitals in comparison with 5f, although the situation might be affected by core shielding (Sternheimer effect).

By paramagnetic resonance of UCl_3 on ^{235}U and ^{233}U Dorain et al.⁷⁾ measured the ratio of the quadrupole moments of the two nuclei:

$|Q_{235}| / |Q_{233}| = 1.17 \pm 0.20$, leaving the signs undetermined. The values from determination by Kaliteevski et al.⁹⁾ and Van der Sluis et al.¹⁰⁾ recalculated by Roberts et al.⁸⁾ agreed with this ratio within the limits of error.

The specific-heat measurements by Roberts et al.¹¹⁾ yielded a value for the quadrupole-coupling constant of ^{235}U $|P/k| = 0.0216$ K, which initially was assigned to be negative¹²⁾.

From systematic behaviour of the quadrupole moments of nuclei in the neighbourhood of the uranium isotopes it seemed likely that ^{235}U and ^{233}U both have positive quadrupole moments, corresponding to prolate nuclei. Nuclear theory by Hill and Wheeler¹³⁾ predicted that for this form of the nucleus α -emission was expected to be very favourable at the poles of the spheroid since the α -barrier would be much thinner at the poles than at the equator.

A conflict situation arose when the anisotropy in the α -emission from ^{233}U aligned in RUN, was measured at low temperatures⁸⁾. The result was that the product of A_2 and f_2 in the formula for the angular distribution was negative:

$$W(\theta) = 1 - \frac{(0.0625 \pm 0.0025)}{T} P_2(\cos\theta).$$

If it was assumed that the considerations by Pryce and Eisenstein⁴⁾ about the positive value of q were correct, then, for a positive quadrupole moment, resulting in a negative P -value and a positive value for the f_2 -parameter, the anisotropy in the α -emission would be interpreted as a favoured emission from the equator of the prolate nucleus, which is in contradiction with the theory by Hill and Wheeler. The other possibility was the assumption of a negative quadrupole

section 1.3.

moment, but this did not agree with nuclear systematics.

The α -decay of ^{233}U was studied theoretically by Chasman and Rasmussen ¹⁴), by which it was tried to make a determination of the mixing ratio and relative phase of S- and D-waves in the α -decay. From this admixing the A_2 -value can be calculated, using the explicit formulae given in section 1.1.2 of this chapter. The decay scheme of ^{233}U is given in fig. 1.3. The results of the numerical integrations

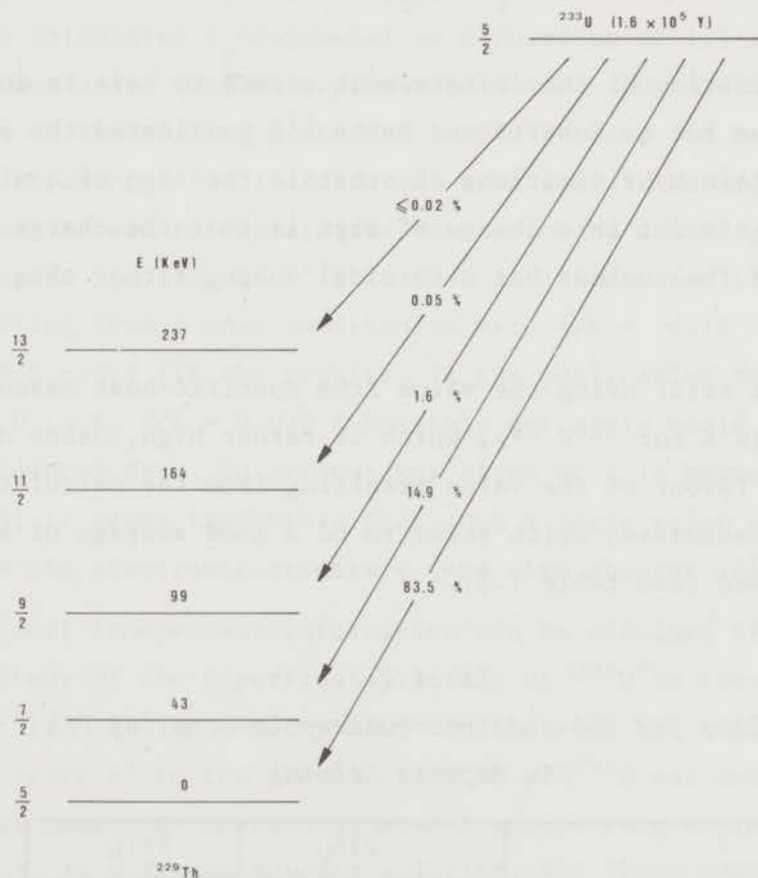


Fig. 1.3.
Alpha-decay of ^{233}U .

to obtain the S- and D-wave amplitudes, seemed to agree with nuclear theory; furthermore, applied to Dabbs' experimental value ⁸), mentioned above, a value for the quadrupole coupling constant of ^{233}U resulted:

$P/k = + 0.0277$ K, if the D-wave part of the decay was assumed to be in phase with the S-wave part and a value $P/k = - 0.0418$ K, if the S- and D-waves were out of phase.

Similar calculations on the relative phases and amplitudes of S- and D-waves were done by Salusti ¹⁵⁾. Dabbs et al.¹⁶⁾ derived a value $P/k = + 0.0221$ K for ^{233}U from these results, however using an experimental angular distribution:

$$W(\theta) = 1 - \frac{0.064}{T} P_2(\cos\theta) .$$

An explanation of the disagreement seemed to have to encounter a positive value for q . Roberts and Dabbs ¹⁷⁾ considered the possibilities that for certain hybridizations of orbitals the sign of q might change. The requirements for this change of sign is that the charge distribution around the nucleus has a toroidal shape, rather than a cigar shape.

At first still using the value from specific-heat measurement $P/k = + 0.0216$ K for ^{235}U ¹⁶⁾, which is rather high, Dabbs decided later ¹⁸⁾ in favour of the value resulting from the calculations by Chasman and Rasmussen, which seems to be a good average of all the values reviewed (see table 1.3).

Table 1.3.
Values for the electric-quadrupole coupling P/k
(in degrees Kelvin)

	^{235}U	^{233}U
Roberts ¹¹⁾	0.0216	0.0389
Chasman ¹⁴⁾ Dabbs ¹⁴⁾	0.0154	0.0277
Salusti ¹⁵⁾ Dabbs ¹⁶⁾	0.0123	0.0221
Ruby ²⁰⁾ present work	0.0205	0.0369

section 1.3.

The measurements of Dabbs et al. on α -anisotropy of ^{235}U and ^{233}U had always been done in the temperature region where the orientation parameter f_2 is inversely proportional to T ; the cooling methods were incapable of going down to temperatures where a deviation can be observed from the linearity of $W(\theta)-1$ versus $1/T$.

Matvienko ¹⁹⁾ cooled RUN-crystals with a coating of ^{233}U down to temperatures as low as 0.05 K. The measured curve of anisotropy vs. $1/T$ does not conform with the expected behaviour. At high temperatures the curve is linear with $1/T$, but saturates already at about $1/T = 5$, whereas the calculated f_2 -parameter as a function of $1/T$ would reach its saturation value only at approximately $1/T = 30$. A difference in temperature of the cooling plate and sample surface did not seem sufficient to account for the abnormal behaviour in an adequate way. It was tried instead to explain the saturation by assuming a sizeable magnetic-dipole coupling of ^{233}U in RUN. An orientation parameter $f_2(T)$ resulting from a spin Hamiltonian with $A/k = -0.16$ K and $P/k = 0.028$ K could fit the results. In the publication the authors give $A/k = 0.16$ K, $P/k = 0.028$ K but this certainly would not agree with the measured data. No account was given of this magnetic-dipole interaction; it seems improbable that such a large value of A/k would result from the electronic structure (see also chapter III, section 4).

Additional independent information can be obtained from a γ -ray resonance study of the hyperfine splitting of $^{238}\text{U}^*$ in several uranium compounds ²⁰⁾. In the α -decay of ^{242}Pu the 44.7 keV γ -line from the rotational level 2^+ to the ground state 0^+ of ^{238}U was measured. The two chemical compounds containing uranyl-groups were $\text{UO}_2(\text{NO}_3)_2 \cdot 6\text{H}_2\text{O}$ and $\text{UO}_2(\text{NO}_3)_2$ in a frozen aqueous solution. For these compounds the results are: $e^2qQ = -6100 \pm 225$ and -6800 ± 340 MHz, averagely equivalent to $e^2qQ = -0.293 \pm 0.001$ K. If it is assumed that the intrinsic quadrupole moments Q_0 of ^{238}U in the 2^+ 44.7 keV level and ^{235}U in the ground state are equal then, from the subsequent formulae in section 1.1.3 of this chapter, the P -value for ^{235}U can be derived:

$$\frac{(e^2qQ)_{235}}{(e^2qQ)_{238}} = \frac{\left\{ \frac{3K^2 - I(I+1)}{(I+1)(2I+3)} \right\}_{235}}{\left\{ \frac{3K^2 - I(I+1)}{(I+1)(2I+3)} \right\}_{238}},$$

$$P = -\frac{3e^2Qq}{4I(2I-1)}.$$

From $(I^\pi, K) = (2^+, 0)$ for ^{238}U in the 44.7 keV level and $(I^\pi, K) = (\frac{7^-}{2}, \frac{7}{2})$ for ^{235}U in the ground state, it follows that for ^{235}U $P/k = +0.0205$ K. This value would tend to confirm the value from Dabbs' specific-heat measurements, rather than the calculations by Salusti and Chasman and Rasmussen, but it has to be considered that the intrinsic quadrupole moments of the two isotopes may be somewhat different.

In table 1.3 a summary of this evaluation is given, by presenting the P-values resulting from the various experiments and calculations; the values refer to either of ^{233}U and ^{235}U , directly or obtained by using the ratio of quadrupole moments from Dorain et al. ⁷):

$$\frac{|Q_{235}|}{|Q_{233}|} = 1.17 \pm 0.20$$

$$\frac{|P_{235}|}{|P_{233}|} = 0.557 \pm 0.095$$

1.3.2. ^{237}Np

An evaluation of the hyperfine-splitting constants for ^{237}Np in $\text{Rb NpO}_2(\text{NO}_3)_3$ is hardly necessary, since there has been one measurement of the parameters which was sufficiently accurate to yield correct estimates for the orientation parameter f_2 , although initially, analogous to the uranium isotopes, some doubt existed about the signs of the constants.

Compared to the UO_2^{++} -ion, NpO_2^{++} has one more electron which is in the 5f-shell. This is the cause of a magnetic field at the location of the ^{237}Np nucleus and therefore of a magnetic-dipole coupling term

section 1.3.

in the effective-spin Hamiltonian. Bleaney et al.²¹⁾ determined the values of the various parameters by the paramagnetic resonance technique:

$$\begin{aligned} A &= \pm 0.166 \pm 0.002 \text{ cm}^{-1} \quad , \\ |B| &= 0.02 \pm 0.02 \text{ cm}^{-1} \quad , \\ P &= \mp 0.030 \pm 0.002 \text{ cm}^{-1} \quad . \end{aligned}$$

Actually, the explicit signs of A and P could not be determined; experimentally it resulted only that the signs were opposite. The considerations by Eisenstein and Pryce⁴⁾ on the electronic structure of the linear NpO_2^{++} -ion indicated that the quadrupole-coupling constant might be negative and hence, A would be positive.

The anisotropy in the α -emission from aligned ^{237}Np nuclei in RNN, measured by Roberts et al.²²⁾, pointed out that the sign of P as given by Pryce did not conform with the theory of Hill and Wheeler¹³⁾, analogous to the situation of ^{235}U and ^{233}U in RUN. Pryce²³⁾ revised the earlier considerations, in which basic wave functions were constructed so that $g_{//}$ was positive, but according to symmetry arguments, this should have been negative. Therefore the signs of A and P became negative and positive respectively. The accuracy of the hyperfine-splitting parameters was improved, as can be seen from the values given in table 1.4. However, the picture of electronic structure in the vicinity of the nucleus was retained. Herewith it was postulated by Pryce that the quadrupole moment of ^{237}Np should be negative, but this again is in contradiction with nuclear systematics.

In the meantime, the measurements on the anisotropy in α -emission from aligned ^{237}Np had been extended to lower temperatures²⁴⁾. The temperature dependency pointed out unambiguously that the combination of negative A and positive P was correct. These results were compared with theoretical expectations for the mixing of S- and D-waves for the α -decay of ^{237}Np ²⁵⁾. The experimental value for the anisotropy coefficients is slightly outside the range of theoretical values, probably because the S- and D-wave amplitudes were not chosen correctly, but agrees with the situation where S- and D-waves are in phase.

Similar to ^{235}U and ^{233}U , Roberts and Dabbs ¹⁷⁾ considered the possibilities that for NpO_2^{++} the electronic-charge distribution might be different from the suggestions of Eisenstein and Pryce ⁴⁾, e.g. a toroidal shape instead of a cigar-like shape, by which the value of q might become negative.

A positive quadrupole-coupling constant was independently confirmed by Mössbauer measurements by Dunlap et al. ²⁶⁾ on the 59.6 keV γ -ray transition in ^{237}Np following the α -decay of ^{241}Am . The values obtained were: $|A| = 0.127 \text{ cm}^{-1}$ and $P = + 0.025 \text{ cm}^{-1}$, for the neptunyl compound $\text{K}_3\text{NpO}_2\text{F}_5$. It is interesting that a small asymmetry term was found in the electric-quadrupole interaction. A strong argument for a positive quadrupole moment of the ground state of ^{237}Np is that these Mössbauer experiments showed the sign of Q for both levels to be equal, since the 59.6 keV level has the same Nilsson configuration as the ground state of ^{241}Am for which a quadrupole moment of +4.9 b was quoted in ref ²⁷⁾.

Table 1.4.

Hyperfine-splitting constants for ^{237}Np
in $\text{RbNpO}_2(\text{NO}_3)_3$ (ref.23)

$g_{//}$	=	$- 3.405 \pm 0.008$
$ g_{\perp} $	=	0.205 ± 0.006
A	=	$- 0.16547 \pm 0.00005 \text{ cm}^{-1}$
$ B $	=	$0.01782 \pm 0.00003 \text{ cm}^{-1}$
P	=	$0.03015 \pm 0.00005 \text{ cm}^{-1}$

References

References

1. J.L. Hoard and J.D. Stroupe, Chemistry of Uranium, USAEC, TID-5290 (1954), Book 1, 323.
2. G.H. Dieke and A.B.F. Duncan, Spectroscopic Properties of Uranium Compounds (Mc Graw-Hill Book Company Inc., New York, 1949), 1st ed., 33.
3. L.H. Jones and R.A. Penneman, Jrn. Chem. Phys. 21 (1953) 542.
4. J.C. Eisenstein and M.H.L. Pryce, Proc. Royal Phys. Soc., London, A229 (1955) 20.
5. W.H. Zachariassen, Acta Cryst. 1 (1948) 281.
6. R.L. Elliott, Phys. Rev. 89 (1953) 659.
7. P.B. Dorain, C.A. Hutchison Jr. and E. Wong, Phys. Rev. 105 (1957) 1307.
8. L.D. Roberts, J.W.T. Dabbs and G.W. Parker, Proc. of 2nd Conf. on Peaceful Uses of Atomic Energy (1959) 322.
9. N.I. Kaliteevsky and M.P. Chaika, Bull. Leningrad Univ. 11 (1955) 121.
10. K.L. Van der Sluis and J.R. McNally, Jrn. Opt. Soc. America 44 (1954) 87.
11. L.D. Roberts, J.W.T. Dabbs and G.W. Parker, Semiann. Progr. Report (1956) ORNL-2204, 60.
12. L.D. Roberts, J.W.T. Dabbs and G.W. Parker, Semiann. Progr. Report (1957) ORNL-2430, 51.
13. D.L. Hill and J.A. Wheeler, Phys. Rev. 89 (1953) 1102.
14. R.R. Chasman and J.O. Rasmussen, Phys. Rev. 115 (1959) 1257.
15. E. Salusti, Nuovo Cimento 30 (1963) 171.
16. J.W.T. Dabbs, F.J. Walter and G.W. Parker, Report ORNL-3425 (1963) 82.
17. L.D. Roberts and J.W.T. Dabbs, Phys. Ann. Progr. Report (1960) ORNL-2910, 62.
18. J.W.T. Dabbs, F.J. Walter and G.W. Parker, Physics and Chemistry of Fission (IAEA, Vienna, 1965) Vol.I, 39.
19. V.I. Matvienko, A.V. Kogan and K.A. Petrzhak, Sov. Jrn. of Nucl. Phys. 7 (1968) 297.

20. S.L. Ruby, G.M. Kalvius, B.D. Dunlap, G.K. Shenoy, D. Cohen, M.B. Brodsky and D.J. Lam, Phys. Rev. 184 (1969) 374.
21. B. Bleaney, P.M. Llewellyn, M.H.L. Pryce and G.R. Hall, Phil. Mag. 45 (1954) 992.
22. L.D. Roberts, J.W.T. Dabbs, H. Postma, G.W. Parker, R.D. Ellison, Phys. Progr. Report (1955) ORNL-1975, 45.
23. M.H.L. Pryce, Phys. Rev. Letters 3 (1959) 375.
24. S.H. Hanauer, J.W.T. Dabbs, L.D. Roberts and G.W. Parker, Phys. Ann. Progr. Report (1960) ORNL-2910, 56.
25. S.H. Hanauer, J.W.T. Dabbs, L.D. Roberts and G.W. Parker, Phys. Rev. 124 (1961) 1512.
26. B.D. Dunlap, G.M. Kalvius, S.L. Ruby, M.B. Brodsky and D. Cohen, Phys. Rev. 171 (1968) 316.
27. T.E. Manning, M. Fred, F.S. Tomkins, Phys. Rev. 102 (1956) 1108.

section 1.4.

1.4. Absorption and scattering of fission fragments

The scattering of fission fragments is a possible systematic error in the measured angular distribution. Substantial scattering over large angles will tend to reduce the measured anisotropy in the angular distribution and as a result of this A_2 -values will be underestimated. It is important to make an estimate of this effect from the known range-energy relations for fission fragments in several materials.

The theory for range-energy relations has been developed especially by Bohr ¹⁾. The slowing-down process for fission fragments is split up into two separate mechanisms for the energy dissipation of incident fission fragments in matter. At higher energies Coulomb interaction between electrons and the highly charged fission fragment is acting as a continuous friction as the fission fragment moves through the material. Deviations from the original direction of the particle are small because of the continuous character of this force. This mechanism is dominant at higher energies. At lower energies nuclear scattering becomes more important and by this process fission fragments suffer large deflections if the mass of the nuclei in the material is comparable to the fragment. The critical speed v_c at which nuclear scattering becomes important is given by the formula:

$$\frac{1}{2} M_1 v_c^2 = \frac{2 Z_1 Z_2 e^2}{a_0} \frac{M_1 + M_2}{M_2} \left\{ Z_1^{\frac{2}{3}} + Z_2^{\frac{2}{3}} \right\}^{\frac{1}{2}},$$

in which Z_1 and Z_2 are atomic numbers of the stopper and stopping nuclei, e is the electronic charge and a_0 is the first Bohr radius: $a_0 = 0.529 \times 10^{-8}$ cm.

A more advanced theory was proposed by Lindhard, Scharff and Schiott ²⁾ (LSS), which also considers electronic and nuclear stopping as uncorrelated processes. It refers especially to the energy region where the two processes are competitive. The nuclear stopping is studied with several potentials for nuclear interaction, simple power potentials, for instance Coulomb interaction, and screened potentials. From the differential scattering cross section a nuclear stopping power can be calculated.

Energy losses are represented in a universal formula with dimensionless parameters ϵ and ρ for the energy (E) and the range (R) respectively:

$$\epsilon = E \frac{a M_2}{Z_1 Z_2 e^2 (M_1 + M_2)} ,$$

$$\rho = R N M_2 4\pi a^2 \frac{M_1}{(M_1 + M_2)^2} ,$$

$$a = \frac{c a_0}{(Z_1^{2/3} + Z_2^{2/3})^{1/2}} .$$

If the range R is expressed in mg/cm², then the constant N is Avogadro's number divided by 1000: $N = 6 \times 10^{20}$; a is the screening parameter and a_0 is the first Bohr radius; in Bohr's treatment the constant c is 1, in LSS-theory 0.8853.

Electronic stopping is governed by a stopping power, which is proportional to the velocity. The relation can be expressed in dimensionless parameters:

$$\frac{d\epsilon}{d\rho} = k\epsilon^{1/2} ,$$

in which the constant k is usually between 0.1 and 0.2. The extrapolated electronic range which is the range in absence of nuclear stopping, is:

$$\rho_e(\epsilon) = \frac{2}{k} \epsilon^{1/2} .$$

The observed range is reduced by the nuclear stopping power and can be written as:

$$\rho(\epsilon) = \rho_e(\epsilon) - \Delta(k, \epsilon) ,$$

in which $\Delta(k, \epsilon)$ is the correction on the electronic range for the nuclear stopping.

section 1.4.

The discontinuous character of nuclear stopping, which becomes important if the nuclei in the stopping material have masses which are comparable to the fission-fragment mass, will induce a certain range straggling³⁾. The range has statistically a gaussian distribution, centered at the mean range value R_0 :

$$P(R) = \frac{1}{\sqrt{2\pi} \sigma R_0} \exp \left[-\frac{(R-R_0)^2}{2 \sigma R_0^2} \right].$$

The range-straggling parameter is:

$$\sigma = \sqrt{3M_1M_2} / 2(M_1+M_2).$$

Cloud chamber experiments by Bøggild et al.⁴⁾ revealed tracks of fission fragments in gases. From the photographs it was obvious that range straggling became rather important towards the end of the track.

The majority of the later theoretical treatment and interpretations of experiments concerning penetrations of fission fragments is based on LSS-theory. Since the main interest here is to estimate the energy losses of fission fragments and the deflections from the original direction of emission, it will be investigated at which energy nuclear scattering becomes important in case of fission fragments transmitted through $\text{RbUO}_2(\text{NO}_3)_3$ and to which degree the angular distribution is disturbed for fission fragments with energies above the discriminator level for the detection of the fission fragments.

Recoil properties of fission products from thermal fission of ^{235}U in aluminium and gold metal were measured by Alexander and Gazdik⁵⁾. A range-energy relation could be fitted by formulae:

$$\rho = k' \epsilon^{\frac{1}{2}} - \Delta$$

or
$$\rho = k'' \epsilon^{\frac{2}{3}}.$$

Self-absorption by target material, which in this case was ^{235}U sprayed onto thin Al-foils could be expressed as an effective stopping power which was 1.4 times the value for pure Al. Bohr's theory would predict about 0.5 for this factor but target inhomogeneities might account for the increase. This ratio was less for the relatively heavier catcher Au. Values for k' , k'' and Δ are presented in table 1.5 for Al and Au, in which M_2 denotes the mass number of the fission fragments; Δ is given separately for the heavy and light fission-fragment groups (HFF and LFF).

Table 1.5.
Range-energy parameters for fission fragments ⁵⁾

	Al	Au
$k' (\text{mg}/\text{cm}^2 \text{MeV}^{\frac{1}{2}})$	$2.84 \cdot 10^{-3} M_1 + 3.206$	$7.28 \cdot 10^{-3} M_1 + 7.91$
$\Delta (\text{mg}/\text{cm}^2)$ (LFF)	1.0	~ 1.3
(HFF)	0.5	~ 0.9
$k'' (\text{mg}/\text{cm}^2 \text{MeV}^{\frac{2}{3}})$	0.19	0.51

Similar experiments on ranges in metallic uranium are reported by Niday ⁶⁾, for which results good theoretical fits are obtained in terms of the LSS-theory, with special adjustment of charge screening. Ranges vary from 7 mg/cm^2 to 11.5 mg/cm^2 over the mass range 75 to 155.

In a semi-empirical treatment by Izui ⁷⁾ of range-energy relations in which a simplified Rutherford approximation was used the relative contributions of electron and nuclear stopping power were calculated. For fission fragments interacting with gold metal, which is resembling the case of uranium rather well, the relative contributions are equal for light fragments at approximately 5 MeV and for heavy fragments at 9 MeV. Recalculated for uranium the range-energy relation would predict that for light fragments the minimum energy to traverse a uranium thickness of 1 mg/cm^2 is 4 MeV, while this is 8 MeV

section 1.4.

for heavy fragments. The conclusion from these investigations is that at an energy level of 15 to 20 MeV nuclear scattering is still not very important. Furthermore, the average energy loss for fission fragments having their initial kinetic energies, transmitted through a target thickness of 2 mg/cm² of uranium, is 20 and 25 MeV for heavy and light fragments respectively.

Experiments on multiple and plural scattering ⁸⁾ of light fission fragments from thermal fission of uranium in foils of thicknesses in the order of 1 mg/cm² (e.g. Au) revealed a narrow angular distribution with a FWHM of 1° to 2°. The results could be explained by specially screened potentials. Although these investigations were done with light fragments, and heavy fragments on the average suffer somewhat larger deflections, scattering over angles of this order would not have any effect on the anisotropy measurements, because these deflections are negligible compared to the solid angle of the detectors

Another investigation ⁹⁾ on range-energy relations, using surface-barrier detectors to measure energies of emitted fission fragments, gave very accurate results confirming the previously mentioned values and interpretations. The experimental range-energy relation in terms of the dimensionless LSS-parameters is:

$$k\rho = 1.158\epsilon^{\frac{1}{2}} [1 - \exp(0.0987\epsilon)] + 0.01939\epsilon ,$$

$$k = \frac{0.0793 Z_1^{\frac{2}{3}} Z_2^{\frac{1}{2}} (M_1 + M_2)^{\frac{3}{2}}}{(Z_1^{\frac{2}{3}} + Z_2^{\frac{2}{3}})^{\frac{3}{4}} M_1^{\frac{3}{2}} M_2^{\frac{1}{2}}} .$$

This relation between $k\rho$ and ϵ has been plotted in fig. 1.4. The ratios ϵ/E and ρ/R were calculated as a function of mass and charge of the stopping material for median heavy and light fission fragments separately.

The results are shown in figs. 1.5 and 1.6 respectively.

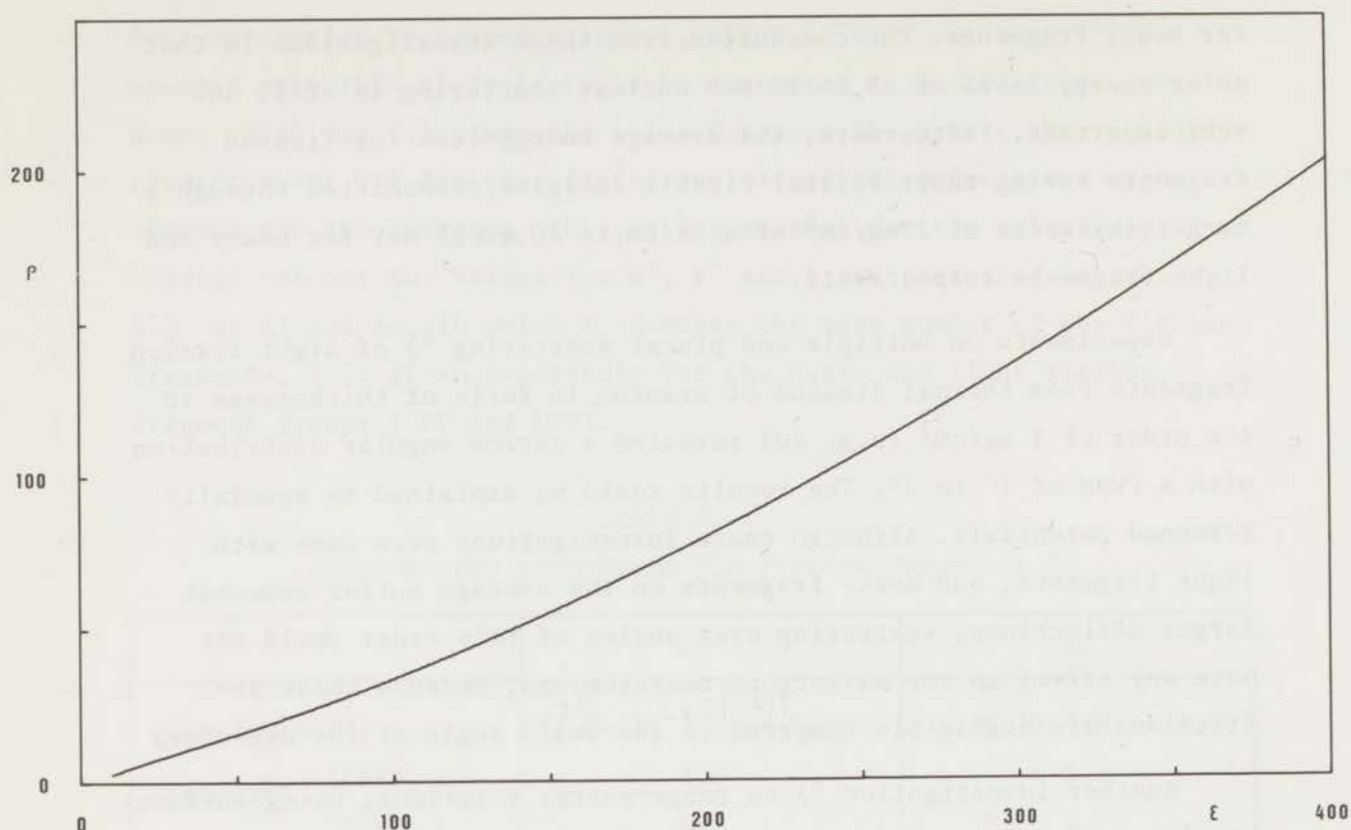


Fig. 1.4.

Range-energy relation for fission fragments expressed in the dimensionless LSS parameters ρ and ϵ ; the curve represents the range values as determined by Kahn and Forgue (ref.⁹).

The crystal $\text{Rb UO}_2(\text{NO}_3)_3$ contains widely varying nuclei and therefore the decrease in velocity as the fission fragment passes the atomic matter cannot be described in a straightforward way by one of the formulae given above. Although heavy elements have more stopping power than light elements, the effective ranges expressed in mg/cm^2 are smaller for the light than for the heavy elements. On the other hand nuclear scattering becomes sooner important for the heavy than for the light elements. A target thickness (t) is increased effectively to a thickness t_{eff} corresponding to the angle of detection of fission fragments. In the experiments presently described the angle of emission of fission fragments is approximately 45° : $t_{\text{eff}} = 1.414 t$.

section 1.4.

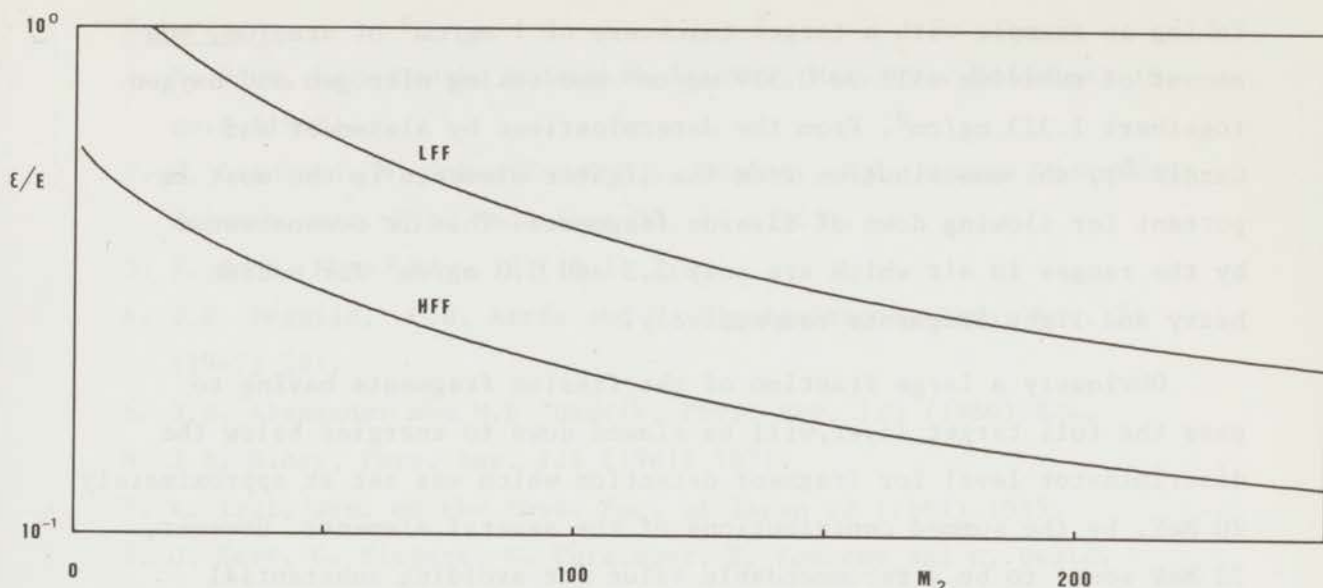


Fig. 1.5.

Ratio of the dimensionless energy ϵ and the energy of the fission fragments in MeV as a function of the mass parameter M_2 of the stopping material for median light fragments (LFF) and median heavy fragments (HFF); the scale of ϵ/E is logarithmic.

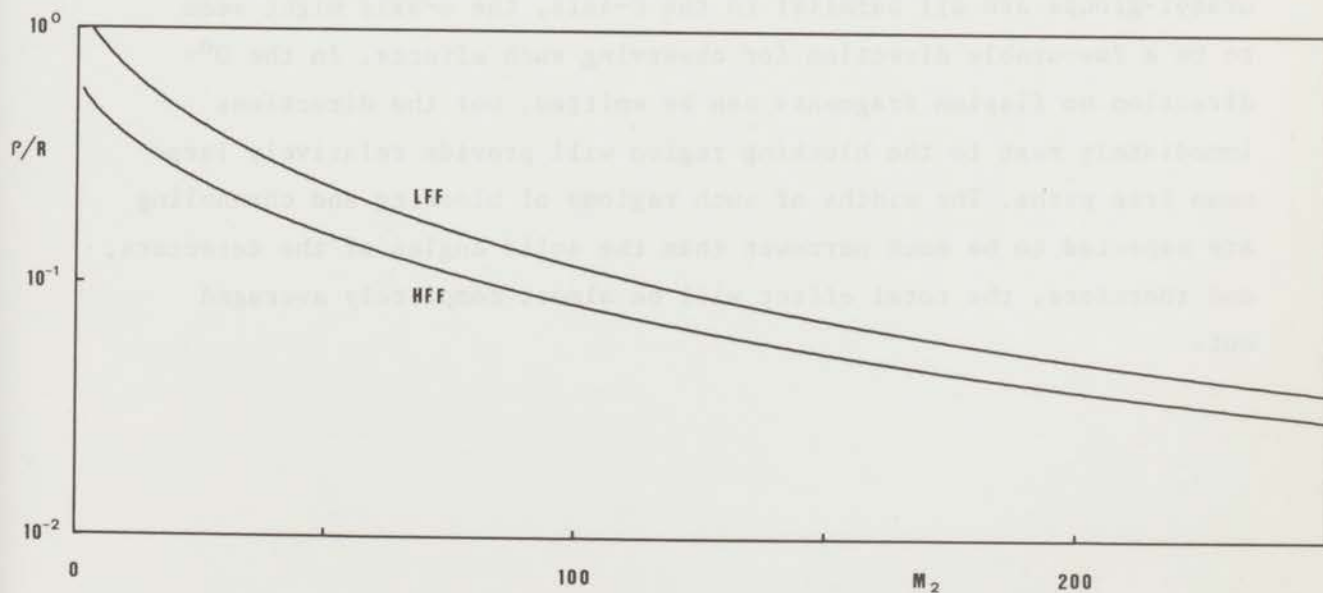


Fig. 1.6.

Ratio of the dimensionless range ρ and the range R expressed in mg/cm^2 as a function of M_2 for median light and heavy fragments; the scale ρ/R is logarithmic.

Taking an example with a target thickness of 1 mg/cm^2 of uranium, the amount of rubidium will be 0.519 mg/cm^2 and taking nitrogen and oxygen together: 1.323 mg/cm^2 . From the determinations by Alexander and Gazdik ⁵⁾, the contribution from the lighter elements is the most important for slowing down of fission fragments. This is demonstrated by the ranges in air which are only 2.3 and 3.0 mg/cm^2 for median heavy and light fragments respectively.

Obviously a large fraction of the fission fragments having to pass the full target layer will be slowed down to energies below the discriminator level for fragment detection which was set at approximately 20 MeV, by the summed contributions of the several elements. However, 20 MeV seems to be a recommendable value for avoiding substantial nuclear scattering.

Finally, there is one factor arising from the discontinuous and anisotropic character of the crystal structure: blocking and channeling of fission fragments may favour certain directions of emission, due to possible clear ways in the crystal. Owing to the fact that the uranyl-groups are all parallel to the c-axis, the c-axis might seem to be a favourable direction for observing such effects. In the 0° -direction no fission fragments can be emitted, but the directions immediately next to the blocking region will provide relatively large mean free paths. The widths of such regions of blocking and channeling are expected to be much narrower than the solid angles of the detectors, and therefore, the total effect will be almost completely averaged out.

References

References

1. N. Bohr, Kgl. Danske Videnskab. Selskab, Mat.-Fys. Meddelser 18, no.8 (1948).
2. J. Lindhard, M. Scharff and H.E. Schiott, Kgl. Danske Videnskab. Selskab, Mat.-Fys. Meddelser 33, 14 (1963).
3. N. Bohr, Phys. Rev. 59 (1941) 270.
4. J.K. Bøggild, O.H. Arrøe and T. Sigurgeirsson, Phys. Rev. 71 (1947) 281.
5. J.M. Alexander and M.F. Gazdik, Phys. Rev. 120 (1960) 874.
6. J.B. Niday, Phys. Rev. 121 (1961) 1471.
7. K. Izui, Jrn. of the Phys. Soc. of Japan 22 (1967) 1015.
8. D. Kerr, G. Siegert, K. Kürzinger, E. Konecny and H. Ewald, Zeitsch. Naturforsch. 22a (1967) 1799.
9. S. Kahn and V. Forgue, Phys. Rev. 163 (1967) 163.

Chapter II

EXPERIMENTAL ARRANGEMENT AND CALCULATIONS

2.1. Experimental geometry

From the theoretical formula for the angular distribution,

$$W(\theta) = 1 + \sum_{k=2,4,6,\dots} A_k f_k P_k(\cos\theta) ,$$

a relevant expression has to be derived which is suitable for calculations on the experimental data. A geometrical integration has to be applied on the Legendre-polynomials $P_k(\cos\theta)$ according to size and position of the sample and the detectors. The averaged polynomial can be determined by integrations over the solid angle of detector towards sample (Ω_d) and over the sample area (S_s):

$$\langle P_k(\cos\theta) \rangle = \frac{\int_{S_s} \int_{\Omega_d} P_k(\cos\theta) d\Omega dS}{\int_{S_s} \int_{\Omega_d} d\Omega dS} .$$

In considering the geometry for sample and detectors, the experimental situation was far from ideal. From the point of required counting statistics a large sample was needed with an area comparable to the $5 \times 5 \text{ cm}^2$ neutron beam and for the same reason also the solid state detectors had to be a fair size. A picture of samples and detectors with respect to the neutron beam for the experiments at Harwell is given in fig. 2.1 and in fig. 2.2 for those at Petten. The samples used for the measurements at Harwell were mostly consisting of a mosaic of about 25 crystals, covering approximately a circular area with a diameter of 4.5 to 5.0 cm. The sensitive area of the diffused-junction detectors was 4 cm^2 . During the last stage of the experiment detectors were used having a surface area of 2 cm^2 . The detectors were all mounted around the sample on a cylindrical frame, as shown in fig. 2.1, at a distance of 4.6 cm to the central axis of the assembly. The distance of the centre of the detectors to the horizontal plane

section 2.1.

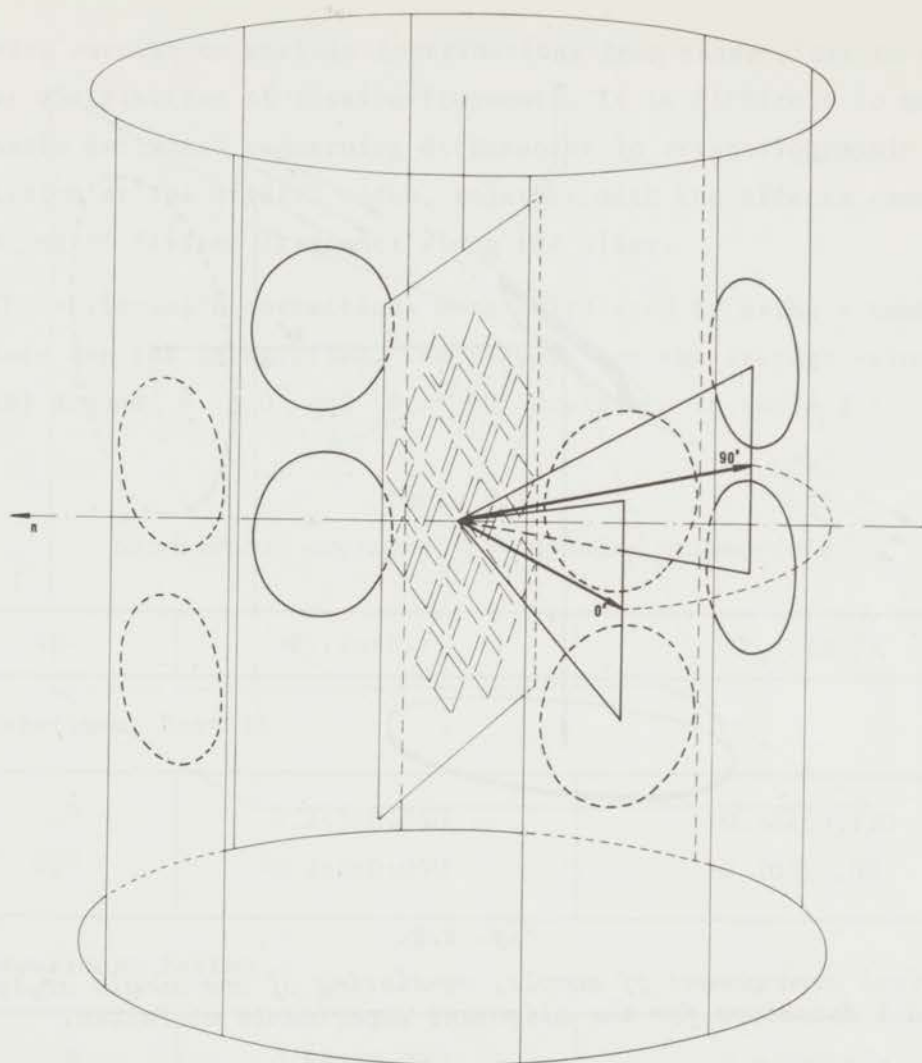


Fig. 2.1.

Geometrical arrangement of sample and detectors for the alignment experiments at Harwell. RUN-crystals are attached to either side of the cooling plate. Each side is viewed by 4 diffused-junction detectors.

through the centre of the sample is 1.45 cm. It is actually this distance which provides effectively the greatest correction on the Legendre polynomials.

In the experiments at Petten only single crystals have been used. These crystals were all approximately square and had a surface area of 0.8 to 1.2 cm². The detectors had a smaller sensitive area than the

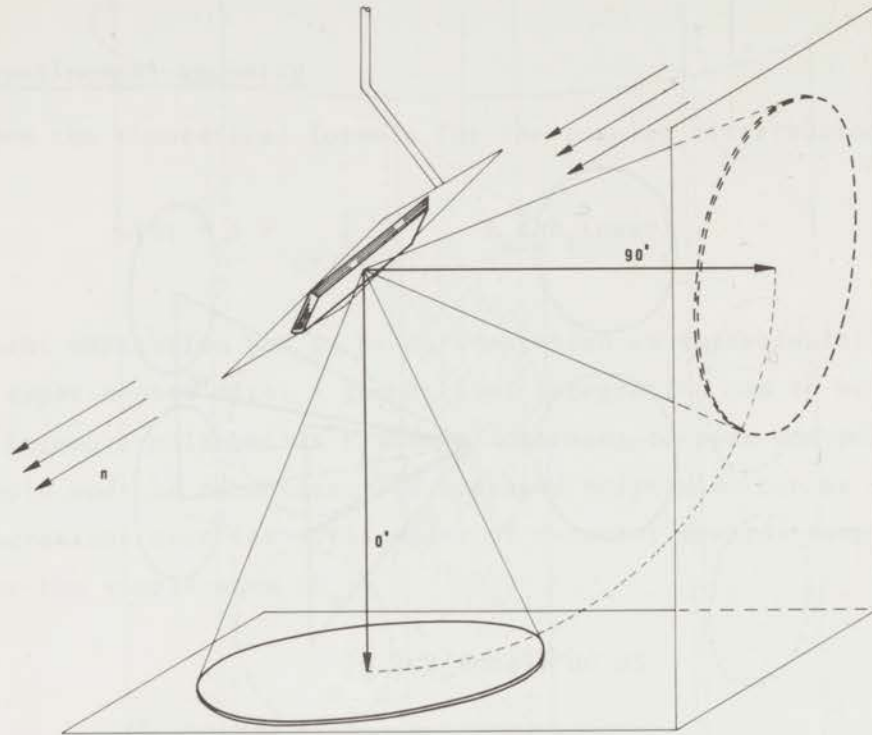


Fig. 2.2.

Geometrical arrangement of sample, consisting of one single crystal of RUN, and 2 detectors for the alignment experiments at Petten.

ones at Harwell: 1.5 cm^2 . One of these detectors was mounted in the direction of the c-axis of the crystal at a distance of 3.0 cm, while the other was perpendicular to the c-axis.

For all calculations the samples at Harwell were considered to be uniformly coated circular surfaces. Any discontinuity due to non-ideal fitting of the mosaic of crystals was neglected, but an estimate of this effect was included in the quotation of errors. In the case where a sample consisted of one crystal only, the exact size of the crystal was taken. The natural surfaces at the sides of the crystals facing the detectors are assumed to have the same crystal structure and orientation. However, for reasons of sample symmetry it is important to keep these sides as small as possible, for instance, by covering

section 2.1.

them with varnish to exclude contributions from these sides to the angular distribution of fission fragments. It is difficult to make reasonable estimates concerning differences in crystallographic orientation at the crystal sides, together with the effects caused by scattering of fission fragments along the sides.

The solid-angle corrections were calculated by using a numerical procedure for the integration. The results for the average values of $P_k(\cos\theta)$ around $\theta \approx 0^\circ$ and $\theta \approx 90^\circ$ are given in table 2.1.

Table 2.1.
Geometrical averages for Legendre polynomials

$\langle\theta\rangle$	$\langle P_2(\cos\theta)\rangle$	$\langle P_4(\cos\theta)\rangle$
experiment Harwell		
0°	0.765 ± 0.050	0.324 ± 0.120
90°	-0.265 ± 0.050	-0.105 ± 0.080
experiment Petten		
0°	0.883 ± 0.030	0.635 ± 0.086
90°	-0.383 ± 0.030	0.108 ± 0.061

The quoted errors are based on estimates of systematic errors due to numerical integration and due to the deviations from sample uniformity.

The problem of deviations in crystal orientation has been mentioned above. Another cause for misorientation is misplacement of the crystal by 180° , resulting in a reversal of the direction of 0° and 90° for that crystal. This would dilute the measured anisotropy, although the effect would depend somewhat on the actual location of the crystal in the sample. Neglecting the last factor the effective Legendre polynomials, assuming a fraction x to be misoriented, would become:

$$\langle P_k(\cos\theta) \rangle'_{\theta=0^\circ} = (1-x) \langle P_k(\cos\theta) \rangle_{\theta=0^\circ} + x \langle P_k(\cos\theta) \rangle_{\theta=90^\circ}$$

$$\langle P_k(\cos\theta) \rangle'_{\theta=90^\circ} = x \langle P_k(\cos\theta) \rangle_{\theta=90^\circ} + (1-x) \langle P_k(\cos\theta) \rangle_{\theta=0^\circ}$$

In first-order approximation the anisotropy effect would be diminished by a factor $1-2x$. It is plausible that in one of the samples with ^{233}U , one or two crystals out of the total of 25 crystals were misoriented indeed. For this reason it was necessary to perform the experiments on single crystals, as has been done at Petten.

2.2. Samples for alignment of ^{235}U , ^{233}U and ^{237}Np

Alignment of the nuclei ^{235}U and ^{233}U can be achieved in the double nitrate $\text{RbUO}_2(\text{NO}_3)_3$, indicated below as RUN. In a similar way ^{237}Np can be aligned in the isomorphous chemical compound $\text{RbNpO}_2(\text{NO}_3)_3$, indicated as RNN.

The crystal structure of RUN and RNN is rhombohedral as described by Hoard and Stroupe ¹⁾ and Dieke and Duncan ²⁾. A model of the crystal structure is shown in fig. 2.3. In the direction of the c-axis Rb^+ -ions and the UO_2^{++} -groups alternate. The UO_2^{++} -groups, which are supposed to be linear, are aligned in this direction.

Since the α -activity of the target nuclei would produce a large heat-input by dissipation of α -particles in the sample material, adequate cooling seemed only possible with a minimum amount of target material, and hence it was decided to coat the crystal surface with only a thin layer in which the target nucleus would be disposed. Furthermore, effective counting of fission fragments is possible only from samples having thicknesses in the order of 1 mg/cm^2 of fissile material. The preparation of the coated single crystals was done at the Applied Chemistry Division, AERE, Harwell ³⁾. RUN-crystals were grown from a solution of rubidium uranyl nitrate in which the uranium was isotopically depleted (0.43% ^{235}U). It was possible to use RUN base crystals also for the ^{237}Np -sample.

section 2.2.

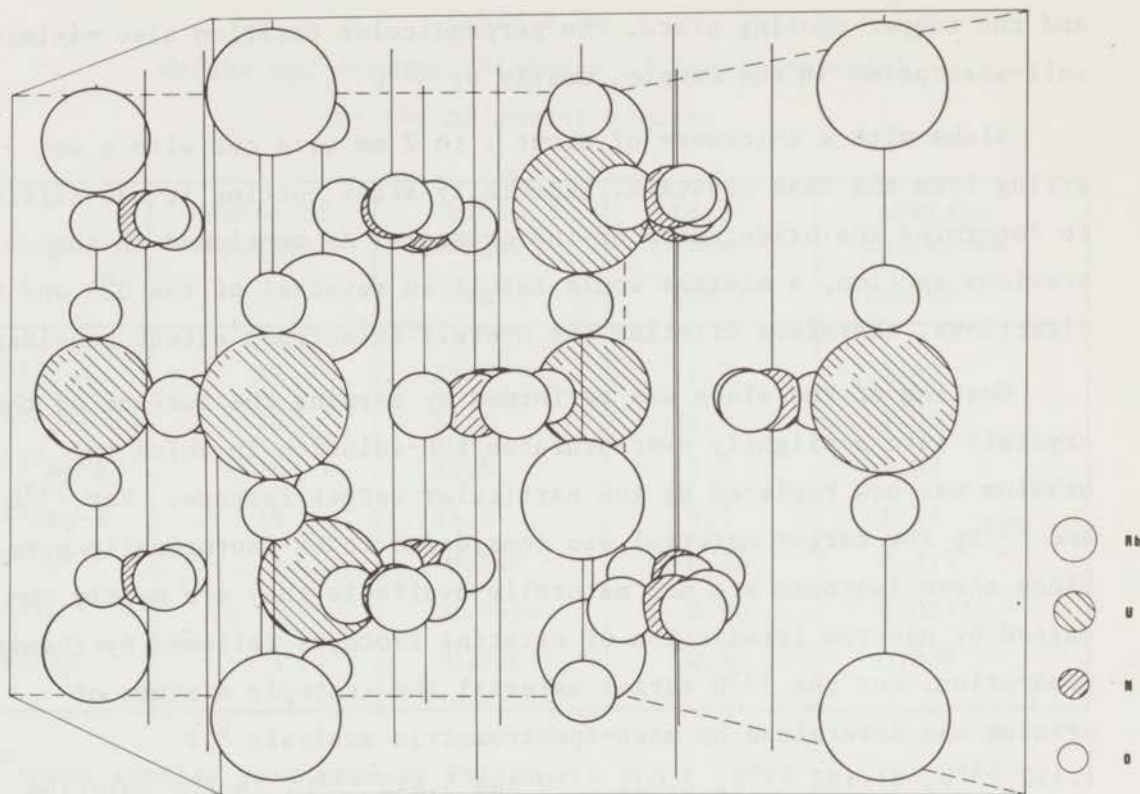


Fig. 2.3.

Crystal structure of $RbUO_2(NO_3)_3$.

A natural surface had to be chosen from the crystals, which would be suitable for the orientation geometry. Since only s-wave capture occurs in the energy range of incident neutrons considered, the direction of the beam was inconsequential to the direction of nuclear orientation. However, the diffused-junction detectors had to be positioned outside the neutron beam. The natural face which was selected for sample surface corresponds to the $10\bar{1}2$ hexagonal planes; the form of this surface is a parallelogram with an angle of 85° . The c-axis emerges at an angle of 49° with the surface in the direction of one of the obtuse angles in the parallelogram.

By placing the sample perpendicular to the neutron beam, it was feasible to have two separate samples, one facing the neutron beam, the other receiving neutrons after transmission through both samples

and the copper cooling plate. The perpendicular position also minimized self-absorption in the sample, mostly by ^{238}U .

Slabs with a thickness of about 1 to 2 mm were cut with a wet string from the base crystals. Especially after cutting it was difficult to determine the orientation of the crystals. As mentioned in the previous section, a mistake would result in reversal of the 0° - and 90° -directions, therefore diluting the overall anisotropy effect considerably.

Coating of the slabs was performed by dipping the surface of the crystals into a slightly oversaturated RUN-solution in which the uranium was now replaced by the particular target isotope. For ^{233}U and ^{237}Np the target material was considered to be isotopically pure. Since these isotopes are not naturally available they are mostly obtained by neutron irradiation of existing isotopes followed by chemical separation. For the ^{235}U target material the isotopic mixture of uranium was determined by mass-spectrometric analysis ⁴): 1.15% ^{234}U , 91.18% ^{235}U , 2.02% ^{236}U and 5.64% ^{238}U . In the solution for the ^{235}U -sample 0.5% ^{237}Np was added to reduce the relaxation time for the alignment of the target nuclei.

To measure the absolute amount of disposed target material and to check on the uniformity of the coating, all the individual crystals were counted on α -activity. In the case of ^{235}U the α -activity was masked completely by the activity of ^{234}U , having a half-life which is roughly 3000 times shorter than ^{235}U . Heavier coated crystals showed a larger full width at half maximum (FWHM) of the α -peak than the lighter ones. A non-uniform coating resulted in an abnormally broad α -peak.

The coated crystals of which the orientations were thought to be well determined were attached with a low temperature varnish on to a copper plate into a mosaic and the c-axes were carefully aligned by eye. In table 2.2 the measured total weights of all samples have been given, together with the number of crystals, total surface area and average thickness.

section 2.2.

Table 2.2.
Weight and average thickness of target material
in the alignment samples

sample	number of crystals	total weight (mg)	total area (cm ²)	average thickness (mg/cm ²)
²³³ U-A	27	25.3	17.2	1.47
²³³ U-B	25	22.1	21.4	1.03
²³⁷ Np-A	26	25.6	13.6	1.88
²³⁷ Np-B	24	23.5	19.7	1.19
²³⁵ U *	1	0.540	0.76	0.711
²³³ U *	1	0.0654	0.80	0.0817
²³⁷ Np *	1	0.720	0.81	0.889

* these samples were used at Petten.

There were several effects dependent on the sample thickness that could not be measured directly and which therefore might have caused systematic errors. The heat input that is developed by the dissipation of α -particles and fission fragments in the sample material is proportional to the amount of target material; it limits efficient cooling of the sample. Varying sample thicknesses will give rise to a difference in effective temperature of the samples. Another possible error is the scattering of fission fragments which diminishes the original anisotropy in the angular distribution. This effect will be less pronounced for α -particles which have a greater penetration length. By giving the two samples, at opposite sides of the sample cooling plate, a different coating thickness, it might be possible to detect these effects and make a correction if necessary.

2.3. Cryostat and thermometry

The various samples of RUN-crystals had to be cooled to temperatures as low as 0.1 K. It was necessary to maintain this temperature for periods of several days. Data had to be collected for total periods up to a few weeks for experiments on ^{233}U and in the case of ^{237}Np , count rates were so low that it was required to take data at low temperatures for a few months. To obtain reasonable alignment of the target nuclei temperatures of only 0.5 K would be sufficient, but in order to rule out systematic errors an increase in the anisotropy effect was desirable. Temperatures lower than 0.1 K seemed to be of little use because of low thermal conductivity of the sample material and poor thermal contact between sample and cooling plate. Observing the requirements for the total time of data collection at low temperatures, it seemed necessary to use a cooling method which would enable maintenance of the minimum temperatures for periods which generally would be considerably longer than the periods obtained by adiabatic demagnetization of paramagnetic salts. For this reason the cooling technique by means of $^3\text{He}/^4\text{He}$ dilution, which is a continuous process, was a much more suitable method for the alignment experiments.

The method was pointed out in principle by London in 1962⁵⁾ and afterwards it was developed at several laboratories⁶⁻⁹⁾. By the time it was decided to make use of $^3\text{He}/^4\text{He}$ dilution to obtain the required cooling, technical know-how was only scarcely available, especially regarding the optimization of the exchange of heat and the rate of circulation of ^3He . The cryostats at Harwell and Petten, together with the $^3\text{He}/^4\text{He}$ refrigerator were designed by Postma, who has given detailed information on the apparatus used at Harwell in refs.^{10,11)}.

Since the $^3\text{He}/^4\text{He}$ dilution refrigerator was only used as an experimental device to obtain low temperatures, a full description of the theory of $^3\text{He}/^4\text{He}$ solutions is not necessary here. Only a general outline of the method will be given, together with a description of the apparatus.

A mixture of liquid ^3He and ^4He which is cooled to temperatures

section 2.3.

below approximately 0.8 K will separate spontaneously into two phases which differ in the ^3He -concentration. As the temperature is reduced further this difference in concentration increases and below approximately 0.05 K the concentrations remain practically constant. The ^3He -rich phase is then nearly pure ^3He whereas the dilute phase is ^4He with 6% ^3He . Taking the final situation below 0.05 K as being particular for the general behaviour of phase separation, there are remarkable differences in cryogenic properties between the two phases. ^3He has a large specific heat compared to the superfluid ^4He . In the dilute phase ^3He behaves as a Fermi-Dirac gas in a medium consisting of $^4\text{He-II}$. Phase transition of ^3He atoms from the concentrated to the dilute phase can be understood as an analogy with evaporation of a liquid, albeit there are important differences with this example; for instance, pure ^3He has a lower density than ^4He and therefore the concentrated phase will float on top of the dilute phase in a mixing chamber. Cooling will result if ^3He atoms from the concentrated phase are passing the phase boundary to the dilute phase. Evaporation from the dilute phase is possible by slightly heating this phase in an evaporation chamber and since there is a sizeable difference in vapour pressure of ^3He and ^4He , mainly ^3He vapour will be pumped off. By constantly taking away ^3He from the dilute phase ^3He will be forced to pass the phase boundary. In view of this, it is important that in the dilute phase the concentration of ^3He is finite at very low temperatures. The concentration rises slowly as the temperature increases. The ^3He gas which has been pumped away from the dilute phase is recondensed at the concentrated side of the mixture and cooled in counterflow by the dilute phase by means of heat exchangers. By constant circulation of ^3He the process has become continuous. A formula for the cooling capacity in the mixing chamber can be given by:

$$\dot{Q}_{\text{mc}} = \dot{n}_3 \{H_{3d}(T_{\text{mc}}) - H_{3c}(T_{\text{mc}}')\} ,$$

in which \dot{n}_3 is the circulation rate of ^3He in mole/sec; $H_{3d}(T_{\text{mc}})$ is the enthalpy of ^3He per mole in the dilute phase at the temperature of the

mixing chamber; $H_{3C}(T_{mc}')$ is the enthalpy of ^3He per mole in the concentrated phase at the temperature of the inflowing ^3He into the mixing chamber. In practice the difference between T_{mc} and T_{mc}' is negligible if the system performs optimally. A simplified expression for the cooling capacity can easily be derived from the specific heat of concentrated and dilute ^3He as a function of temperature,

$$\dot{Q}_{mc} = R \dot{n}_3 9.9 T_{mc}^2 \quad (\text{erg/sec})$$

in which $R = 8.3 \times 10^7$ erg/mole is the gas constant.

There are a few experimental restrictions on ideal cooling with a continuous $^3\text{He}/^4\text{He}$ dilution refrigerator.

1. To assist evaporation of ^3He from the dilute phase the evaporation chamber has to be heated externally which is an additional heat input to the system.
2. The ^3He which is condensed and put into the concentrated phase is precooled before reaching the mixing chamber by the returning flow of ^3He in the dilute phase. The type of heat exchangers, used for this purpose in the refrigerator described, is a copper cylinder with two chambers containing sintered copper to enlarge the exchange surface. Ideal cooling is limited by the heat conductivity of copper and the Kapitza resistance of ^3He to copper, both in the concentrated and dilute phase. This factor is very important in the mixing chamber to which the sample is connected by a copper cooling rod.
3. Considerable heat development may occur by the viscous flow of ^3He in the dilute and concentrated phase if the refrigerator has a high flow resistance. This effect is mainly important for the lower sections of the refrigerator. The resistance of the sintered copper in the heat exchangers may give rise to this frictional heating if the volume of the chamber is too small.
4. The condensation of ^3He is done in a spiral of copper tubing which is situated inside the He-bath at 1 K. Heat input from condensing ^3He gas inside the heat exchangers is prevented by a flow restriction, mounted in a position before the first heat exchanger. This also

section 2.3.

adjusts the total resistance of the system by which a suitable circulation rate can be obtained.

The cryostat used for the alignment experiments at Harwell is shown in a cut-away view in fig. 2.4, and the detailed view of the tail section containing the dilution refrigerator in fig. 2.5. The nitrogen bath (77 K) with a volume of 14 l is the annular bath, which shields the two helium baths. The upper bath having a volume of 10 l was operated at 4 K; the lower bath (4.2 l) was reduced by pumping to 1 K. Evaporation of this bath amounted only 12 to 15 ml/hour and under normal circumstances continuous operation of the dilution refrigerator could be obtained for periods up to 10 days. The 4 K bath had to be refilled every two days, but this could be done during normal operation and did not effect the temperature of the sample.

The $^3\text{He}/^4\text{He}$ dilution refrigerator was designed for ^3He circulation rates up to 10^{-4} mole/sec. At a temperature of 0.1 K on the mixing chamber this would ideally give a cooling capacity of about 800 erg/sec. The refrigerator has never been tested to obtain the minimum temperature, because of the α -activity of the samples which gave a considerable heat input. In the beginning there were only three porous copper heat exchangers. The dilute and concentrated side of these are exactly equal: 2 cylindrical chambers of 12 mm diameter and 10 mm high in a copper block are filled with sintered copper (density: 60% copper). A better performance of the refrigerator can probably be obtained by making the volume of the heat exchangers larger, especially at the dilute side because of internal friction of ^3He . In the course of the experiments on ^{233}U a fourth heat exchanger was mounted in order to diminish the heat load on the mixing chamber by the inflow of ^3He . The heat input of the sample, however, was too large to observe an improvement in the lowest temperature achieved.

The $^3\text{He}/^4\text{He}$ gas mixture consisted of 10 l (NTP) 30% ^3He , determined by mass-spectrometric analysis. During operation the restriction capillary which was wound around the mixing chamber gradually became blocked. This resulted in a slow extraction of ^3He from the total

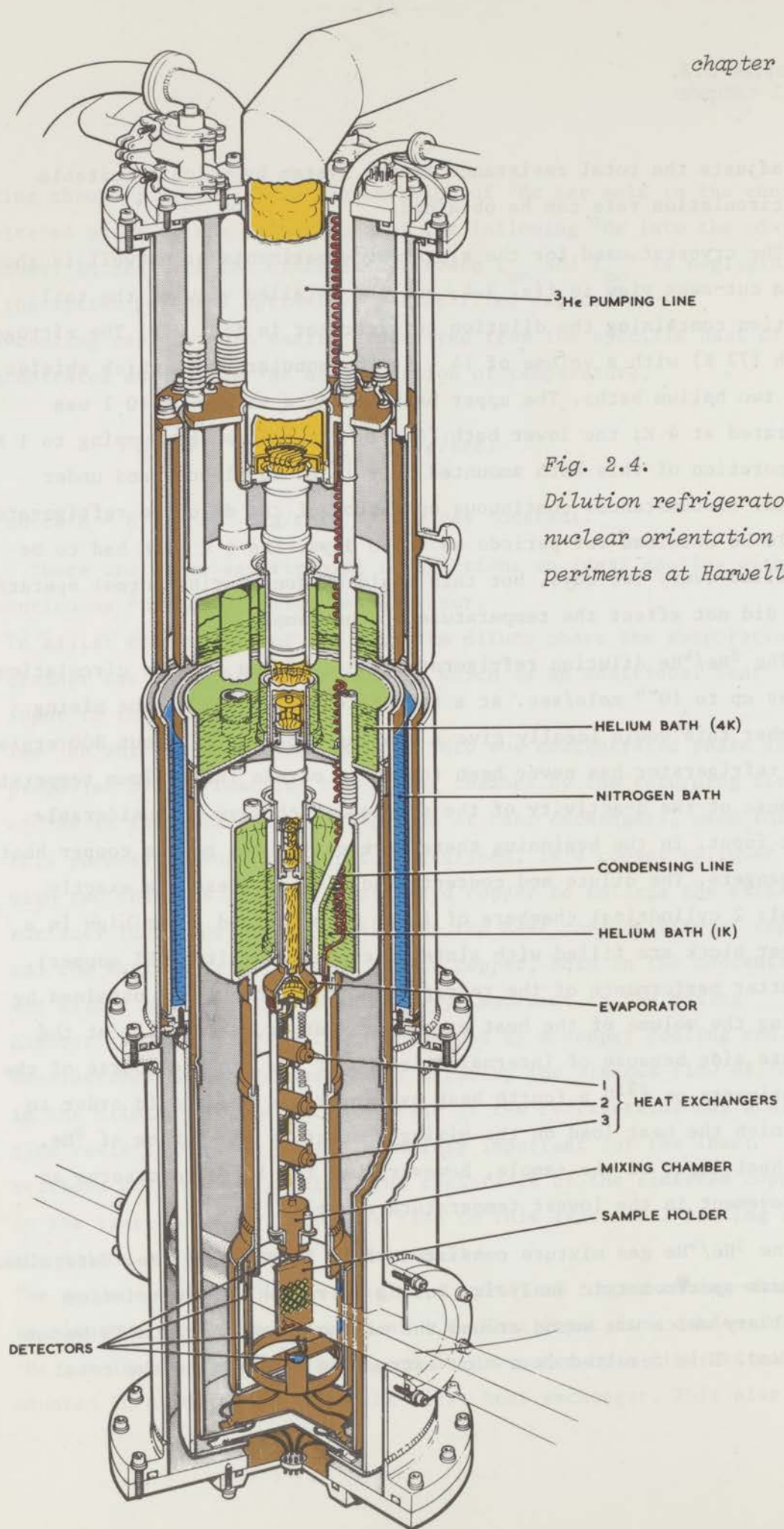


Fig. 2.4.
Dilution refrigerator for
nuclear orientation ex-
periments at Harwell.

section 2.3.

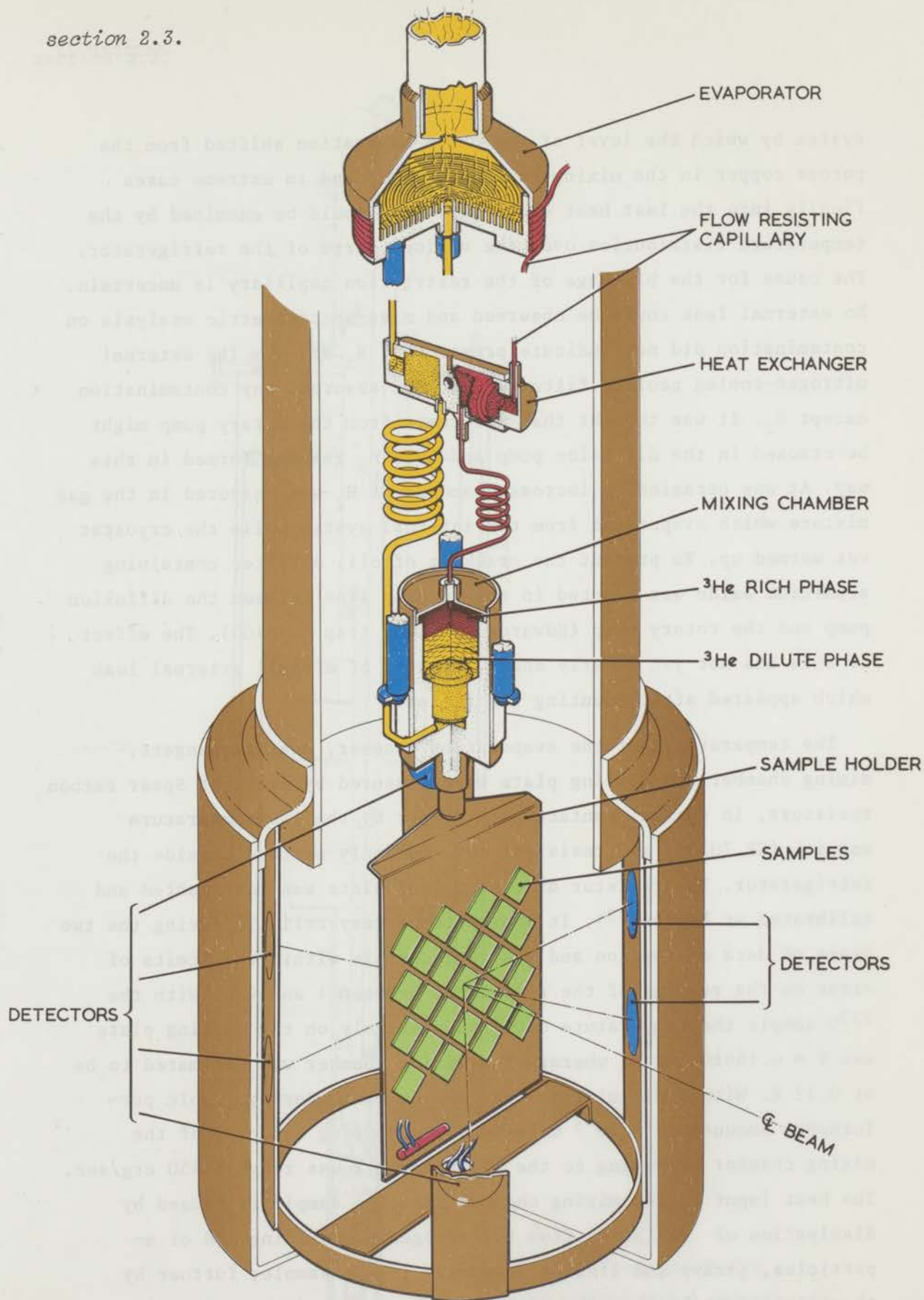


Fig. 2.5. Tail section of Harwell cryostat including dilution system, sample and detector assembly.

system by which the level of the phase separation shifted from the porous copper in the mixing chamber upwards and in extreme cases finally into the last heat exchanger. This could be examined by the temperature distribution over the various parts of the refrigerator. The cause for the blockage of the restriction capillary is uncertain. No external leak could be observed and mass-spectrometric analysis on contamination did not indicate presence of N_2 and O_2 . The external nitrogen-cooled zeolite filter would have absorbed any contamination except H_2 . It was thought that oil fumes from the rotary pump might be cracked in the diffusion pump and that H_2 gas was formed in this way. At one occasion an increased amount of H_2 was measured in the gas mixture which evaporated from the internal system while the cryostat was warmed up. To prevent the cracking of oil, a filter containing aluminium oxide was mounted in the pumping line between the diffusion pump and the rotary pump (Edwards foreline trap 0.1/100). The effect of this has not yet clearly shown, because of a small external leak which appeared after mounting the filter.

The temperatures of the evaporation chamber, heat exchangers, mixing chamber and cooling plate were measured by means of Speer carbon resistors, in thermal contact with copper by the low-temperature varnish (GE 7031); all resistors were commonly earthed outside the refrigerator. The resistor at the cooling plate was constructed and calibrated at Leyden¹³⁾. It proved to be very reliable during the two years of data collection and was reproducible within the limits of error on the reading of the resistance between 1 and 4 K. With the ^{233}U sample the temperature obtained averagely on the cooling plate was $T = 0.166 \pm 0.002$ K, whereas the mixing chamber was estimated to be at 0.12 K. With a circulation rate of 3He which during stable performance amounted 4×10^{-5} mole/sec, the cooling capacity of the mixing chamber according to the given formula was roughly 450 erg/sec. The heat input to the mixing chamber from the sample is caused by dissipation of radiation from the cryogenic shielding and of α -particles, γ -rays and fission fragments in the sample; further by thermal conduction through the heat exchangers and the suspension.

section 2.3.

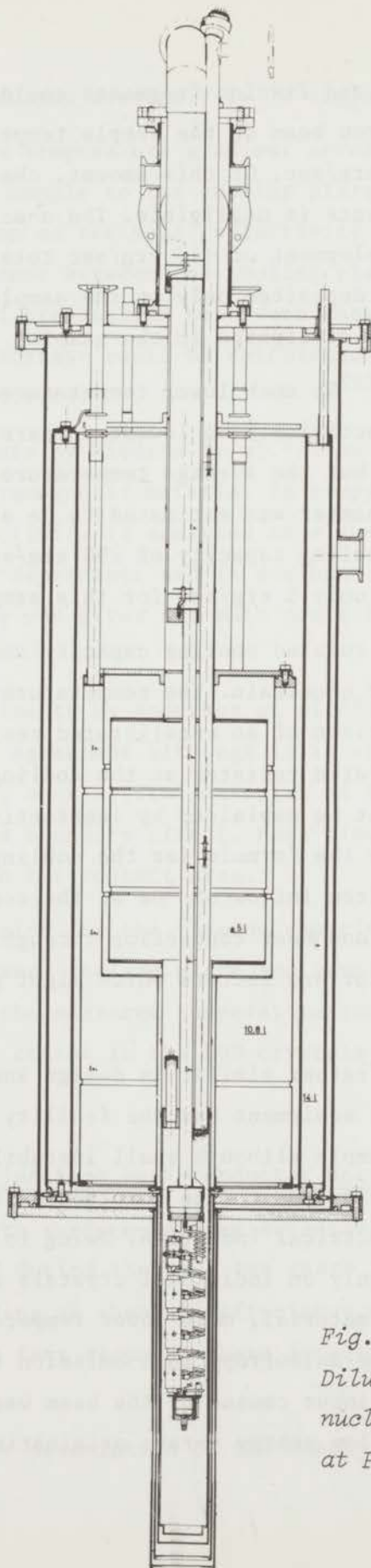


Fig. 2.6.
Dilution refrigerator for
nuclear orientation experiments
at Petten.

The heating effect by γ -rays and fission fragments could be measured by the influence of the neutron beam on the sample temperature. This is estimated to be 15 to 20 erg/sec. Of this amount, the relative contribution from fission fragments is negligible. The α -activity of ^{233}U gave rise to a heat development of 140 erg/sec totally, but regarding that ^{233}U nuclei are deposited only on the sample surface, about half of the activity is dissipated in the sample.

For the experiments with ^{237}Np much lower temperatures were obtained because of a lower α -activity. The lowest temperature was 0.09 K on the cooling plate, but the average temperature was typically 0.11 K, whereas the mixing chamber was estimated to be at 0.095 K. This would correspond to a cooling capacity of 290 erg/sec. The heat input due to α -particles was only 5 erg/sec for this sample.

The difference between calculated cooling capacity and heat load on the refrigerator is rather uncertain. The temperature of the mixing chamber was derived by comparison of an uncalibrated resistor at the mixing chamber and the calibrated resistor at the cooling plate. For the rest the discrepancy might be explained by ineffective cooling at higher temperatures, at which the formula for the cooling capacity is no longer valid. Heat input from inflow of ^3He at the concentrated side into the mixing chamber and heat conduction through the suspension and spacers of the refrigerator are factors which might partly account for the difference.

The cryostat at Petten is rather similar in design and it has been described before ^{13,14}). This equipment has the facility for a magnetic field to be applied on the sample although small instabilities of the magnet strongly affect the behaviour of the dilution refrigerator because of heating due to electrical induction. Owing to the fact that measurements were performed only on individual crystals which mostly had a thin coating of target material, much lower temperatures could be obtained; for instance, the anisotropy in α -emission from ^{233}U was measured down to 40 mK. Heat input caused by the beam was probably mainly due to interaction of low energy γ -rays originating from the

section 2.4.

reactor and amounted averagely to 10 erg/sec.

Concerning a temperature gradient across the sample from the active surface of the sample to the cooling plate, it is important to have some information on the heat conductivity of the RUN-crystals and of a thermal resistance between the cooling plate and the crystals. If the exact amount of transferred heat were known an effective temperature of the sample surface could be calculated under additional assumptions of heat conductivity.

In experiments by Miedema et al.¹⁵⁾ on a thermal link between a solution of paramagnetic material in propyl alcohol and a CrK alum the heat conductivity is analysed as a sum of two components: the first has a T^3 -dependence and is dominant above 0.2 K; the second has a T -dependence and gives the main contribution to the heat conductivity below 0.2 K.

Other experiments by Anderson et al.¹⁶⁾ on a copper heat link are in qualitative agreement although it is suggested that the distribution of temperatures over crystal material is homogeneous and that thermal resistance is a boundary effect. Heat flow has a T^3 -dependence and is proportional to the contact area.

As a conclusion for the fission experiments, a possible temperature difference between cooling plate and sample surface may assume a T^3 -dependence in the measured temperature range. Finally, it should be mentioned that cracks in the RUN-crystals may severely limit the heat conductivity.

2.4. Diffused-junction semi-conductor detectors

Together with surface-barrier detectors diffused-junction detectors were developed during the past ten years for the detection of charged particles. Having an absolute efficiency together with a high resolution and a fast response these detectors proved to be suitable for many purposes.

An extensive description of the theory and experimental properties

of diffused-junction detectors is given by Gibson, Miller and Donovan 17).

The surface-barrier detectors have a slightly better energy resolution, but are less stable and less rugged than the diffused-junction detectors. For the former, n-type silicon is being used, for the latter, p-type. For the diffused-junction detectors which were used in the experiments described, the n-p junction is made by diffusing phosphorous into an oxidized layer of the silicon.

The detectors are now widely used and many different types, depending on the requirements, are commercially available. However, relatively little is known about applications at very low temperatures and therefore some investigations were done about pulse-height characteristics, radiation damage, stability under varying temperatures and varying pressure of the surrounding gas in the sample space.

The detectors chosen for the fission experiments at Harwell are Harshaw multi-diffused junction semi-conductor detectors, with an active area of 400, 200 or 150 mm² and a depletion depth of 100 μ ; they were delivered with flying aluminium leads which are point-welded to the active surface. The backing of the detectors is a thin gold plating; the electrical earthing is provided by mounting the detector on a copper plate. To ensure electrical insulation, quartz had been grown on the sides of the active surface and for the detectors used at Petten also more inward as a separate guard ring. The specifications for resistivity ranged from 2,000 to 12,000 Ω cm and a noise level was guaranteed to be below 30 to 60 keV.

For the experiments at Harwell a total of 8 detectors was used in a symmetric arrangement around the sample as shown in fig. 2.1 in section 2.1. The outputs of detectors with equivalent geometrical positions were paralleled in pairs, so that only four detector sets resulted. All detectors were commonly earthed; positive bias voltage was applied to the active surface area. All the detectors were tested at 1 K before operation, by measuring the spectra of the α -particles from the sample at various bias voltages and further by measuring leak

section 2.4.

currents as a function of bias.

With one detector, whose behaviour seemed to be average for the whole set of detectors, measurements were taken at several temperatures with the ^{235}U sample: the results are given in fig. 2.7. The lower part of the picture shows a relative measure of the resolution as a function of bias voltage. This is the FWHM of the α -peak divided by the peak position.

The ratio loses its meaning as an absolute measure of resolution as soon as this resolution becomes negligible in comparison with the width of the α -peak. It would have been advantageous to make these tests at different temperatures using a source of ^{241}Am with a very narrow α -peak, instead of the heavy samples of coated RUN-crystals having a considerably broadened α -spectrum; at room temperature the relative resolution for the α -peak from ^{241}Am was 1% at an applied bias of 50 V.

The relative resolution for 300 K and 77 K is rather constant over the full range of bias voltages. For 4 K and 1 K it is gradually decreasing to the value which is determined solely by the width of the α -spectrum and at 100 V the resolution has become independent of temperature.

The leak current through the semi-conductor changes appreciably from 300 K to 77 K, but it is rather constant below 77 K, as shown in the upper part of fig. 2.7. Quite a general feature of the detectors is abnormally high leak currents at higher bias voltages, which shows remarkably well in the curve at 77 K. At about 100 V the current suddenly becomes very high and any increase in bias will boost it further. It is unknown whether this is an intrinsic property of the detector, in which case the leak current is a diffusion current, or whether it is due to a surface current. The detector considered did not have a quartz guard ring on the surface to prevent surface leakage currents.

A high current could be correlated with a high noise level which sometimes was comparable to the pulse heights of α -particles.

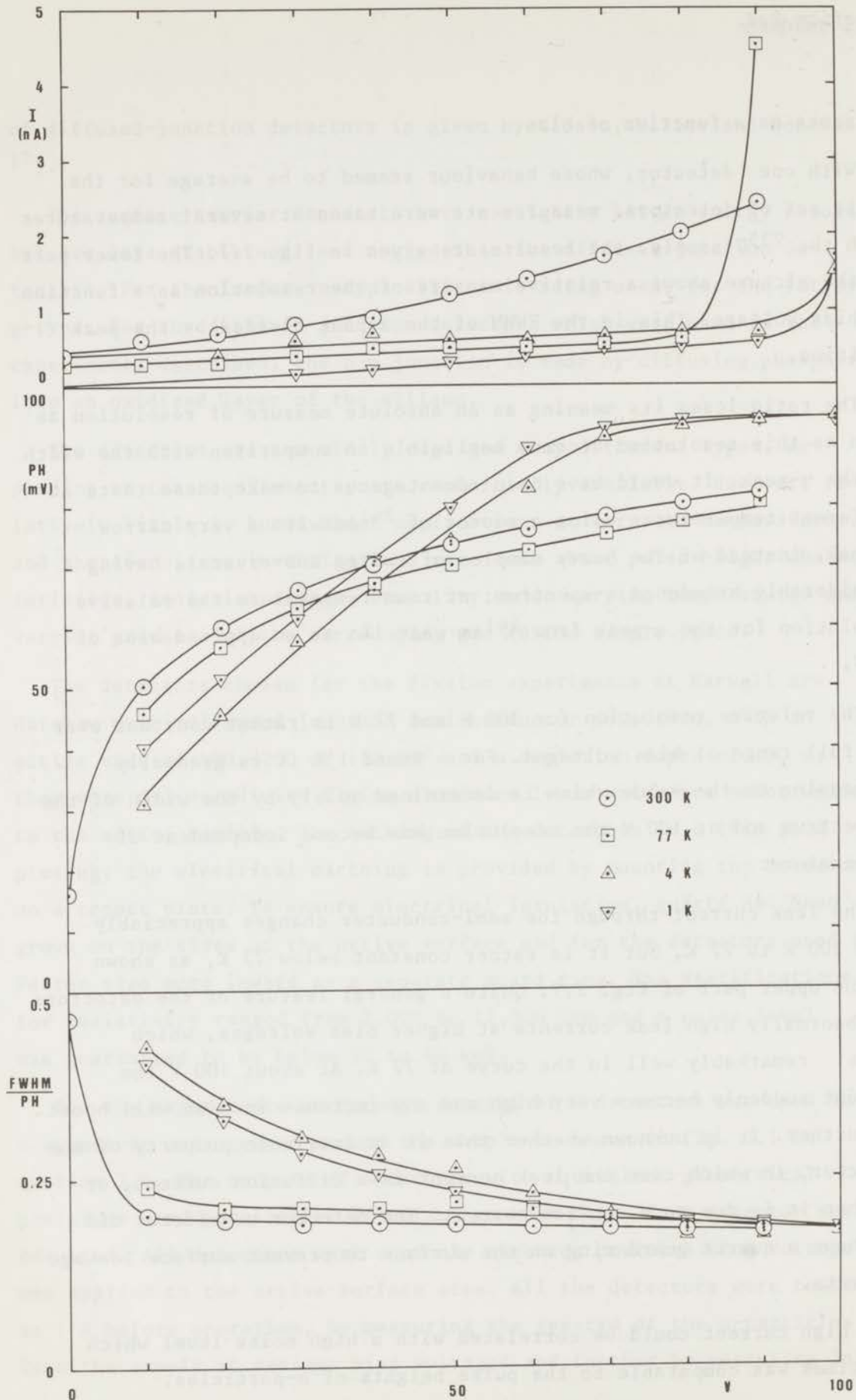


Fig. 2.7. Diffused-junction detector characteristics; peak current, pulse height and resolution as a function of applied bias voltage, measured at various temperatures.

section 2.4.

Leakage currents and related noise levels were also affected by a current in the order of 5 to 10 mA through the heater on the mixing chamber of the refrigerator. Another cause of abnormally high leak current was gas in the sample space: even a very low pressure of He gas could upset the detector in its normal performance. After pumping away the gas the detectors would settle down in a period which was typically in the order of a few hours.

At low temperatures the leak current still seemed to be very sensitive to temperature changes. Since pulse heights and noise levels were also influenced by this effect, it was necessary to operate the detectors under very stable circumstances. The temperature was kept constantly at 1 K during data collection and the bias was set to zero if the 1 K bath to which the detector assembly was connected had to be warmed up. After applying normal bias again it would take 2 to 6 hours before the detectors had reached a stable noise level. After a long duration of correct performance, sometimes the current suddenly jumped to high values. The detector could be used again after allowing it to "cool down" by removing the bias for some time and then reapplying it. However, it proved to be rather unreliable afterwards. To protect the data collection from the break down of detectors, alarms were set on α -count rate monitors, so that a run would be stopped if the count rate exceeded a permissible level. Some of these observations showed that the behaviour of the leak current was rather similar to that of the primary photocurrent in CdS-crystals¹⁸⁾.

The pulse-height characteristics show the biggest change between 77 and 4 K unlike the leak current characteristics. At low temperatures there is a saturation in pulse height: at about 80 V an increase in bias voltage does not result in a higher pulse height, whereas at higher temperatures this saturation has not yet been reached at 100 V. This behaviour is qualitatively in agreement with observations by Walter et al.¹⁹⁾ on germanium surface-barrier counters which also operated at very low temperatures. Saturation in pulse height is attained if the hole and electron trapping length, which are proportional to the bias voltage, are long compared to the thickness of

the sensitive layer.

Effects of radiation damage could clearly be observed in the case of the experiment on ^{233}U , where the sample had a high α -activity. At the detectors the intensity was $\sim 3 \times 10^4$ $\alpha/\text{cm}^2\text{sec}$ of 4.5 MeV α -particles, which over the whole period of data-collection gives 3×10^{11} α/cm^2 . The impair was observed as a decrease in pulse height, which is caused by attenuation of the average trapping length due to lattice imperfections. Because of fixed discriminator levels for pulse heights from fission fragments and α -particles the decrease in pulse height resulted in a decrease in count rates.

Another effect of radiation damage was an increase of leakage current and related problems with detector break-down as described above. This behaviour seems to be very similar to other studies of irradiation damage to surface-barrier detectors ^{20,21}.

It was noticed that there was an improvement in pulse height again after having the detectors at room temperature for some time, which indicated that part of the lattice imperfections had been annihilated at higher temperatures.

The average lifetime of the detectors, including detector drop-out due to breaking of the point-welded electrical contact on the detector during performance, amounted effectively to 4 months of operation.

2.5. Time-of-flight technique

The orientation experiments were performed at the 45 MeV electron linear accelerator at AERE, Harwell. Neutrons are produced by the impact of pulses of accelerated electrons in a mercury target. The resulting neutron pulses are boosted by a subcritical assembly of uranium enriched in the isotope 235. The neutrons produced are slowed down to a useful distribution of energies by a moderator of 2.5 cm polyethylene. The flight path used for the alignment experiments had a measured length of 10.0 meters and made in the horizontal plane an angle of 20° with the direction perpendicular to the electron beam. The neutron flight-path arrangement is shown in fig. 2.8.

section 2.5.

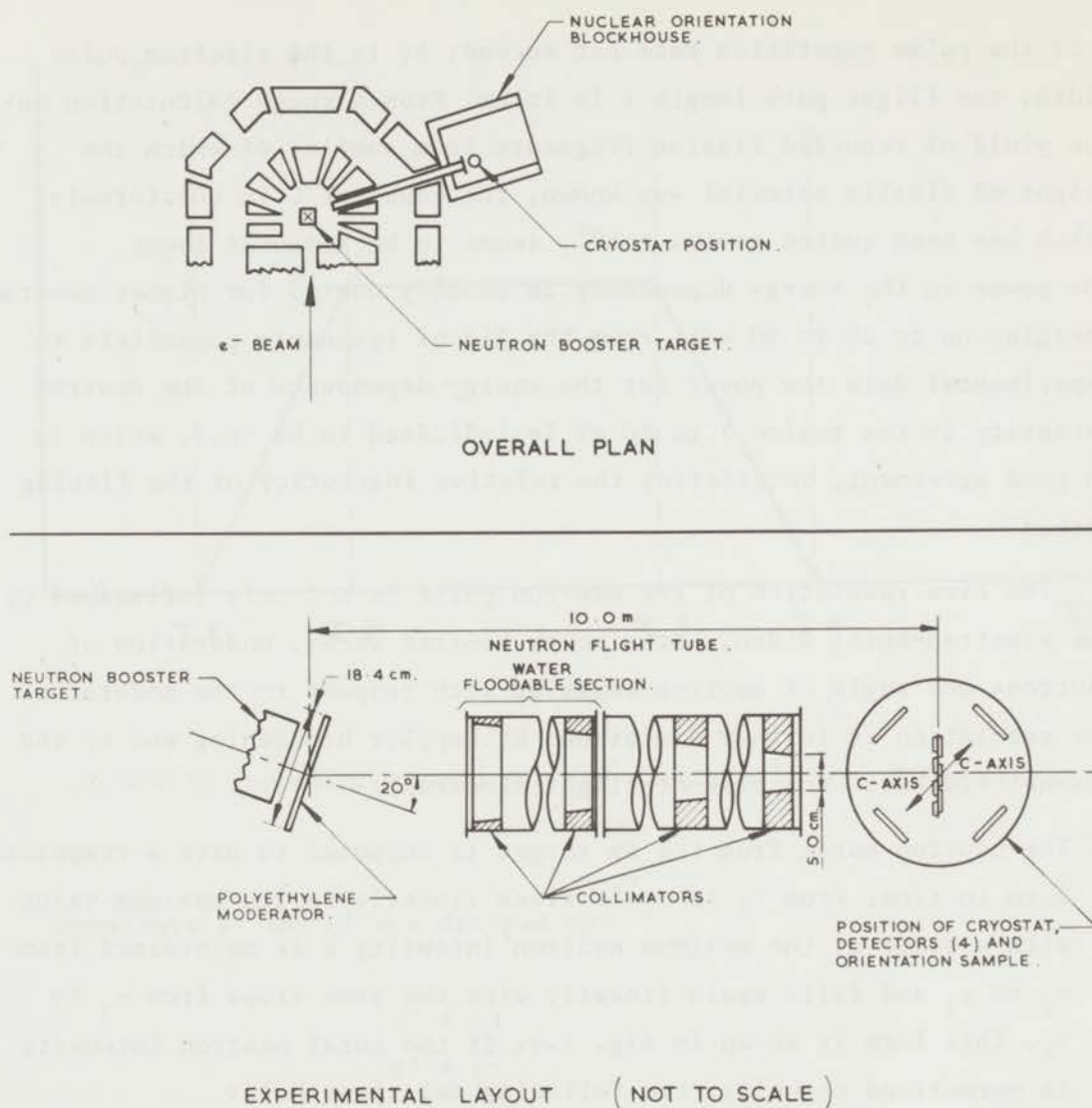


Fig. 2.8.

Neutron flight-path arrangement and experimental beam layout.

The neutron spectrum of the machine as a function of energy is not accurately known, but in general an expression has been given²²⁻²⁴⁾ for the flux:

$$N(E)\Delta E = C f \Delta \tau 1^{-2} E^{-0.78} \Delta E \text{ (n/cm}^2\text{sec).}$$

f is the pulse repetition rate per second; $\Delta\tau$ is the electron pulse width; the flight path length l is in cm. From a rough calculation on the yield of recorded fission fragments from samples of which the weight of fissile material was known, the constant C in the formula, which has been quoted as 1.4×10^7 , seems to be somewhat lower. The power in the energy dependency is usually quoted for higher neutron energies up to 20 to 30 keV. From the fit of resonance parameters to experimental data the power for the energy dependence of the neutron intensity in the region 1 to 60 eV is indicated to be -0.7 , which is in good agreement, considering the relative inaccuracy of the fitting method.

The time resolution of the neutron pulse is not only influenced by the electron-burst width, but also by booster decay, moderation of neutrons and angle of neutron emission with respect to the moderator. The resolution is further diminished by Doppler broadening and by the channel widths of the time-of-flight electronics ²⁵).

1. The neutron burst from the Hg target is supposed to have a trapezoidal form in time. From τ_1 to τ_2 it rises linearly to its maximum value with a slope c ; the maximum neutron intensity a is maintained from τ_2 to τ_3 and falls again linearly with the same slope from τ_3 to τ_4 . This form is shown in fig. 2.9. If the total neutron intensity is normalized to unity, the following relations hold:

$$a = 2/(\Delta\tau_1 + \Delta\tau_2)$$
$$c = 4/(\Delta\tau_1^2 - \Delta\tau_2^2)$$

where:

$$\Delta\tau_1 = \tau_3 - \tau_2$$
$$\Delta\tau_2 = \tau_4 - \tau_1 .$$

2. The neutron booster is subcritical and therefore the induced neutron intensity decays with a time constant λ . The neutron intensity can be calculated as a function of time for the various time regions from a differential equation on decay and production. Assuming a production of ϵ neutrons in the booster per incident neutron, the

section 2.5.

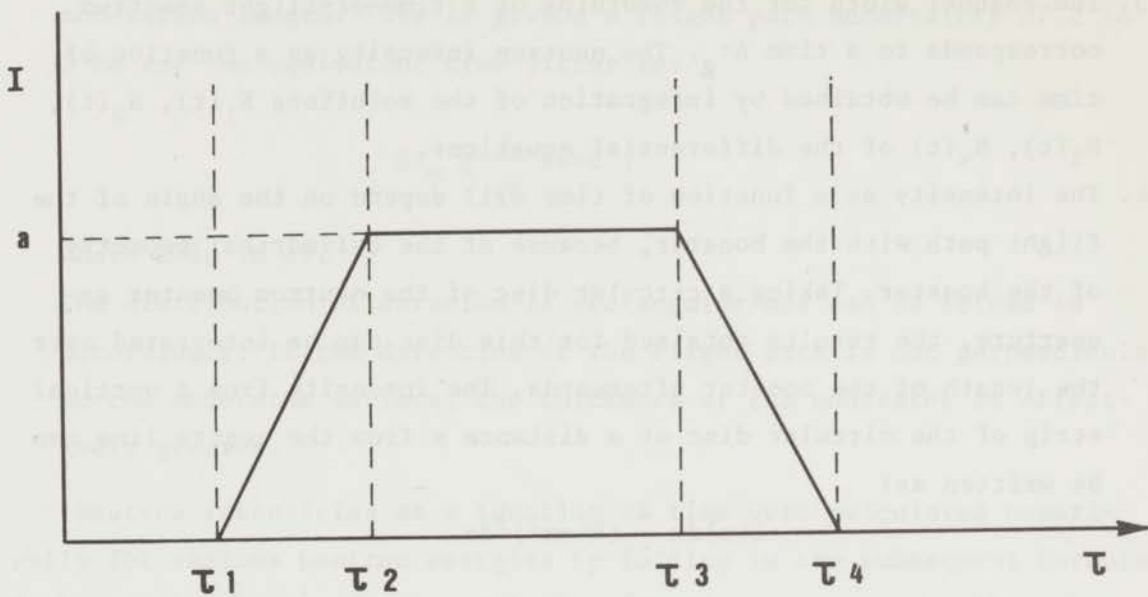


fig. 2.9.

Intensity function assumed for the electron burst of the linear accelerator.

constants a' and c' are defined by:

$$a' = \epsilon a$$

$$c' = \epsilon c .$$

Thus, the following differential equations are obtained:

$$\tau_1 \leq t \leq \tau_2: \quad \frac{d N_1(t)}{dt} = c' (t - \tau_1) - N_1(t) \lambda$$

$$\tau_2 \leq t \leq \tau_3: \quad \frac{d N_2(t)}{dt} = a' - N_2(t) \lambda$$

$$\tau_3 \leq t \leq \tau_4: \quad \frac{d N_3(t)}{dt} = c' (\tau_4 - t) - N_3(t) \lambda$$

$$t \geq \tau_4: \quad \frac{d N_4(t)}{dt} = - N_4(t) \lambda .$$

3. The channel width for the recording of a time-of-flight spectrum corresponds to a time $\Delta\tau_g$. The neutron intensity as a function of time can be obtained by integration of the solutions $N_1(t)$, $N_2(t)$, $N_3(t)$, $N_4(t)$ of the differential equations.
4. The intensity as a function of time will depend on the angle of the flight path with the booster, because of the cylindrical geometry of the booster. Taking a circular disc of the neutron booster as aperture, the results obtained for this disc can be integrated over the length of the booster afterwards. The intensity from a vertical strip of the circular disc at a distance x from the centre line can be written as:

$$I(x)dx \div (R^2 - x^2)^{\frac{1}{2}} dx,$$

where R is the radius of the booster disc. At that point time differences due to a difference in the length of the flight path can be given by:

$$t = x \sin\theta \cdot 72.3/\sqrt{E}$$

$$t_{\max} = R \sin\theta \cdot 72.3/\sqrt{E},$$

where E is in eV; θ is the angle between the flight path and the incoming electron beam.

Resultingly:

$$I(t)dt \div (t_{\max}^2 - t^2)^{\frac{1}{2}} dt$$

for:

$$-t_{\max} \leq t \leq t_{\max}.$$

5. The time jitter due to moderation is the last factor influencing the time resolution. Taking an infinite slab of moderator material, the intensity as a function of time and neutron velocity v is ²⁶⁾:

$$I(t) = \frac{1}{2} \left(\frac{vE}{\lambda}\right)^2 e^{-\frac{vt}{\lambda}}.$$

λ is the mean collision path of neutrons in the moderator, which for polyethylene amounts to approximately 1.0 cm. The optimal yield of neutrons is reached with a moderator thickness of 3 to 5 times the

section 2.5.

moderation length. This is giving a flight path uncertainty of 2 to 3 cm and the equivalent time jitter is:

$$\Delta\tau_m \approx \frac{2}{\sqrt{E}} \mu\text{sec} ,$$

where E is in eV.

The distribution of duration is rectangular and can be folded in accordingly. If the direction of the flight path is not perpendicular to the moderator surface, the thickness of the moderator is effectively greater.

Neutron intensities as a function of time were calculated numerically for various neutron energies by folding in the subsequent formulae. Although the shapes of the resolution functions are essentially non-Gaussian, for processing the experimental results it is mostly sufficient to use Gaussian functions, of which the center (τ_{r0}) and FWHM (τ_{r1}) correspond to those of the calculated resolution functions. The results are given in fig. 2.10.

The values of the parameters τ_{r0} and τ_{r1} as functions of energy are fitted by functions of the type:

$$a_1 E^p + a_2 .$$

Another uncertainty on the energy in time-of-flight spectra is Doppler broadening, due to thermal vibrations of the target nuclei. The energy has to be defined in the centre-of-mass coordinate system of neutron and target nucleus. The centre of Doppler broadening function (τ_{d0}) is the recoil correction, which is independent of temperature; the broadening is given by the FWHM (τ_{d1}) of this Doppler function:

$$\tau_{d0} = \frac{t}{M+1}$$

$$\tau_{d1} = \frac{4t}{M+1} \left(\frac{kT}{E} \frac{M}{M+1} e_{\ln 2} \right)^{\frac{1}{2}} ,$$

time-of-flight : $t = \frac{72.3 \text{ l}}{\sqrt{E}}$

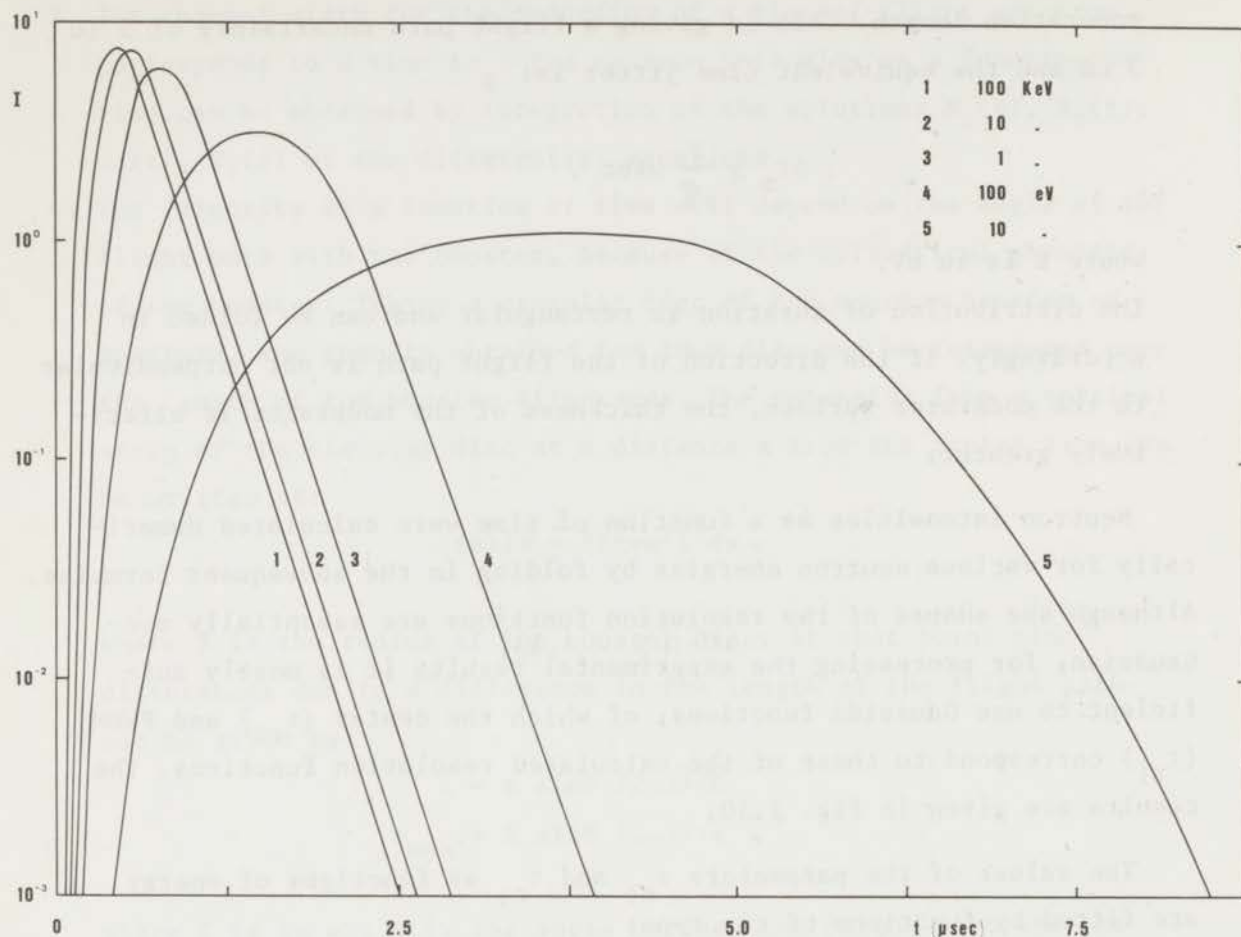


Fig. 2.10.

Resolution functions for several neutron energies.

length of flight path: l

neutron energy in laboratory coordinate system: E

mass of target nucleus: M .

Since the temperature of the sample is extremely low the FWHM (τ_{dl}) of the Doppler broadening function as calculated from the above formula is negligible in comparison with the machine resolution. Even for the warm runs at 6 K the contribution from the Doppler broadening would hardly be significant.

The above formula for τ_{dl} is based on the Maxwell-Boltzmann distribution of velocities of target nuclei, which is valid for gases.

section 2.5.

For a crystal the velocity distribution will be considerably different. At temperatures which are very low compared to the Debye temperature θ_D for the crystal an effective temperature can be given ^{27,28}):

$$T_{\text{eff}} = \frac{3}{8} \theta_D .$$

An estimate of θ_D for UO_2 has been obtained by Michaudon et al.²⁹) from a measurement of the broadening of a neutron resonance of ^{238}U . The value resulting from this measurement, $\theta_D = 205$ K, would give an effective temperature of 77 K. Such a value might become of any importance to the resonance broadening only for neutron energies below a few electron volt and therefore the above formula was taken a first-order approximation for the Doppler broadening.

The combined resolution function will have a centre at:

$$\tau_0 = \tau_{r0} + \tau_{d0} ,$$

and FWHM:

$$\tau_1 = \sqrt{\tau_{r1}^2 + \tau_{d1}^2} .$$

In fig. 2.11 the parameters τ_{r0} , τ_{d0} and τ_0 are plotted as a function of energy. The parameters τ_{r1} , τ_{d1} and τ_1 are given in fig. 2.12. The Doppler broadening τ_{d1} is given for two temperatures $T = 0.2$ K and $T = 6$ K. The resulting total resolution width τ_1 for $T = 0.2$ K coincides completely with τ_{r1} and for $T = 6$ K, τ_1 is only visibly different from τ_{r1} below a few eV.

In the neutron spectrum observed at the target, there is a background of neutrons whose energies do not correspond to the time-of-flight within the calculated limits of resolution. This background is due to emission of delayed neutrons in the booster, but even more so to scattering of neutrons in surrounding concrete and other materials. A considerable fraction of the background is consisting of thermal neutrons, smeared out over the entire time-of-flight spectrum. In general the background can be split up into a time-dependent and a time-independent part.

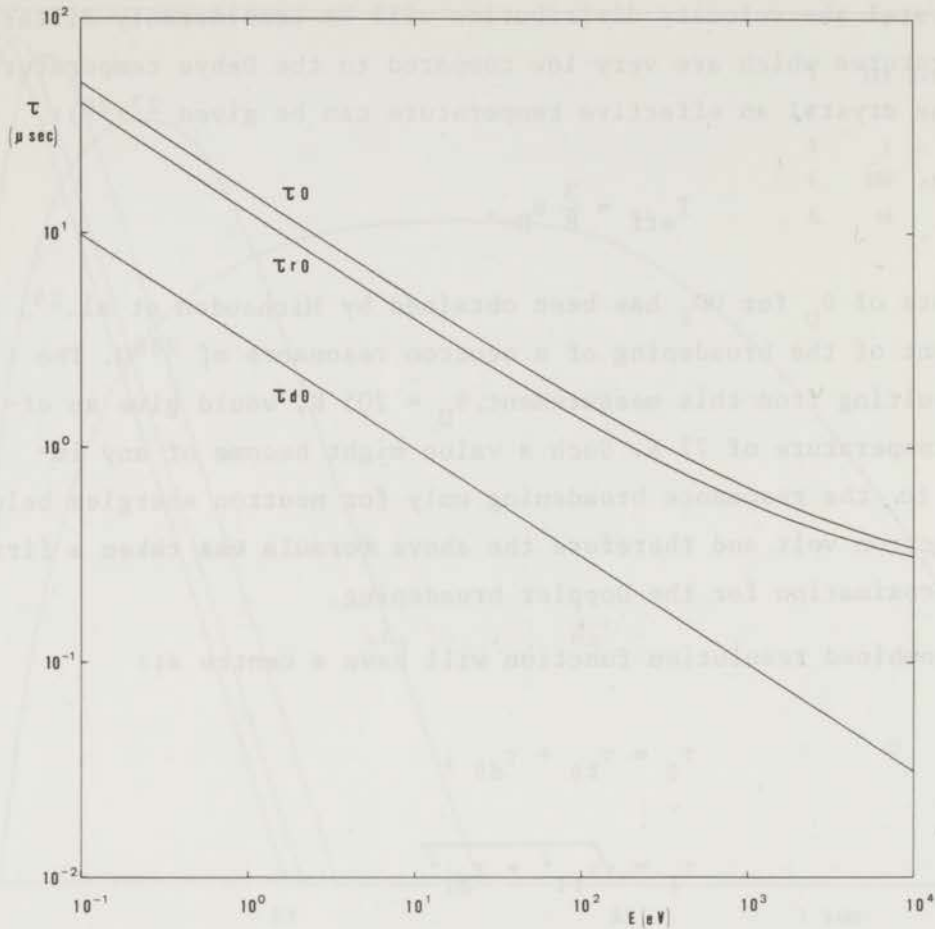


Fig. 2.11.

Centre of resolution function (τ_{r0}), of Doppler broadening function (τ_{d0}) and total time shift (τ_0) as a function of neutron energy.

The most suitable method to determine the background is by placing black resonance filters in the beam at a short distance from the target. Neutrons with energies corresponding to the resonance energies will be filtered out completely, except for those which are scattered into the target from outside the beam. This method tends to underestimate the real background since the neutrons of which the energies correspond to resonances of the absorbers are filtered out completely. By placing too many absorbers in the beam the background determination would become inaccurate. In table 2.3 the absorber

section 2.5.

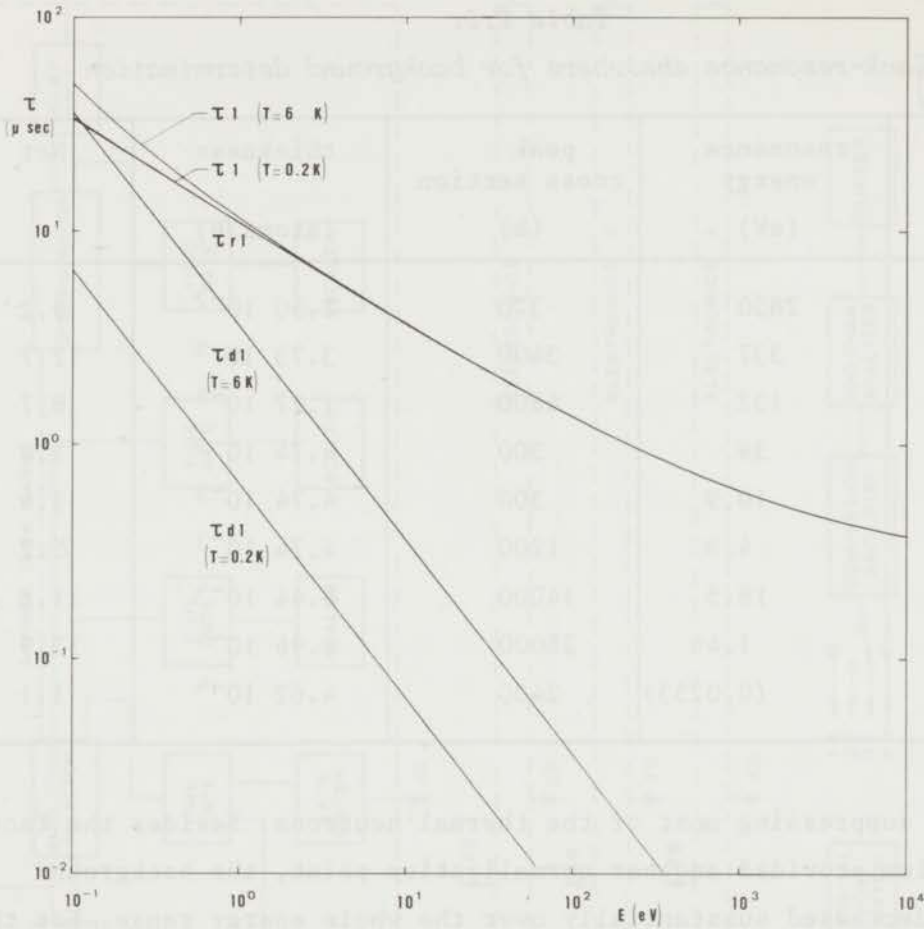


Fig. 2.12.

Width of resolution function (τ_{r1}), of Doppler broadening function (τ_{d1}) and total width (τ_1) as a function of neutron energy.

materials are listed together with the thicknesses of the materials, energies of relevant resonances, cross sections at the centre of the resonances and transmission parameters $N\sigma_t$. Sodium having the highest observable resonance energy of this group was put in the beam during normal data collection. It served as a normalization point for the background to be subtracted from the time-of-flight spectra. It proved, that the background subtraction was not sufficiently accurate if only sodium was used and especially at lower neutron energies this would lead to uncertainties. Therefore, cadmium was put in the beam in

Table 2.3.
Black-resonance absorbers for background determination

absorber element	resonance energy (eV)	peak cross section (b)	thickness (atoms/b)	Not
Na	2850	370	$2.50 \cdot 10^{-2}$	9.2
Mn	337	3400	$3.73 \cdot 10^{-3}$	12.7
Co	132	6800	$1.27 \cdot 10^{-3}$	8.7
Ta	39	300	$4.74 \cdot 10^{-3}$	1.4
	10.9	300	$4.74 \cdot 10^{-3}$	1.4
	4.3	1200	$4.74 \cdot 10^{-3}$	5.7
W	18.5	14000	$8.44 \cdot 10^{-4}$	11.8
In	1.46	28000	$4.96 \cdot 10^{-4}$	13.9
Cd	(0.0253)	2400	$4.62 \cdot 10^{-4}$	1.1

addition, suppressing most of the thermal neutrons. Besides the fact that cadmium provided another normalization point, the background herewith decreased substantially over the whole energy range. For the data collection on ^{233}U a few runs were made without cadmium in the beam but the results from these runs were very unreliable and were not used for further analysis.

In the case of ^{237}Np it was necessary to suppress the background as much as possible and cadmium was used throughout the data collection. It was not necessary to take separate background runs since the counts between the groups of resonances in the fission cross section of ^{237}Np were essentially due to background. No sodium was used in order to extend the useful energy range to higher energies.

2.6. Electronics and data-handling

A block-diagram of the electronic amplifying and recording equipment is shown in fig. 2.13. Four identical sets of preamplifiers and main amplifiers are connected to the four pairs of silicon detectors.

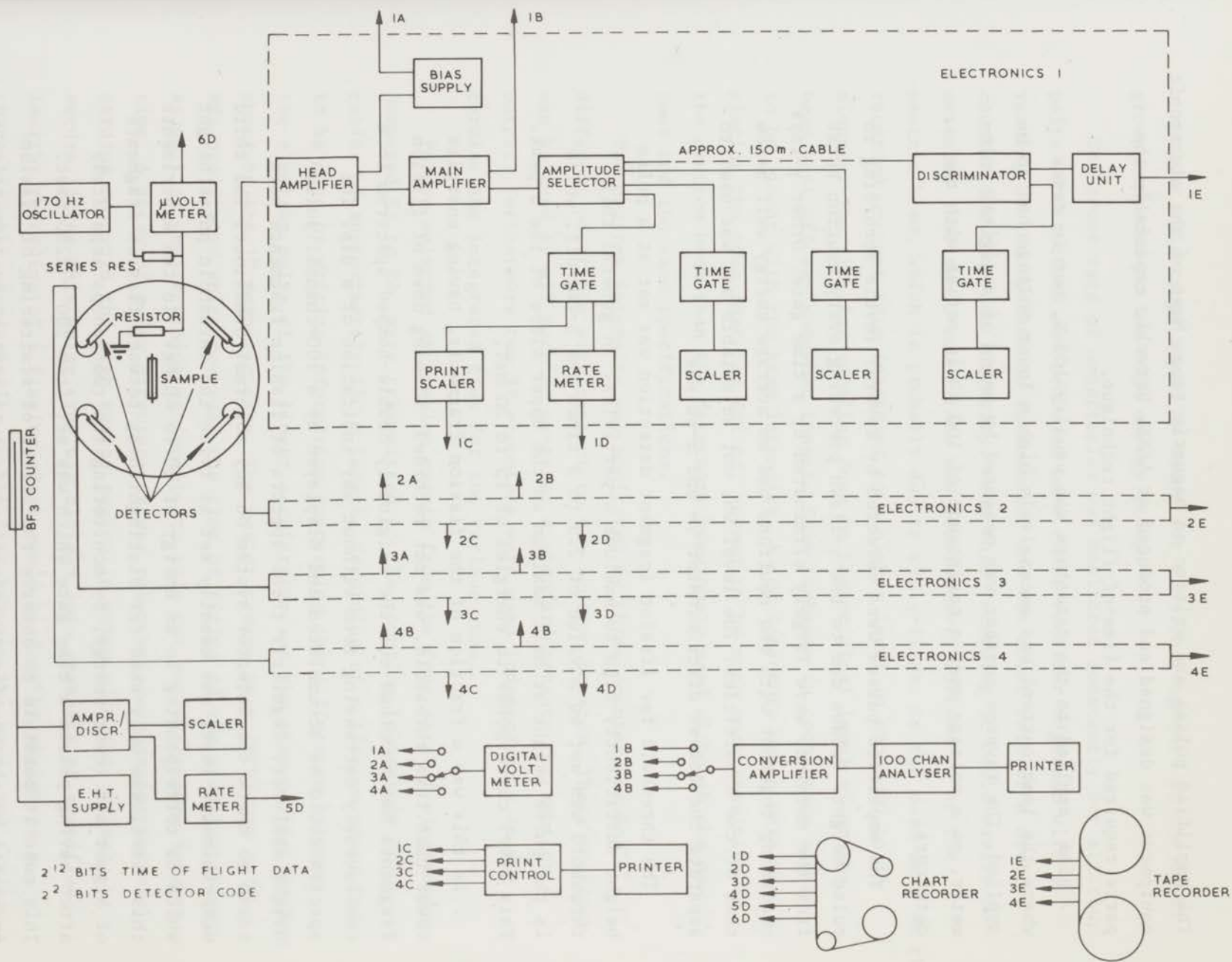


Fig. 2.13. Block diagram of electronic equipment.

The amplified pulses are written on magnetic tape. Most of the electronic equipment was designed and produced at AERE, Harwell, especially the parts required for the time-of-flight technique.

Bias applied to the detectors was usually 100 V, but in cases where the leak current was excessively high a lower voltage had to be applied. The reverse current was measured by means of a digital voltmeter, as a voltage over a resistance of 100 k Ω in series with the detectors.

The amplified pulses were selected by several levels according to pulse height. Pulses due to the γ -flash preceding every neutron burst from the machine, were largely eliminated by a time gate. Other γ -rays occurring together with the neutrons had an average energy well below that of the α -particles. The level was not adjustable and was used to separate the lowest discriminator γ - and α -pulses.

The threshold for fission fragment detection was set at a pulse height sufficiently high to exclude α -particles. In general this threshold was set at a value of 2.5 to 3 times the α -cut-off, which is the pulse height at half maximum on the upper slope of the α -peak. This level corresponds to energies of 15 to 20 MeV.

In this way a fraction of the fission fragments, having energies lower than this threshold, was not recorded. Slowing down of fission fragments had smoothed out the originally double-humped spectrum to a continuously decreasing form without any indication of a dip. The spectra could be accumulated and displayed by a 100-channel pulse-height analyzer. Regularly these spectra of fission fragments were taken to check the detector system on any abnormal behaviour. The third discriminator level was usually set at twice the threshold pulse height which is corresponding to an energy of 30 to 40 MeV. In the experiments this level was only used for distinguishing between fission fragments of higher and lower energy, by monitoring the two groups separately after having passed a time gate which was set from 200 - 2200 μ sec. This made it possible to observe the effect of scattering of fission fragments on the angular distribution. If this effect were significant

section 2.6.

a smaller anisotropy would be found for fission fragments in the lower group compared to the high energy group.

The count rate of α -particles was monitored constantly for all four pairs of detectors and recorded on a chart recorder together with a reading of the resistance thermometer and the count rate of a neutron counter for the beam intensity. From this recording it could easily be detected that the α -count rate was considerably influenced by the neutron beam, which is probably due to the γ -flash. As the beam went on the recorded α -count rate increased to a higher level in about 10 to 15 minutes. The time for settling down to the original level after the beam went off was somewhat longer. This increase in count rate seemed to be linear with the beam intensity. A few detectors which were replacing the ones that had failed, seemed to be much more sensitive to the neutron beam than the detectors previously used although the new ones had the same specifications.

The neutron intensity was monitored by three counters having different positions with respect to the neutron booster. These monitors can be used by all machine users as a standard measure for neutron output. Furthermore two BF_3 -counters were used independently to determine the integrated flux for the various runs.

Pulses selected as fission events from the four sets of electronics, numbered E1 to E4, were transmitted to the counting laboratory by cables of approximately 150 m length. Recording of a fission event had to be done by writing information concerning the difference between the electron pulse of the linear accelerator and the time of the fission event on the 1" magnetic tape. The master timing unit (MTU) was a 16 MHz oscillator which governed the time of firing of the electron pulse, as well as any recording equipment, to rule out any difference in zero time. A delay of a few microseconds was taken before starting the recording to avoid the high energy region in which also the γ -flash occurs. After this delay time was divided into channels of specified length; recording of a fission event could be done by assigning a channel number corresponding to the time between the event and firing

of the machine. A total number of 16384 (2^{14}) channels was available which had to be divided into 4 sets of 4096 (2^{12}) channels for the 4 electronic sets. For this purpose the first 2 bits of a recorded word of 14 bits were reserved for the coding of the 4 electronic sets: E1 (0,0), E2 (0,1), E3 (1,0), E4 (1,1). The division of the 4096 channels into suitable time regions could be equal for the experiments with ^{233}U and ^{237}Np , namely 2048 channels of $1/8 \mu\text{sec}$, 1024 of $1/2 \mu\text{sec}$, 512 of $1 \mu\text{sec}$ and 512 of $2 \mu\text{sec}$. The magnetic tape recorder was operated in a single shot mode where, for each cycle of the machine, only one event can be recorded for each set of 4096 channels, after which the recorder is blocked until release at the start of the next machine cycle. Because of the low count rates, especially with ^{237}Np , a count-loss correction which accumulates as the time increases is practically negligible. The tape could be run at low speed so that it would last at least for 24 hours of data collection.

The fission fragments were monitored once more in the counting laboratory through a time gate in order to be able to localize spurious counts which might be generated by the electronic equipment.

The first phase of processing data could be done with a PDP-4 computer. The channel numbers written on magnetic tape were accumulated into 4 separate time-of-flight spectra. These were labelled and archived on $\frac{1}{2}$ " magnetic tapes for further analysis. Also the summing of runs was done on this computer. The many calculations which were necessary to bring the results into a practical form were performed on the IBM-360/65 computer at Harwell, during the last stage of experiments on an IBM-360/75.

First of all a background had to be subtracted from the measured time-of-flight spectra. As described above background runs were taken with black resonance absorbers in the beam to determine the relative form of the background. A curve was fitted through the channel regions of absorption and normalized to the absorption regions of sodium and cadmium in the actual runs. The analytical curve fitting the background points best was mostly of the type:

section 2.6.

$$BG(t) = a_0 + \frac{a_1}{t} + \frac{a_2}{t^2} + \frac{a_3}{t^3} .$$

At this stage of processing also the small count-loss correction was made.

Further calculations were performed to calculate the anisotropies of resonances. The effects could be calculated directly from the ratio of counts in a certain channel region if the relative normalizations between the detectors at 0° and 90° were known. In principle the measurements at higher temperature (6 K) should yield this relative efficiency with great accuracy and indeed the normalization ratio had a very small statistical error. However, drift in the pulse height characteristics made considerable changes in the relative efficiency during the periods when cold runs were taken between two series of warm runs. In a few cases the normalization ratio had to be corrected because of drop-out of detectors. Also uncertainty in background subtraction introduced small systematic deviations in the normalization ratio. Finally, there was a small residue of nuclear alignment at the temperature of about 6 K for the warm runs; this factor would at the most change the normalization ratio by 0.5%. An estimate of the total systematic error in the normalization ratio based on these considerations and on the actual spread in the calculated ratios, led to 2% for the measurements on ^{233}U .

For ^{237}Np the method for determination of the relative efficiencies had been simplified by assuming that for the warm runs the number of counts under resonances in the fission cross section of ^{237}Np was proportional to the number of counts in the background. Since a few warm runs would give a normalization ratio which was statistically very inaccurate, it was attempted to see whether a good normalization ratio would result if the total number of counts from background and resonances were taken. Since the background counts exceeded the resonance counts by far, despite reduction of the background by the cadmium filter, it was sufficient to determine the normalization from the total counts in the cold runs. By comparison with corresponding warm runs, it was verified that there were no noticeable temperature effects in the background.

This method of normalizing between detectors eliminated a few systematic errors, for instance the error due to inappropriate fitting of a parameterized curve through the background of the warm runs, at the expense of introducing an uncertainty over small temperature effects in the background and a possible effect of inhomogeneities in intensity of the background. The total systematic error in the normalization ratio is estimated to be 3 to 4%.

The calculation of anisotropies and A_2 -values of resonances was straightforward. Sums of counts were taken over channel regions where one resonance was predominant and the anisotropy for a group was taken as the normalized ratio of counts in the 0° - and 90° -direction. A_2 -values were obtained by feeding in the values for f_2 , $\langle P_2(\cos\theta) \rangle_{\theta=0^\circ}$ and $\langle P_2(\cos\theta) \rangle_{\theta=90^\circ}$. A statistical error in A_2 was only due to counting statistics in the cold runs. The estimated systematic error was consisting of the following components, as evaluated in the analysis of the data:

- 1) The uncertainty in background subtraction was estimated from statistical errors in the experimental background points and from the deviations between fitted curve and experimental points. This error amounted usually to 10 to 20% on the background in the cold runs.
- 2) The error in the normalization ratio was estimated at 2% for ^{233}U and at 3 to 4% for ^{237}Np .
- 3) The solid angle correction on the Legendre polynomials and related errors have been given in section 1 of this chapter.
- 4) The uncertainty in the value of the f_2 -parameter, resulting from temperature differences in the sample and from estimates on the error in the hyperfine splitting constants, was an important contribution to the total systematic error.

The total systematic error was taken as the square root of the sum of the various components. Other possibilities for systematic errors arising in the experiment have been discussed elsewhere.

A standard routine for the display of the distribution of A_2 -values for resonances in the fission cross section of ^{233}U was the pseudo-

section 2.6.

histogram, which was first used by Dabbs³⁰). A probability function is calculated as a sum of Gaussian functions: the A_2 -value and related statistical error ΔA_2 of each resonance are represented by a Gaussian function, with peak position A_2 , FWHM ΔA_2 and total area unity:

$$F(A_2) = \sum_i \frac{1}{\sqrt{2\pi} \Delta A_{2i}} \exp \left[- \frac{(A_2 - A_{2i})^2}{2\Delta A_{2i}^2} \right]$$

References

1. J.L. Hoard and J.D. Stroupe, Chemistry of Uranium, USAEC TID-5290 (1953), Book 1, 323.
2. G.H. Dieke and A.B.F. Duncan, Spectroscopic Properties of Uranium Compounds (McGraw-Hill Book Company, Inc., New York, 1949), 1st ed., 33.
3. J.C. Waldron, report AERE-R6141 (1969).
4. The analysis has been done by E.A.C. Crouch, Chemistry Division, AERE, Harwell.
5. H. London, G.R. Clarke and E. Mendoza, Phys. Rev. 128 (1962) 1992.
6. T.P. Das, R. de Bruyn Ouboter and K.W. Taconis, Proc. of 9th Intern. Conf. on Low Temperature Physics Columbus, Ohio (1965), Part B, 1253.
7. B.S. Neganov, N. Borison and M. Liburg, Soviet Phys. - J.E.T.P. 23 (1966) 959.
8. H.E. Hall, P.J. Ford and K. Thompson, Cryogenics 6 (1966) 80.
9. J.C. Wheatley, O.E. Vilches and W.R. Abel, Physics 4 (1968) 1.
10. H. Postma, report AERE-R 6169 (1969).
11. H. Postma, Nucl. Instr. and Meth. 88 (1970) 45.
12. This calibration was done by J.N. Haasbroek, Kamerlingh Onnes Laboratorium, Leyden.
13. J. Mellema and H. Postma, Nucl. Phys. A 154 (1970) 385.
14. E.R. Reddingius, Thesis, University of Leyden (1970).
15. A.R. Miedema, H. Postma, N.J. v.d.Vlught and M.J. Steenland, Physica 25 (1959) 509.
16. A.C. Anderson, G.L. Salinger and J.C. Wheatley, Rev. Scient. Instr. 32 (1961) 110.
17. W.M. Gibson, G.L. Miller and P.F. Donovan, Alpha-, Beta- and Gamma-Ray Spectroscopy (ed. K. Siegbahn, North-Holland Publishing Company, Amsterdam, 1965), Vol. 1, 345.
18. P.J. van Heerden, Phys. Rev. 106 (1957) 468.
19. F.J. Walter, J.W.T. Dabbs and L.D. Roberts, report ORNL-2877 (1960).
20. H.C. Britt and H.E. Wegner, Rev. Sci. Instr. 35 (1964) 842.
21. I. Purica, L. Schächtler and M. Badanoiu, Rev. Roum. Phys. 14 (1969) 809.

References

22. E.R. Rae, Fundamentals in Nuclear Theory, Lect. of Intern. Course, Trieste (IAEA, Vienna, 1967) 831.
23. W.M. Good and E.R. Rae, report AERE-NP/GEN 21 (1962).
24. E.R. Rae and W.M. Good, Experimental Neutron Spectroscopy (Acad. Press Inc., New York, 1970).
25. M.C. Moxon, Nucl. Phys. Div. AERE, Harwell, private communications.
26. H.J. Groenewold and H. Groendijk, Physica 13 (1947) 141.
27. W.E. Lamb, Phys. Rev. 55 (1939) 160.
28. J.E. Lynn, Theory of Neutron Resonance Reactions (Clarendon Press, Oxford, 1968).
29. A. Michaudon, H. Derrien, C. Le Pipec and P. Ribon, Comptes Rendus 255 (1962) 2086.
30. J.W.T. Dabbs, C. Eggerman, B. Cauvin, A. Michaudon and M. Sanche, Proc. of 2nd Symposium on Physics and Chemistry of Fission, IAEA, Vienna (1969) 321.

Chapter III

ANISOTROPY OF α -EMISSION AND OF FISSION BY THERMAL NEUTRONS

3.1. Introductory remarks

The emission of α -particles by heavy nuclei is generally a complicating factor in the measurements of the angular distribution of fission fragments. Besides the fact that the α -activity makes it difficult and dangerous to handle the samples, it gives a considerable heat input to the crystals, preventing efficient cooling of the target to low temperatures. The α -activity is also a problem because of the radiation damage induced to the semi-conductor detectors and possibly to the samples.

On the other hand however, the α -particles, having a preferential direction of emission for non-spherical nuclei, may be measured separately from the neutron-induced fission, since the energy of the α -particles is much lower than the average energy of fission fragments and therefore easily discriminated. Hence, the anisotropy in the α -emission may yield useful additional information about the actual degree of orientation of the heavy nuclei and about the quality of various samples.

Independent measurements on the anisotropy of the α -activity from ^{237}Np and ^{233}U , where the target nuclei were oriented in relatively thin samples, were performed to check on possible systematic errors in the experiments with thick samples consisting of many crystals. The α -particles from ^{235}U are masked completely by the strong α -activity from ^{234}U ; this even-even isotope is not oriented and hence, no anisotropy will be observed in this emission. It is a serious disadvantage that details of the α -decay are insufficiently known to predict quantitative results on the anisotropy in the α -emission in an accurate way.

The anisotropy effect in the fragments from fission by thermal neutrons of aligned ^{233}U and ^{235}U as measured at the High Flux Reactor at Petten will provide extra normalization points to the measurements of the anisotropy as a function of neutron energy from the experiments at the Harwell linac. ^{237}Np does not have a perceivable thermal fission

section 3.2.

cross section and thus, only the α -anisotropy can be determined. Results on measurements of the anisotropy in α -emission and in fission by thermal neutrons from the High Flux Reactor at Petten are presented, together with an interpretation which intends to come to a conclusion about the relative influences of several effects which may be causes of systematic errors:

1. There are uncertainties about the relative contributions from detectors in 0° - and 90° -direction, caused by instability of the detectors.
2. A temperature gradient across the RUN-crystals makes it necessary to calculate an effective temperature in order to correct a temperature difference; this effect is combined with uncertainties in hyperfine-splitting parameters.
3. The scattering of fission fragments, especially in thick samples, might reduce the measured anisotropies.
4. Misorientation of the target material as a coating on the base RUN-crystals and misorientation of individual crystals in samples consisting of many crystals, can be checked by measuring single crystals with very thin coatings.

3.2. ^{237}Np

The anisotropy effect in the α -emission, for the composite samples A and B intended for fission-fragment counting, was measured several times during the period in which the fission experiments were carried out, as a function of temperature. Measured at the beginning of the experiment, as well as one year later during the last stage of data collection, no deterioration in the absolute effect at the lowest temperatures could be observed over this period, although the crystals were badly cracked and therefore inappropriate cooling easily might have occurred.

An example of these measurements is shown in fig. 3.1. Normalization of the experimental data, according to the relative efficiencies of the detectors in the 0° - and 90° -direction, has to be done by extrapolation to $1/T = 0$ of the experimental curve of

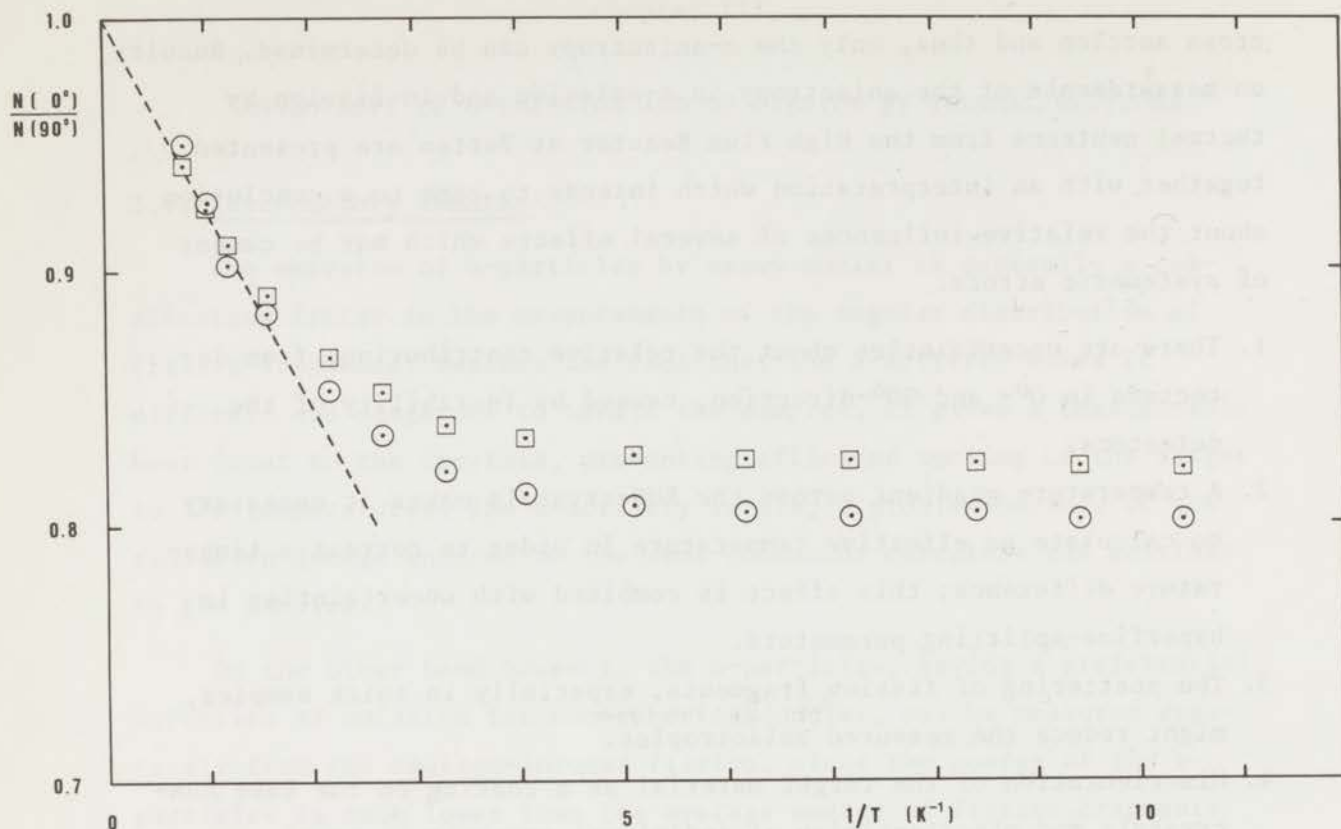


Fig. 3.1.

Anisotropy in the α -emission from ^{237}Np as a function $1/T$ measured at the composite samples A (squares) and B (circles).

$N(0^\circ)/N(90^\circ)$. Experimental points at higher temperatures can be taken by heating of the mixing chamber. Extrapolation to zero-orientation at $1/T = 0$ is not always accurate and hence, the absolute maximal effect is somewhat uncertain. The chosen example in fig. 3.1 shows that sample B had a greater effect than the heavily coated sample A, but in other measurements with the same samples, then with less experimental points, the effects were more equal.

An important feature in the relative form of the curves, which is more reliable than the absolute height, is that the anisotropy is quickly saturating and hardly changing below 0.2 K. This saturation temperature is equal for both curves.

The f_2 -parameter as a function of temperature can be calculated

section 3.2.

using the hyperfine-splitting parameters given by Bleaney ¹⁾, and shown in table 1.4. These values are known very accurately and thus the f_2 -parameter will show little variation within the limits of error on the hyperfine-splitting parameters. The f_2 -parameter according to a single electric-quadrupole term has been given in chapter I, section 1.1.3. A positive value of P would result into a negative alignment parameter f_2 , which at high temperatures would be proportional to $1/T$. The magnetic-dipole term alone yields positive values of f_2 , irrespective of the sign of the constant A ; at high temperatures the f_2 -parameter is proportional to $1/T$. The two hyperfine terms together would have counteracting effects in the f_2 -parameter, if P is positive. At high temperatures the electric-quadrupole interaction is dominant.

The f_2 -parameter is shown as a function of $1/T$ together with the relatively unimportant f_4 -parameter in fig. 3.2. The f_2 -curve calculated shows a plateau from approximately $1/T = 6$ to 10 K^{-1} . At lower temperatures the absolute value of f_2 increases slightly again. Comparison of the two experimental curves in fig. 3.1 and the dependency of the computed f_2 -parameter on temperature shows that saturation of the anisotropy occurs roughly at the temperature where the plateau in the f_2 -parameter starts.

The measurements of the α -anisotropy with one single crystal only could be extended to somewhat lower temperatures, although not sufficiently low to detect a possible increase in anisotropy, beyond the plateau on the f_2 -curve. The crystal had a total weight of 0.72 mg ^{237}Np and a total area of 0.81 cm^2 . Normalization of the counters in the 0° - and 90° -direction was still problematic, but the results for the various runs seemed to be consistent. The last run, when normalized independently, gave a difference of 10% in the measured anisotropy with the other runs; the experimental points at higher temperatures in that run were somewhat in error and therefore the normalization ratio was corrected by such a value, that the anisotropy at low temperature was equal to the other runs. In fig. 3.3 the values for $N(0^\circ)/N(90^\circ)$ have been plotted against $1/T$. For the slope at high temperatures an experimental value can be given:

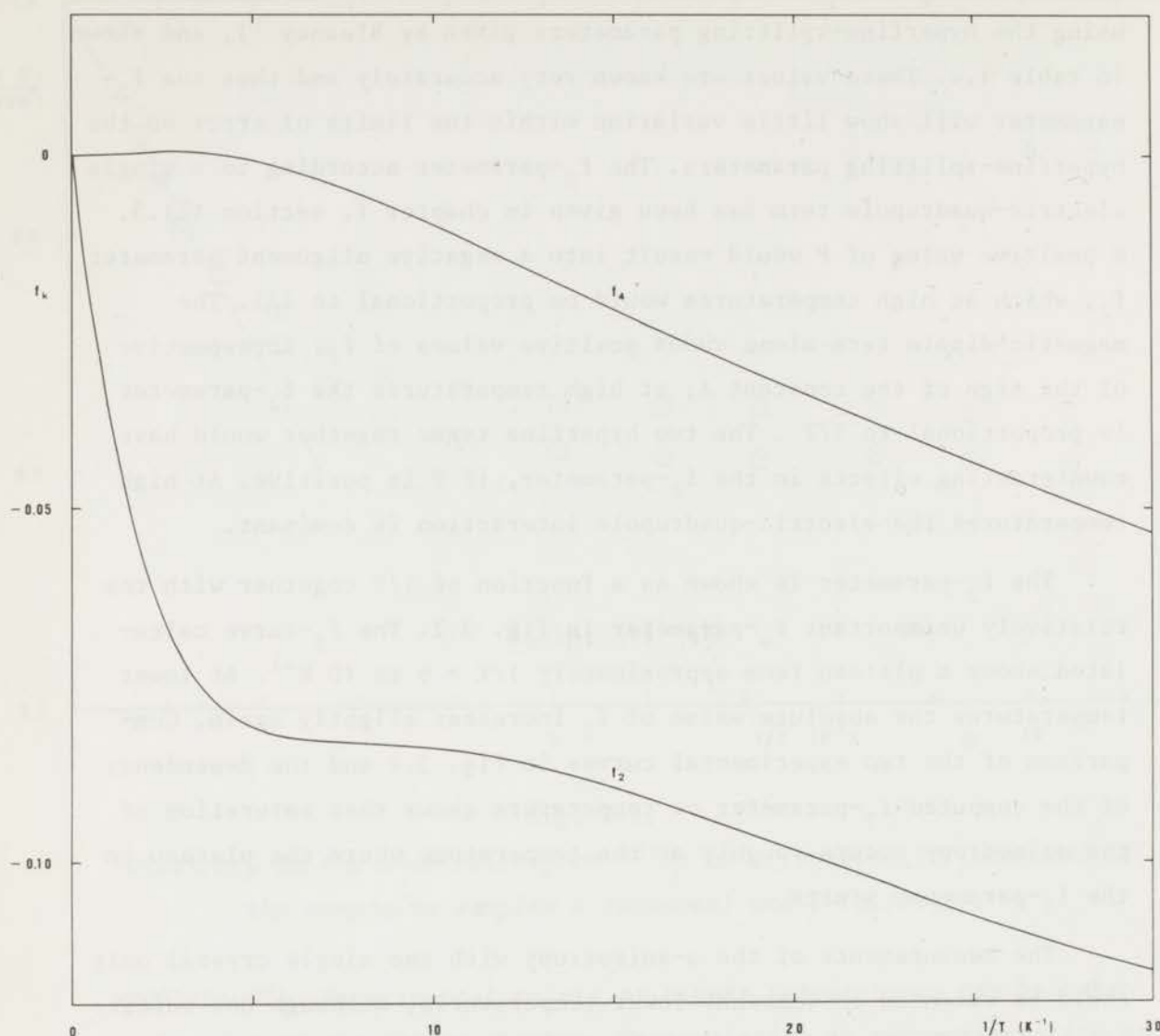


Fig. 3.2.

Orientation parameters f_2 and f_4 as a function of $1/T$ for ^{237}Np in RNN, according to the hyperfine-splitting parameters by Bleaney ¹).

$$\frac{N(0^\circ)}{N(90^\circ)} - 1 = - \frac{(0.102 \pm 0.005)}{T} .$$

The solid curve in fig. 3.3 is the calculated anisotropy corresponding to a value for $A_2 = 2.24$. This curve seems to fit the experimental data rather well; the slope of this fitted curve at high temperatures is -0.098 which is within the limit of the error quoted on the ex-

section 3.2.

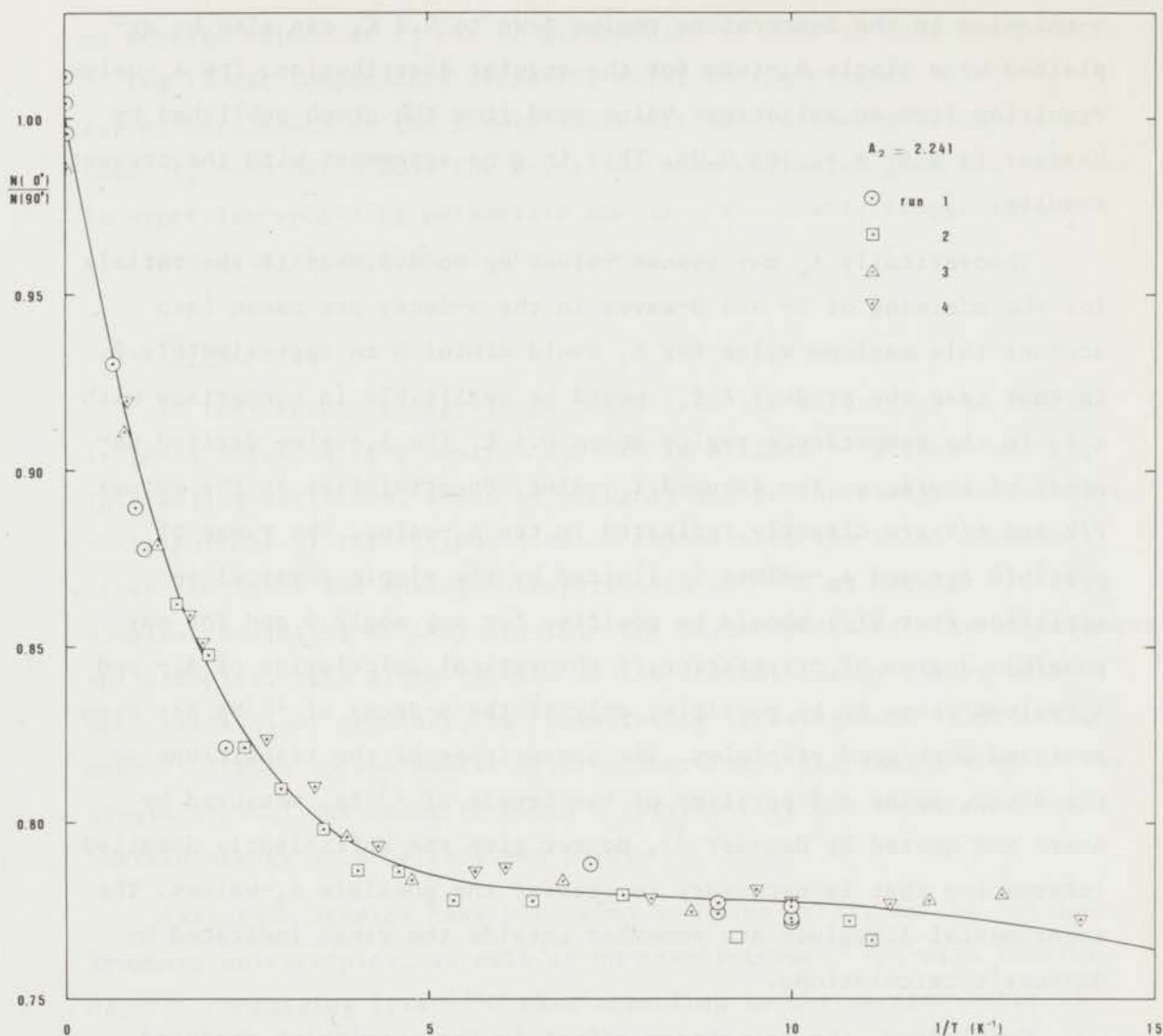


Fig. 3.3.

Anisotropy in the α -emission from ^{237}Np as a function of $1/T$ measured at one crystal; the solid curve represents the theoretical dependence for an A_2 -value of 2.24.

perimental value. A systematic error of about 10% has to be put on the value for A_2 , mainly because of the normalization ratio.

It is impossible to derive a value for A_4 from the experimental data, since the f_4 -parameter is very small in the temperature range obtained in the experiment. Measurements by Hanauer et al.³⁾ on the

α -emission in the temperature region down to 0.2 K, can also be explained by a single A_2 -term for the angular distribution. The A_2 -value resulting from an anisotropy value read from the graph published by Hanauer is : $A_2 = +2.16 \pm 0.06$. This in good agreement with the present results.

Theoretically A_4 may assume values up to 6.3, but if the ratio's for the admixing of S- and D-waves in the α -decay are taken into account this maximum value for A_4 would diminish to approximately 2. In that case the product $A_4 f_4$ would be negligible in comparison with $A_2 f_2$ in the temperature region above 0.1 K. The A_2 -value derived depends of course on the assumed f_2 -value. Uncertainties in the values P/k and A/k are directly reflected in the A_2 -value. The range of possible A_2 - and A_4 -values is limited by the simple physical restriction that $W(\theta)$ should be positive for any angle θ and for any possible degree of orientation. A theoretical calculation of A_2 - and A_4 -values seems to be possible, only if the α -decay of ^{237}Np has been analyzed with good precision. The intensities of the transitions in the decay, spins and parities of the levels of ^{233}Pa , measured by Asaro and quoted by Hanauer ³⁾, do not give the sufficiently detailed information that is necessary to predict the possible A_2 -values. The experimental A_2 -values are somewhat outside the range indicated by Hanauer's calculations.

Concluding, the anisotropy effect in the α -emission measured down to $T = 0.07$ K can be fitted simply by an angular distribution which does not include a term with A_4 . It is important to note that in the case of ^{237}Np it is a priori not necessary to introduce a difference between effective sample temperature and measured temperature on the cooling plate, although such a difference may be present below $T = 0.2$ K, because of the invariance of the f_2 -value in that temperature region.

For the experiment on the fission-fragment anisotropy from ^{237}Np

section 3.3.

an average value for f_2 can be given which is more or less independent of the lowest temperature obtained, owing to the plateau in the f_2 -curve. Regardless of the sample thickness the following value can be used: $f_2 = -0.082 \pm 0.004$. The error has been estimated from the variance in hyperfine-splitting parameters and from reasonable temperature deviations from the middle of the plateau.

3.3. ^{235}U

In the neutron energy range below 1 eV the anisotropy in fission-fragment emission from neutron capture in aligned ^{235}U shows an interesting variation, which is probably due to the change in relative contributions of the various fission channels to the total fission cross section. The analogous experiments on ^{235}U at Harwell ⁴⁾, with samples consisting of many crystals for measurements of fission-fragment anisotropies, have given results in the thermal energy region with good statistical accuracy, but uncertainty in background subtraction made it liable to systematic errors. Therefore, the measurement at the single crystal was meant to yield a correct absolute value of A_2 at a certain energy as a calibration point.

Extensive studies have been done by Dabbs et al. on the fission-fragment anisotropies, as well as on α -anisotropy ⁵⁻⁸⁾, with samples of ^{235}U containing less ^{234}U than according to the natural ratio of the two isotopes. Correcting for the α -emission from ^{234}U , which is an even-even nucleus and therefore not aligned, it was possible to measure the relatively weak α -emission from ^{235}U .

The target material enriched in ^{235}U that was used for the preparation of the samples at Harwell was of such a composition that the α -decay of ^{235}U was completely hidden under the strong contribution from ^{234}U . Therefore, no additional information could be derived from the α -anisotropy and a calibration measurement, necessary for the lowest neutron energy region, had to rely solely on the fission-fragment anisotropy at thermal neutron energy.

The single crystal used for the calibration experiment had a

coating thickness of $0.7 \text{ mg } ^{235}\text{U}/\text{cm}^2$, comparable to the average thickness of the thinnest sample in the Harwell experiments. The fission fragment spectrum was smeared out, but the originally double-humped structure was still perceivable as shoulders in the measured spectrum. The fission-fragment anisotropy was measured at a neutron energy $E_n = 0.034 \text{ eV}$ in the temperature range from 4.2 K down to 0.032 K. The results are shown in fig. 3.4 as a plot of the ratio of counts in the 0° - and 90° -direction versus the reciprocal of temperature.

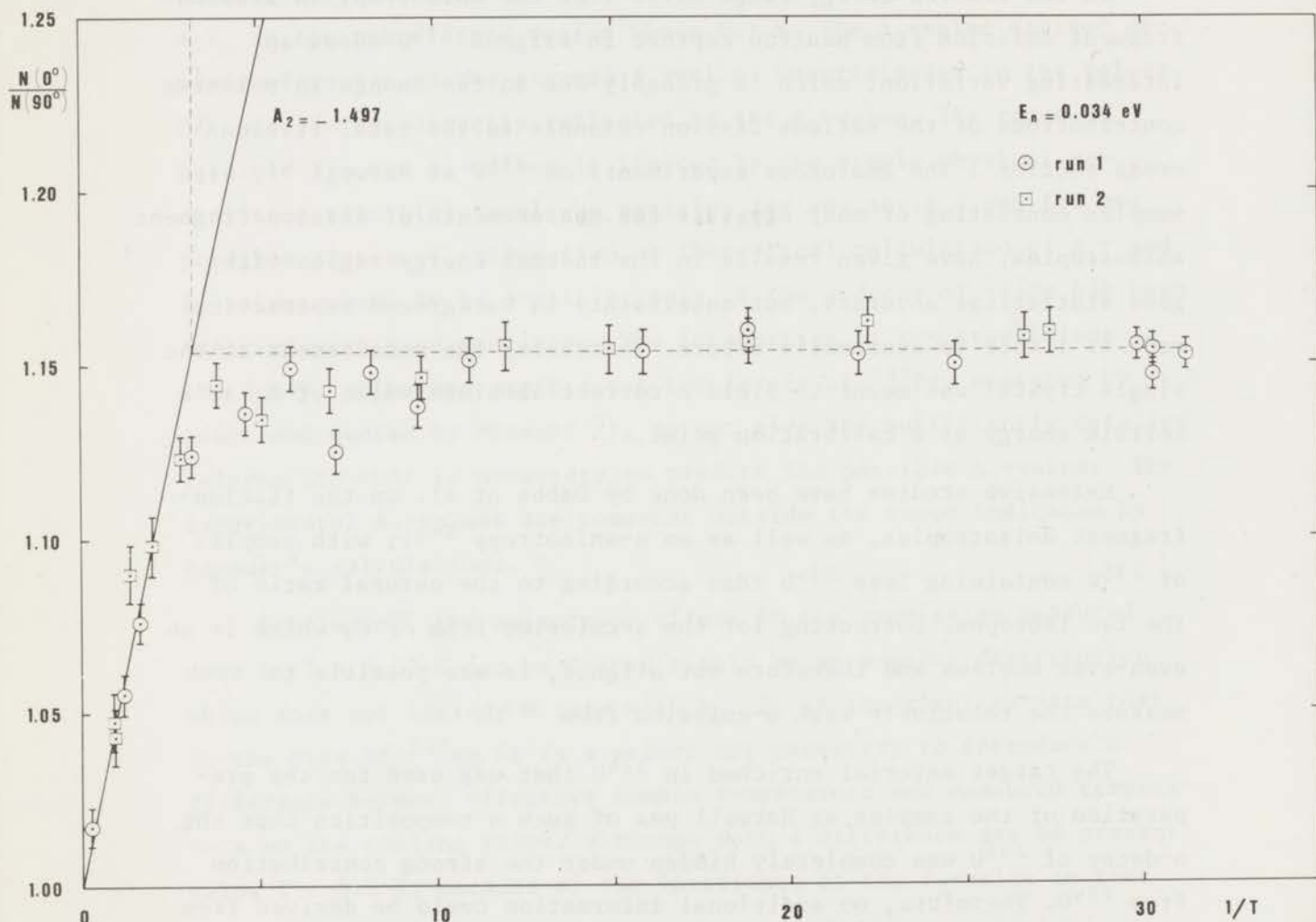


Fig. 3.4.

Anisotropy as a function of $1/T$ for fission fragments from capture of thermal neutrons in ^{235}U measured at one crystal. The solid curve represents a theoretical dependence according to an A_2 -value of -1.50 .

section 3.3.

The data obtained in two separate runs are consistent with one another over the whole energy range. It is striking that the anisotropy effect is quickly saturated and already at $1/T = 6$ the maximum value has been reached.

A theoretical calculation of the anisotropy effect, based on an effective-spin Hamiltonian which consists exclusively of an electric-quadrupole coupling term, will show a variation at high temperatures which is proportional to $1/T$. In fig. 3.5 the orientation parameters f_2 , f_4 and f_6 are presented as a function of temperature, calculated from the quadrupole constant $P/k = +0.0154$ K. At high temperatures only the f_2 -parameter can give a contribution to the anisotropy. Hence, the value for A_2 can be derived already from the slope in the experimental anisotropy above $T = 0.5$ K. In that region:

$$N(0^\circ)/N(90^\circ) = 1 + \frac{0.050 \pm 0.002}{T} .$$

The high-temperature approximation for f_2 is $-\frac{12}{7} \frac{P}{kT}$. The resulting value of $A_2 = -1.50$, with an experimental error of 4%. With this value for A_2 somewhat closer limits can be drawn on A_4 ; this parameter can be estimated to be roughly between +2 and -4. The f_4 -parameter is positive and increases to such values that below 0.1 K the term with $k = 4$ might have a slight influence on the anisotropy if A_4 assumes a large value. The term with $k = 6$ is completely negligible even for an A_6 -parameter having the maximum theoretical value. The saturation of the experimental curve below 0.1 K cannot be explained by these higher-order terms.

The saturation effect on the anisotropy in the lower temperature region as shown in fig. 3.4 has to be explained, either by a temperature gradient over the sample material, or by a magnetic-dipole term additional to the electric-quadrupole term in the effective-spin Hamiltonian. These effects may also occur simultaneously.

As to the first possibility for a cause of the discrepancy, it was estimated in chapter II, section 3, that thermal contact resistances and low heat conductivity might become important below 0.2 K. For these estimates a more or less ideal thermal contact had been assumed; this might not be the case under experimental circumstances.

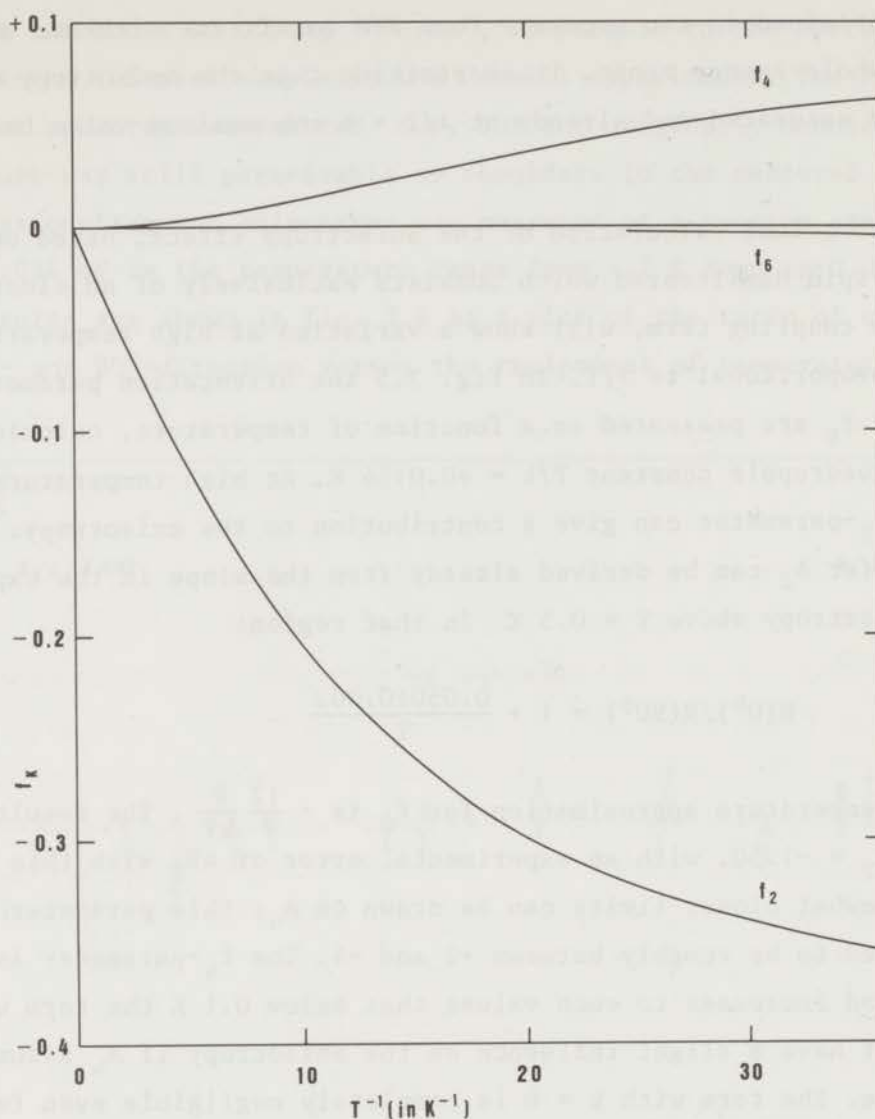


Fig. 3.5.

Orientation parameters f_2 , f_4 and f_6 as a function of $1/T$ for ^{235}U in RUN, according to a quadrupole-coupling constant $P = 0.0154$ K.

The experimental curve however, shows deviations from the calculated anisotropy already at $1/T = 3 \text{ K}^{-1}$, and at $1/T = 6 \text{ K}^{-1}$ the effect is completely saturated. Since in the case of ^{237}Np , having exactly the same experimental circumstances, the measured temperature dependence of the anisotropy effect was fitted precisely by the calculated curve, it seems that temperature differences between sample surface and

section 3.3.

cooling plate are probably not sufficient to explain the discrepancy, albeit below $T = 0.1$ K effective temperature differences are likely to occur. Measurements on ^{235}U at Harwell ⁴⁾ showing a considerably lower saturation temperature indicate that the thermal contact between RUN-crystals and cooling plate is not very reproducible.

It was also considered that the relaxation times for nuclear orientation in RUN might be rather long. In order to assist the alignment 0.5% RNN-solution was added to the RUN-solution which was used for the coating of the base crystals. Since the sample at Petten constantly remained at the lowest temperature obtained for at least 24 hours and did not show any change in anisotropy over such a period it is believed that relaxation in nuclear orientation can safely be ruled out as a possible cause for the discrepancy.

The second possibility is more difficult to evaluate, since there is no way to examine the effect independently from a measurement of the angular distribution of fission fragments and α -particles. If there is magnetic-dipole coupling, an external magnetic field will give a polarization parameter f_1 different from zero, but the even orientation parameters f_2 and f_4 are hardly influenced by a magnetic field. The value of f_1 might be determined by measuring the circular polarization from neutron-capture gamma-rays, but this is experimentally very tedious for fissile nuclei.

As discussed in chapter I, section 3, Pryce and Eisenstein made definite predictions about the electronic structure of the linear UO_2^{++} -group. The conclusion was that there are no unpaired electrons in the ground state of the uranyl-group and hence, magnetic-dipole interaction for the uranium nucleus should be absent.

If the crystal structure of the coating is not purely conforming with the structure of $\text{RbUO}_2(\text{NO}_3)_3$ - possible misorientation is inconsequential to this discrepancy in the anisotropy effect - a fraction of the uranium atoms might have a different valency, giving an extra electron which might occupy a level in the 5f-shell. This might give rise to magnetic-dipole interaction. The value of A/k that is necessary to account for the saturation is in the order of 0.1 K. In order to explain such a value with a magnetic-dipole moment of 0.35 n.m. for

^{235}U , the hyperfine field generated by one 5f-electron would have to be 1.4×10^7 Oe, which is excessively large.

Whatever cause there is for the rapid saturation of the anisotropy effect, an effective value of the f_2 -parameter can be determined unambiguously from the slope of the anisotropy curve at high temperatures, by projecting the maximum anisotropy on the calculated curve and reading an effective temperature corresponding to that point. The procedure has also been shown in fig. 3.4. The effective temperature is 0.31 K and the value for the orientation parameter is:

$$f_2 = -0.080 \pm 0.001 .$$

A systematic error was estimated to be 17%, resulting from the following components: 15% error in P/k , 5% in the geometrical factors, 4% experimental error on the slope, and 3% error on the value for the maximal anisotropy.

Measurements of the anisotropy effect were performed at two more neutron energies using another monochromator for the neutron beam. At these energies only the maximal effect was measured and no check was done on the temperature dependence. Neutron energies, corresponding A_2 -values, statistical and systematic errors are given in table 3.1.

Table 3.1.

E_n (eV)	A_2	STAT.ERROR	SYST.ERROR
0.034	-1.497	0.018 (1.2%)	18 %
0.047	-1.15	0.11 (9.4%)	39 %
0.125	-1.79	0.08 (4.7%)	24 %

Comparing these results to the measurements at low energy by Dabbs et al.⁸⁾, agreement seems to be satisfactory. At an energy $E_n = 0.14$ eV a value $A = 0.050 \pm 0.002$ was given in the published graph, where the quantity A is defined by:

$$W(\theta) = 1 + \frac{A}{T} P_2(\cos\theta).$$

section 3.3.

The corresponding value from the measurements at Petten at $E_n = 0.125$ eV is $A = 0.047 \pm 0.002$, which is at a slightly different energy, but the expected behaviour from a multilevel fit analysis on the resonances of ^{235}U done by Dabbs ⁸⁾ is rather invariant for a change in neutron energy in this region. At $E_n = 0.03$ eV this calculated curve indicates $A = 0.042$; the point presently measured at $E_n = 0.034$ eV, corresponds to $A = 0.0395 \pm 0.005$. The experimental value at $E_n = 0.047$ eV seems to disagree with the curve calculated by Dabbs, but this point was less accurate.

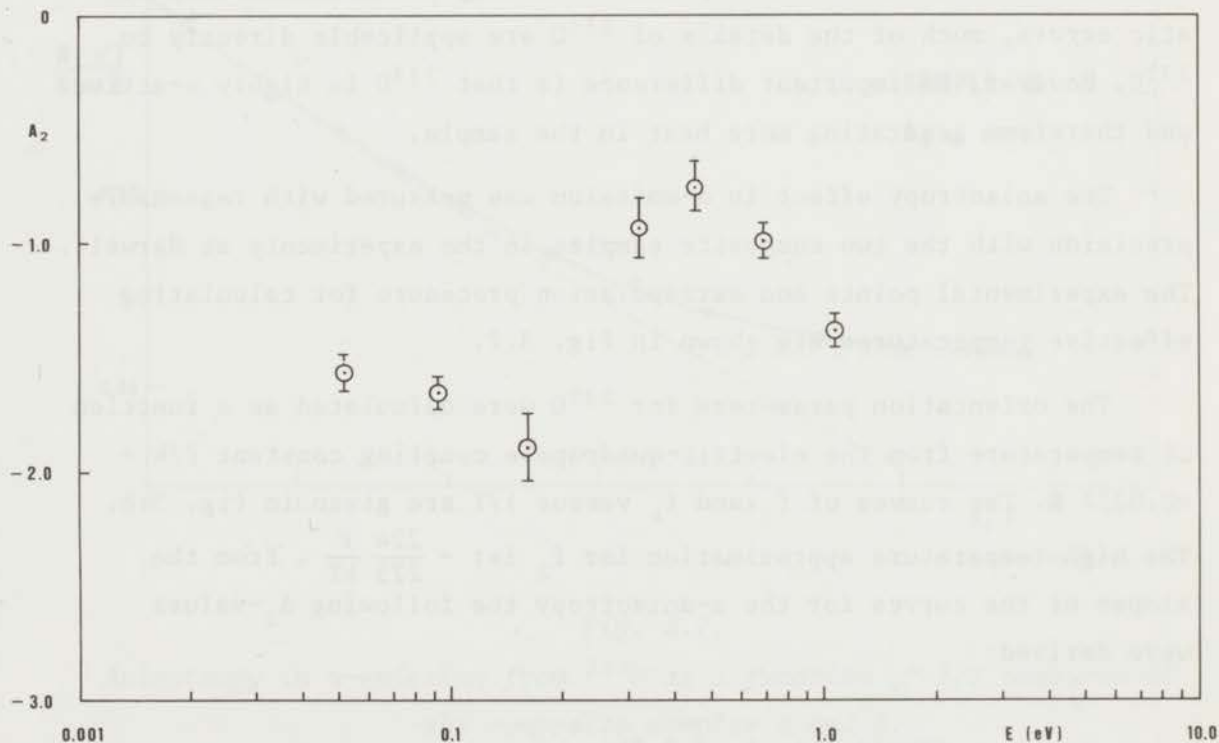


Fig. 3.6.

A_2 -values for fission fragments from ^{235}U in the low neutron energy region from the experiment at Harwell, renormalized to the A_2 -value at $E_n = 0.034$ eV measured at Petten.

The results from the experiment at Harwell for the A_2 -values at low neutron energies have been renormalized to the A_2 -value at 0.034 eV, given above. The original A_2 -values were larger by about 20%,

which is within the systematic error quoted by Pattenden and Postma ⁴⁾ for the A_2 -values over the neutron energy region from 0.4 to 60 eV. The renormalized results are presented in fig. 3.6. The form of the curve is very similar to the results by Dabbs et al. ⁸⁾ and shows a remarkable change in anisotropy over the 0.28 eV resonance. A detailed multilevel analysis is required to explain this asymmetric behaviour in the anisotropy.

3.4. ²³³U

The situation with ²³³U is completely analogous to that for ²³⁵U described above. Since this experiment is subject to the same systematic errors, much of the details of ²³⁵U are applicable directly to ²³³U. However, an important difference is that ²³³U is highly α -active and therefore generating more heat in the sample.

The anisotropy effect in α -emission was measured with reasonable precision with the two composite samples in the experiments at Harwell. The experimental points and extrapolation procedure for calculating effective temperatures are shown in fig. 3.7.

The orientation parameters for ²³³U were calculated as a function of temperature from the electric-quadrupole coupling constant $P/k = +0.0277$ K. The curves of f_2 and f_4 versus $1/T$ are given in fig. 3.8. The high-temperature approximation for f_2 is: $-\frac{224}{225} \frac{P}{kT}$. From the slopes of the curves for the α -anisotropy the following A_2 -values were derived:

$$\text{sample A : } A_2 = 2.36$$

$$\text{sample B : } A_2 = 1.97 .$$

Both values have a systematic error of about 20%. With an average temperature of 0.166 K measured on the cooling plate, sample A was effectively at a temperature of 0.31 K giving an alignment parameter $f_2 = -0.084 \pm 0.005$. For sample B this was 0.28 K and $f_2 = -0.095 \pm 0.005$ respectively. The saturation behaviour is rather

section 3.4.

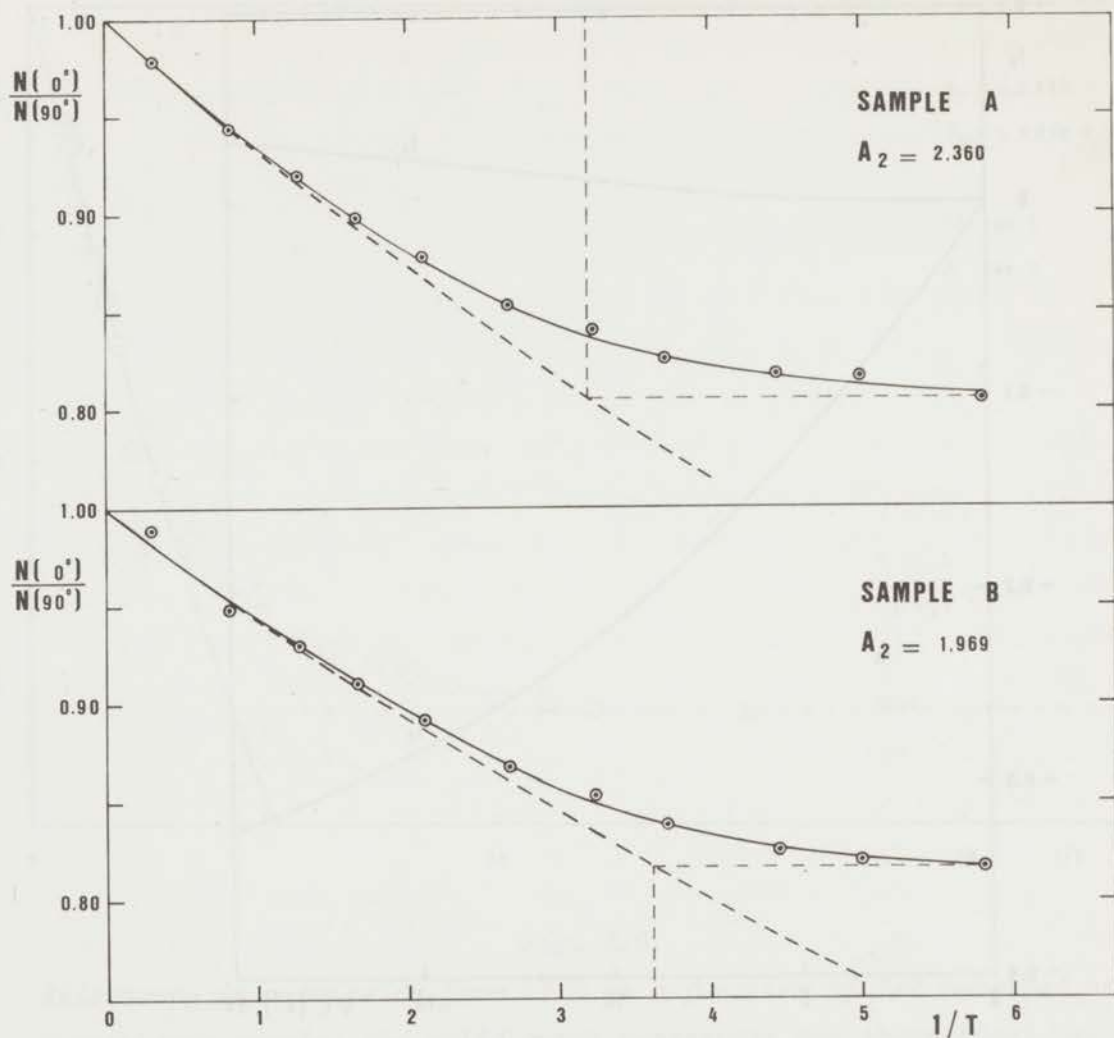


Fig. 3.7.

Anisotropy in α -emission from ^{233}U as a function of $1/T$ measured at the composite samples A and B.

similar for both samples and from the curves it is deduced, that the lowest effective temperature is reached at approximately $1/T = 6 \text{ K}^{-1}$.

The heat development from the α -activity prevented to reach lower temperatures. Normalization measurements therefore, had to be done at an extremely thin sample, which was prepared especially for this purpose. Its thickness of $0.082 \text{ mg } ^{233}\text{U}/\text{cm}^2$ is about 12 times less

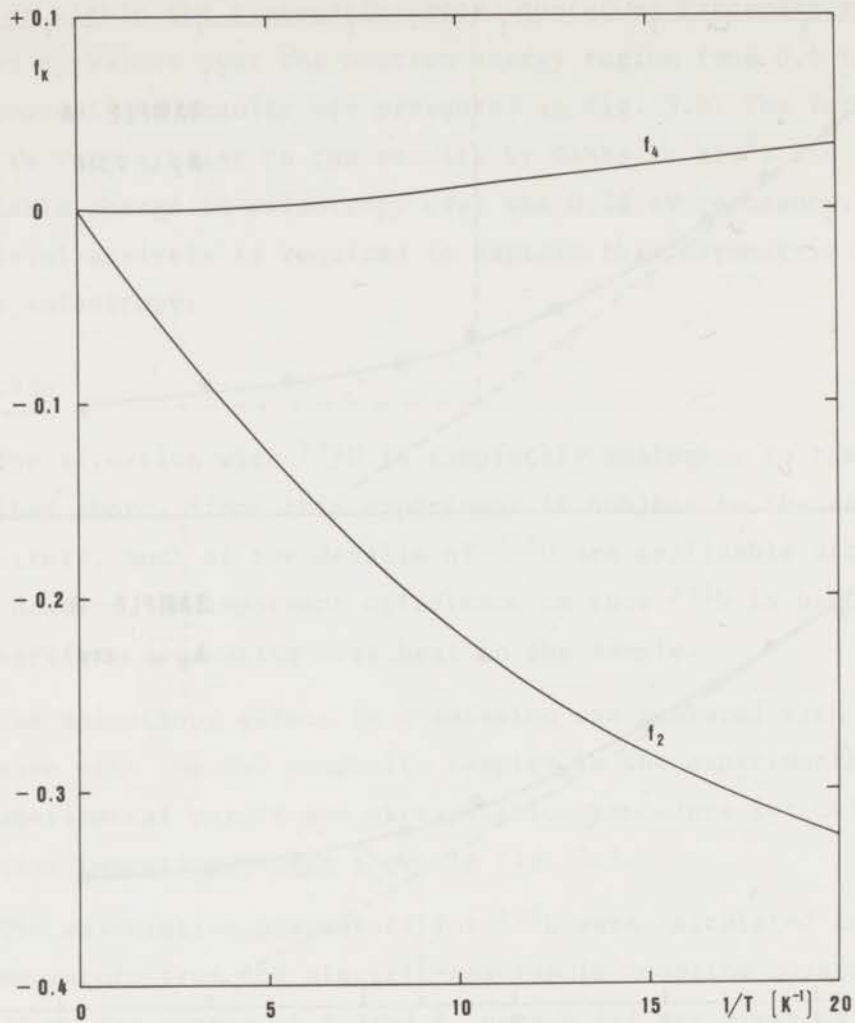


Fig. 3.8.

Orientation parameters f_2 and f_4 as a function of $1/T$ for ^{233}U in RUN, according to quadrupole-coupling constant $P = 0.0277$ K.

than for sample B. The spectrum of fission fragments showed a good separation between the high and low energy group so that systematic deviations due to scattering of fission fragments can be ruled out for these measurements.

The α -anisotropy was measured down to 0.043 K in two separate runs, as shown in fig. 3.9. The absolute statistical errors on the experimental points are about 0.0024. The saturation of the anisotropy is

section 3.4.

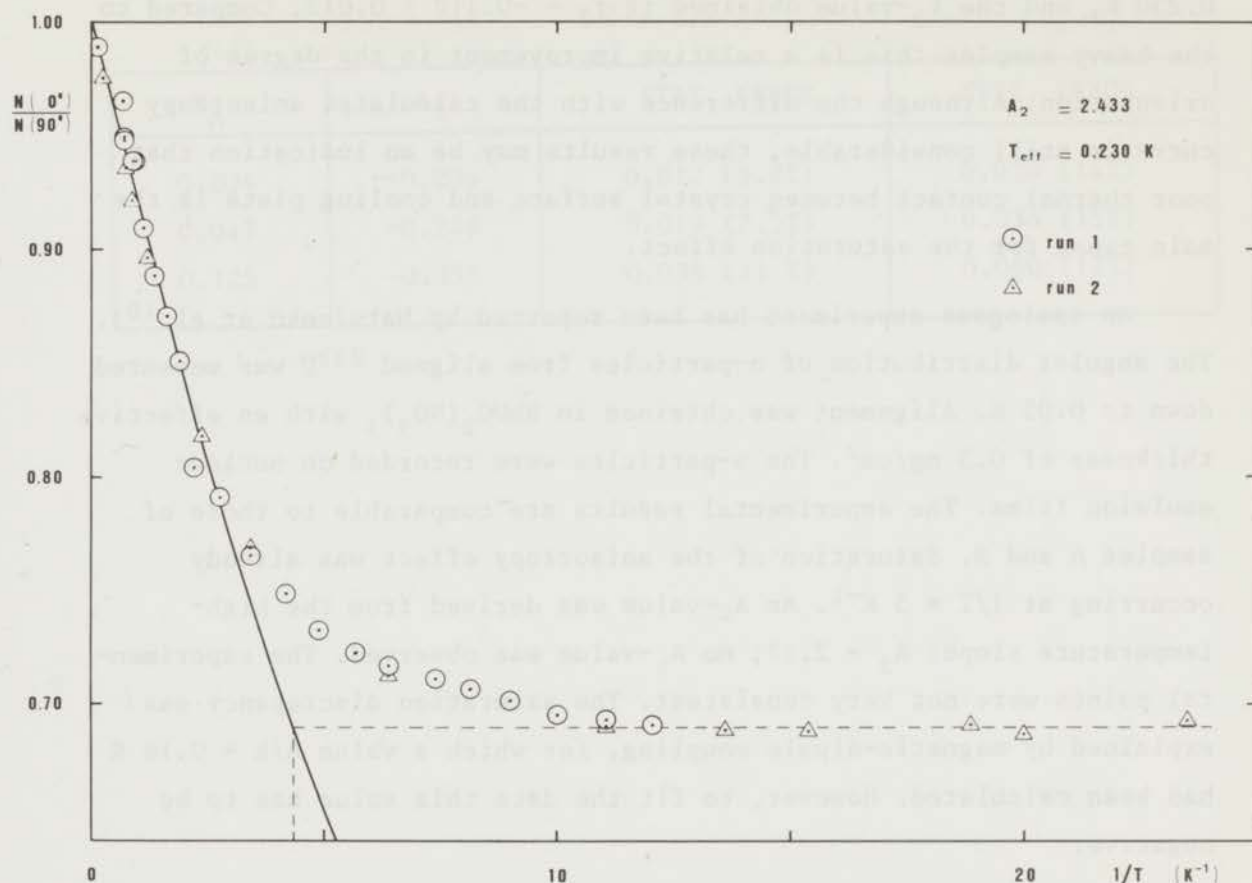


Fig. 3.9.

Anisotropy in α -emission from ^{233}U as a function of $1/T$ measured at a very thin sample; the solid curve represents the theoretical dependence for an A_2 -value of 2.433.

reached at $1/T = 11 \text{ K}^{-1}$, which is at a lower temperature than for the heavy samples, but the curve still shows a large discrepancy with the calculated anisotropy which corresponds to an A_2 -value of 2.433. The error on this value due to uncertainty in normalization is 2%.

Investigations on the α -emission from aligned ^{233}U by Roberts et al.⁹⁾ yielded a value of -0.0625 for the slope A of the anisotropy at high temperature, as defined in the previous section. This corresponds to an A_2 -value of 2.27.

The effective temperature for the maximum anisotropy effect is

0.230 K, and the f_2 -value obtained if $f_2 = -0.112 \pm 0.012$. Compared to the heavy samples this is a relative improvement in the degree of orientation. Although the difference with the calculated anisotropy curve is still considerable, these results may be an indication that poor thermal contact between crystal surface and cooling plate is the main cause for the saturation effect.

An analogous experiment has been reported by Matvienko et al.¹⁰). The angular distribution of α -particles from aligned ^{233}U was measured down to 0.05 K. Alignment was obtained in $\text{RbUO}_2(\text{NO}_3)_3$ with an effective thickness of 0.5 mg/cm^2 . The α -particles were recorded on nuclear emulsion films. The experimental results are comparable to those of samples A and B. Saturation of the anisotropy effect was already occurring at $1/T = 5 \text{ K}^{-1}$. An A_2 -value was derived from the high-temperature slope: $A_2 = 2.17$; no A_4 -value was observed. The experimental points were not very consistent. The saturation discrepancy was explained by magnetic-dipole coupling, for which a value $A/k = 0.16 \text{ K}$ had been calculated. However, to fit the data this value has to be negative.

Comparing the A_2 -values of the three different samples in the present experiment, the value for sample A agrees satisfactory with the A_2 -value from the thin single crystal. The low A_2 -value for sample B however, might indicate that roughly 10% of the target material was misoriented in this sample. On the other hand, a systematic error arising from the normalization of the data may partly cover the difference.

Fission-fragment anisotropies were measured for the same neutron energies as in the case of ^{235}U . The experimental results have been given in table 3.2. The comparatively low A_2 -values are in agreement with Dabbs et al.⁵), reporting anisotropies for thermal fission which are zero within the limits of statistical errors.

section 3.4.

Table 3.2.

E_n	A_2	STAT. ERROR	SYST. ERROR
0.034	-0.205	0.012 (5.8%)	0.028 (14%)
0.047	-0.249	0.019 (7.5%)	0.036 (15%)
0.125	-0.355	0.038 (11 %)	0.060 (17%)

References

1. B. Bleaney, P.M. Llewellyn and M.H.L. Pryce, Phil. Mag. 45 (1954) 922.
2. M.H.L. Pryce, Phys. Rev. Letters 3 (1959) 375.
3. S.H. Hanauer, J.W.T. Dabbs, L.D. Roberts and G.W. Parker, Phys. Rev. 124 (1961) 1512.
4. N.J. Pattenden and H. Postma, to be published in Nucl. Phys.
5. J.W.T. Dabbs, F.J. Walter, L.D. Roberts, G.W. Parker and J.O. Thomson, Phys. Progr. Report, ORNL-2910 (1960) 60.
6. J.W.T. Dabbs, F.J. Walter and G.W. Parker, Phys. Progr. Report, ORNL-3425 (1963) 82.
7. J.W.T. Dabbs, F.J. Walter and G.W. Parker, Phys. Progr. Report, ORNL-3582 (1964) 121.
8. J.W.T. Dabbs, F.J. Walter and G.W. Parker, Proc. of Conf. on Physics and Chem. of Fission, IAEA (Salzburg, 1965) Vol. I, 39.
9. L.D. Roberts, J.W.T. Dabbs and G.W. Parker, Proc. of 2nd U.N. Conf. on Peaceful Uses of Atomic Energy (Geneva, 1959) 322.
10. V.I. Matvienko, A.V. Kogan and K.A. Petrzhak, Sov. Jrn. of Nucl. Phys. 7 (1968) 297.

Chapter IV

ANISOTROPY IN THE ANGULAR DISTRIBUTION OF FISSION FRAGMENTS FROM
FISSION OF ORIENTED ^{233}U BY LOW ENERGY NEUTRONS

4.1. Introduction

The target nucleus ^{233}U in the ground state has spin and parity $\frac{5}{2}^+$. The compound nucleus $^{234}\text{U}^*$ resulting from s-wave neutron capture therefore can have spin and parity 2^+ and 3^+ . The transition states, as the available fission channels, can be taken from the table of transition states for even-even nuclei, as initially proposed by Wheeler ¹⁾ (see chapter I, section 3), on the basis of theoretical and experimental investigations.

The excitation energy of $^{234}\text{U}^*$ for capture of low-energy neutrons in ^{233}U is 6.78 MeV. The fission threshold of ^{234}U is lying approximately 1.4 MeV below this level, as measured by Northrop et al. ²⁾ and Usachev et al. ³⁾. From this excess in energy at the deformation saddle point the available transition states can be predicted, as given in table 4.1. From measurements of the angular distribution of fission fragments at higher excitation energies by Britt et al. ⁴⁾ and Griffin ⁵⁾ as reviewed by Huizenga ⁶⁾ and Lynn ⁷⁾, it could be concluded that the pairing gap at saddle-point deformation was about 2.2 MeV. Therefore, at low neutron energies the spectrum of available transition states will be relatively simple, not including single-particle excitations. Lynn ⁷⁾ indicated that for resonances having spin and parity $J^\pi = 2^+$, between two and four fission channels will be available and for 3^+ -resonances between one and two. The various channels are characterized by the spin and parity J^π and by the projection K of the spin on the nuclear symmetry axis. Fission proceeding through a certain channel will result in a well defined angular distribution of the fission fragments. The A_2 -value for the angular distribution is defined unambiguously by the K-value of the transition state, since K is supposed to be conserved throughout the non-collective part of the fission process, which is a rapid deformation of the nucleus after passage of the deformation barrier.

Table 4.1
Transition states for $^{234}\text{U}^*$

Energy	J^π	K	type of vibrational mode
11 keV	2^+	0	transition ground state
~ 0.7 MeV	$2^+, 3^+$	2	γ -vibration
~ 1.4 MeV	$2^+, 3^+$	1	mass-asymmetry plus bending vibration
~ 1.6 MeV	2^+	0	γ -vibration (2 quanta)

For a certain compound nuclear level possibly a few transition states contribute to fission and therefore the A_2 -value observed from the angular distribution for a certain neutron resonance will correspond to an effective K-value, which is the average of K-values for individual transition states weighted according to the partial fission widths for those states from the particular compound nuclear level.

The theoretically calculated A_2 -values for the various integral values of K in combination with spin and parity 2^+ and 3^+ have been given in table 4.2. The combination $(J^\pi, K) = (3^+, 0)$ is parity forbidden.

Table 4.2
 A_2 -values for the possible combinations of (J^π, K)

K \ J^π	2^+	3^+
	0	-2.68
1	-1.34	-2.01
2	+2.68	0
3		+3.35

section 4.2.

Although the A_2 - values for available transition states are different for the two spin states, the experimental A_2 -values for resonances of different spin may be rather close due to the mixing of transition states. This effect will make the distribution of A_2 -values for resonances narrower. Taking a large number of resonances however, it might be expected that there is a difference in the average A_2 -value of the resonances belonging to different spin groups.

It has been the purpose of the experiment to measure the distribution of A_2 -values for resonances. Since the split-up in the experimental distribution of A_2 -values of many resonances according to the spin groups would be small, the chances for spin assignment of resonances by the measured A_2 -values were expected to be low. The experimental distribution will be affected by overlapping of neighbouring resonances. This admixing of A_2 -values of resonances will make a distribution narrower. Interference between resonances of the same spin also might be an influence on the distribution of A_2 -values, but it is difficult to predict whether this effect will make the distribution narrower or wider.

The average behaviour of partial fission widths in the energy region, where the resonances cannot be resolved, is supposed to change at neutron energy intervals where new transition states open up. In the theory of Bohr ⁸⁾, further developed by Wheeler ¹⁾, the spacing of the vibrational levels at the saddle point having the same spin and parity is in the order of 0.2 to 0.5 MeV. In view of this, it cannot be expected that the average A_2 -values of energy intervals containing many resonances will change substantially over the neutron energy range 0 to 2000 eV in which the anisotropy of fission-fragment emission was observed. At most the opening of a particular channel might be noticed as a very gradual change in the average anisotropy.

4.2. Data-taking, calculations and results

In order to obtain results with reasonable counting statistics, so that not only accurate anisotropies would be derived for the neutron resonances, but also a form analysis might be applied onto the time-of-flight spectra of fission fragments, 4 months of data collection were required.

The resolution of the electron linear accelerator providing the necessary neutrons with a repetition rate of 192 pulses per second, combined with a flight-path length of 10.0 m, should enable to distinguish individual resonances up to a neutron energy of 80 eV, the average spacing of resonances being approximately 1 eV for ^{233}U . However, the counting statistics was too poor to make a useful separation of resonances in the ^{233}U fission cross section above 60 eV. Altogether, the anisotropy in the angular distribution of fission fragments was measured over the neutron energy range from 0 to 2000 eV. For a resonance analysis only the region from 0.4 to 60 eV proved to yield valuable information.

In the fission-fragment detection the time delay at the beginning of the time-of-flight spectrum amounted to 11 μsec , which was set up to avoid the gamma flash preceding every neutron pulse and to cut off the irrelevant high energy region as described in Chapter II. The pulse-height level for the discrimination of low-energy fission fragments against α -particles was sufficiently high to reduce the chances of deflection of fission fragments due to nuclear scattering. The monitor readings of the groups of high and low-energy fission fragments, did not result in a systematic difference in the anisotropy of both groups.

The background in the runs taken at high and low temperatures, which is due to fission fragments produced in the sample by neutrons scattered in surrounding materials, could be subtracted by analyzing the relative form from the background runs taken at the respective temperatures and normalizing this form to the absorption regions of sodium and cadmium in the actual runs.

The normalization factor between the detectors in the 0° - and 90° -direction was calculated from the corresponding warm runs, unless the drop-out of a detector made it impossible to use this calculated normalization factor. In the latter case a correction was applied, so that the average anisotropy was equal to that for the other series of runs.

The results for the measurements of the anisotropy in α -emission have been given in the previous chapter. Assuming that the value of

section 4.2.

Table 4.3.

Measured anisotropy of fission fragments for the samples A and B from 0 to 60 eV, together with an average of both samples obtained after re-normalization of sample B to sample A.

Energy interval in eV	Sample A		Sample B		Average results		
	A ₂	ΔA ₂	A ₂	ΔA ₂	A ₂	ΔA ₂	syst. error
0.255- 0.753	-1.08	0.27	-0.99	0.25	-1.12	0.18	0.21
0.753- 2.14	-1.30	0.04	-1.15	0.03	-1.33	0.03	0.21
2.14 - 2.84	-1.88	0.09	-1.62	0.07	-1.89	0.06	0.25
2.84 - 4.03	-1.23	0.13	-1.30	0.10	-1.41	0.08	0.22
4.03 - 5.45	-1.64	0.14	-1.58	0.11	-1.77	0.09	0.24
5.45 - 6.24	-1.39	0.20	-1.32	0.15	-1.49	0.12	0.22
6.24 - 7.35	-1.79	0.13	-1.63	0.08	-1.87	0.07	0.25
7.35 - 8.12	-1.65	0.30	-1.43	0.23	-1.66	0.18	0.25
8.12 - 9.04	-1.93	0.33	-0.83	0.23	-1.28	0.19	0.24
9.04 - 9.68	-1.38	0.30	-1.32	0.23	-1.48	0.18	0.23
9.68 - 11.14	-0.37	0.11	-0.28	0.08	-0.34	0.07	0.17
11.14 - 11.72	-1.27	0.27	-1.02	0.21	-1.22	0.17	0.21
11.72 - 13.41	-1.28	0.14	-1.21	0.10	-1.37	0.08	0.21
13.41 - 14.78	-1.36	0.24	-1.33	0.18	-1.48	0.14	0.22
14.78 - 15.89	-0.65	0.22	-0.57	0.16	-0.66	0.13	0.18
15.89 - 16.49	0.79	0.24	0.46	0.18	0.63	0.14	0.17
16.49 - 17.46	-0.68	0.24	-0.22	0.18	-0.40	0.14	0.18
17.46 - 18.32	-1.49	0.37	-1.42	0.28	-1.60	0.22	0.23
18.32 - 18.80	-1.17	0.40	-1.41	0.30	-1.47	0.24	0.22
18.80 - 19.98	-0.94	0.19	-0.55	0.14	-0.74	0.11	0.19
19.98 - 21.3	-0.61	0.28	-0.11	0.17	-0.25	0.14	0.17
21.3 - 22.2	0.17	0.21	0.36	0.15	0.34	0.12	0.17
22.2 - 22.6	-0.78	0.23	-0.39	0.16	-0.56	0.13	0.17
22.6 - 23.5	-1.37	0.22	-0.67	0.15	-0.97	0.12	0.20
23.5 - 24.9	-1.20	0.28	-1.11	0.20	-1.26	0.16	0.21
24.9 - 26.2	-1.22	0.29	-0.75	0.20	-0.99	0.17	0.20
26.2 - 27.6	-0.82	0.33	0.02	0.23	-0.25	0.19	0.18
27.6 - 28.7	-0.32	0.41	-0.93	0.31	-0.81	0.25	0.20
28.7 - 30.1	-1.29	0.29	-1.18	0.21	-1.35	0.17	0.22
30.1 - 31.3	-0.94	0.39	-0.62	0.29	-0.80	0.23	0.20
31.3 - 31.9	-0.46	0.50	-0.46	0.37	-0.51	0.30	0.18
31.9 - 32.7	-0.59	0.37	-0.48	0.27	-0.57	0.22	0.18
32.7 - 33.9	0.15	0.36	-0.05	0.26	0.02	0.21	0.17
33.9 - 35.2	-0.62	0.30	0.14	0.21	-0.09	0.17	0.18
35.2 - 36.2	-0.12	0.44	-0.34	0.33	-0.30	0.26	0.18
36.2 - 37.2	-1.28	0.61	-0.68	0.28	-0.88	0.25	0.21
37.2 - 38.4	-1.52	0.51	-0.64	0.35	-1.00	0.29	0.22
38.4 - 39.7	-0.27	0.56	-1.26	0.44	-1.02	0.34	0.22
39.7 - 40.8	-0.71	0.47	-0.40	0.34	-0.56	0.27	0.19
40.8 - 41.8	-0.58	0.58	-0.90	0.43	-0.89	0.35	0.21
41.8 - 43.3	-1.81	0.56	-1.09	0.40	-1.45	0.32	0.25
43.3 - 44.3	-1.65	0.78	-1.34	0.56	-1.59	0.45	0.26
44.3 - 45.8	-2.56	0.83	-1.67	0.60	-2.17	0.49	0.33
45.8 - 46.8	-1.45	0.77	-0.92	0.59	-1.21	0.47	0.26
46.8 - 48.1	-0.90	0.63	-0.20	0.45	-0.46	0.37	0.21
48.1 - 50.0	0.01	0.39	-0.36	0.29	-0.27	0.23	0.18
50.0 - 51.2	-1.08	0.73	-1.09	0.54	-1.21	0.43	0.24
51.2 - 52.5	-2.28	1.00	-0.33	0.66	-0.97	0.55	0.30
52.5 - 55.8	-0.85	0.31	-1.08	0.23	-1.12	0.19	0.21
55.8 - 57.3	-1.11	0.35	-1.05	0.26	-1.18	0.21	0.21
57.3 - 59.9	-1.54	0.33	-1.07	0.24	-1.35	0.19	0.22
59.9 - 62.5	-1.73	0.45	-1.22	0.33	-1.54	0.26	0.24

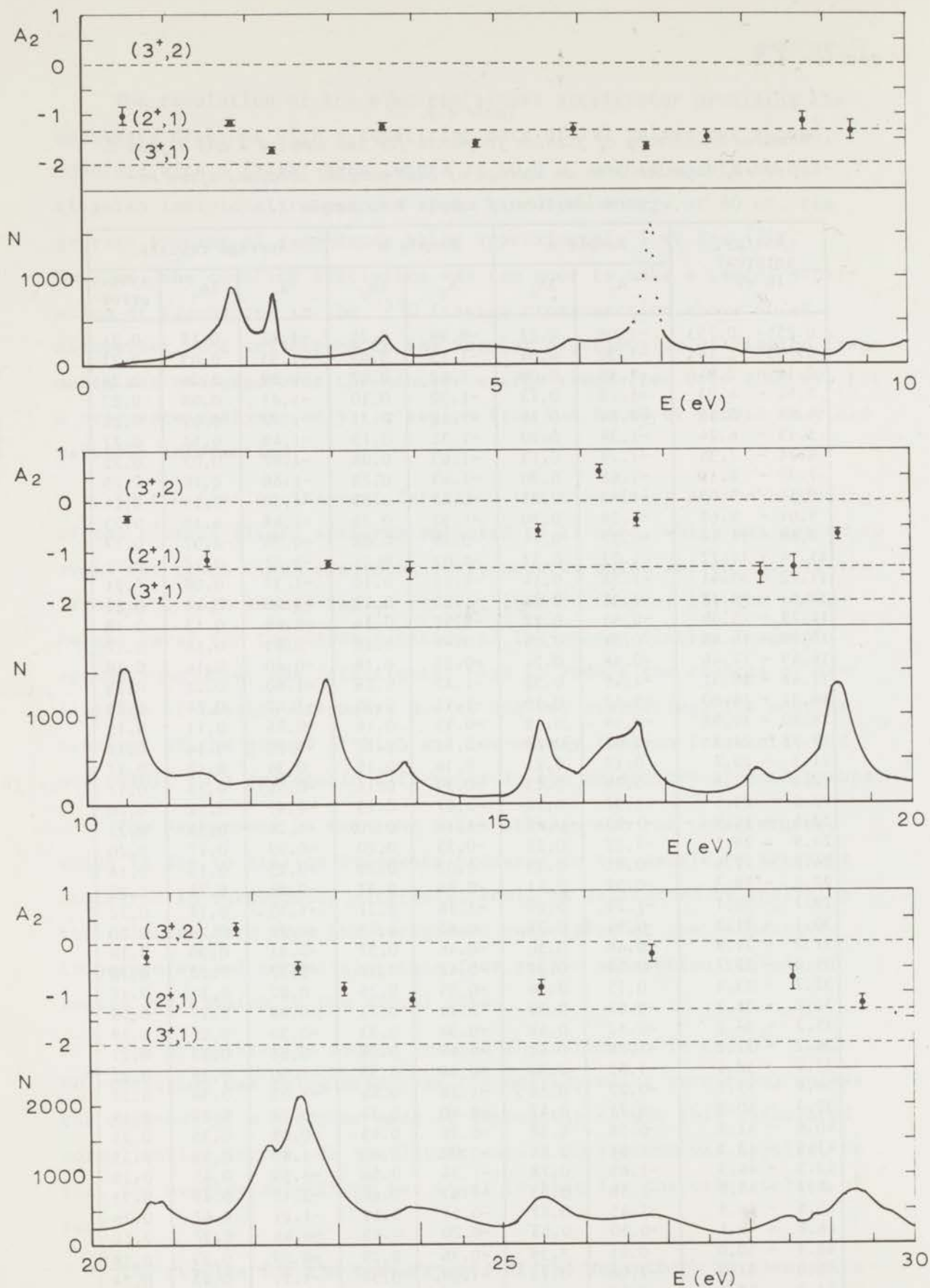


Fig. 4.1.1

Fission-fragment spectrum and A_2 -values for resonances from 0 to 30 eV; a solid line has been drawn through the experimental points where the statistical errors are sufficiently small.

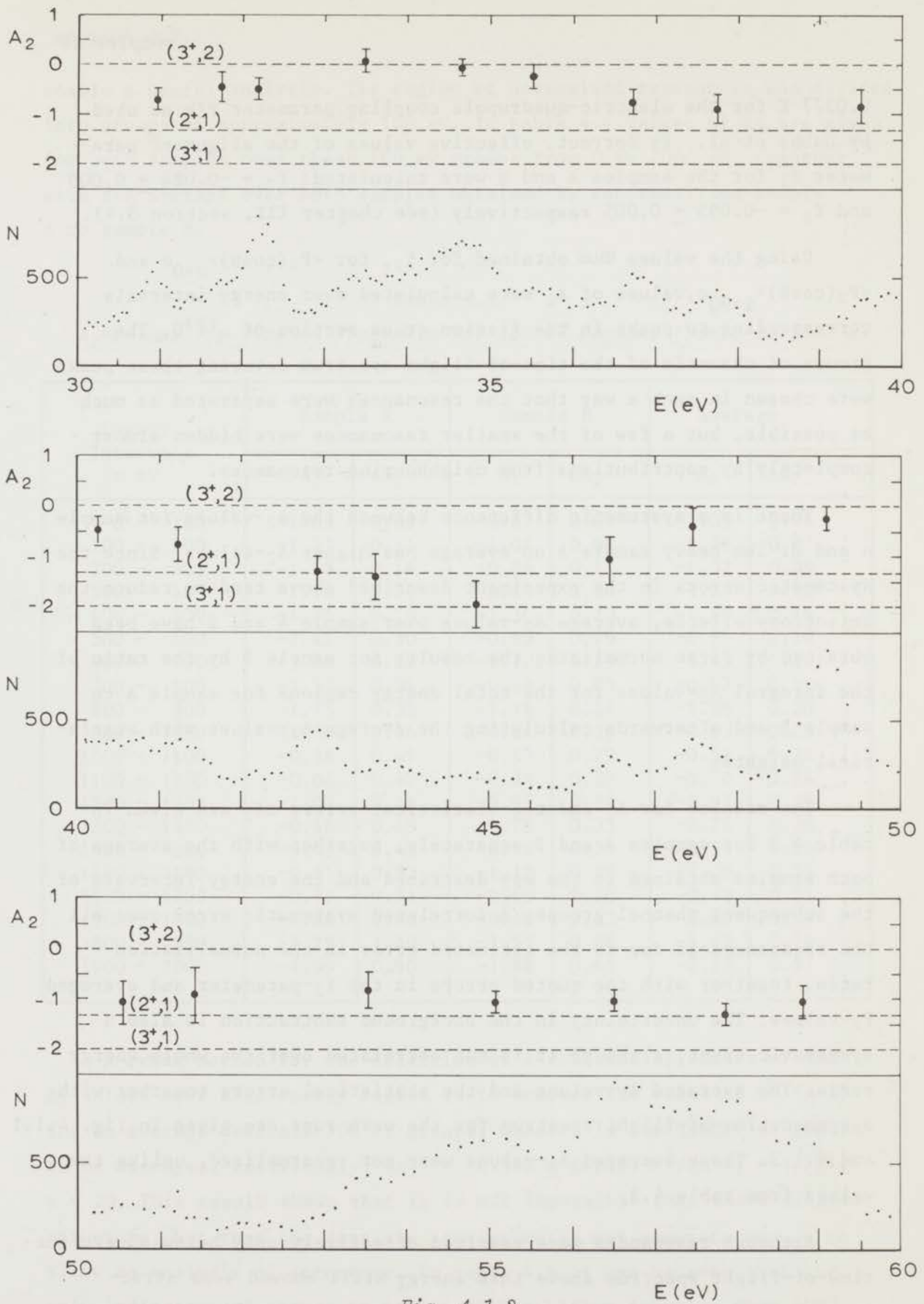


Fig. 4.1.2

Fission-fragment spectrum and A_2 -values for resonances from 30 to 60 eV.

0.0277 K for the electric-quadrupole coupling parameter P/k as used by Dabbs et al. is correct, effective values of the alignment parameter f_2 for the samples A and B were calculated: $f_2 = -0.084 \pm 0.005$ and $f_2 = -0.095 \pm 0.005$ respectively (see chapter III, section 3.4).

Using the values thus obtained for f_2 , for $\langle P_2(\cos\theta) \rangle_{\theta=0^\circ}$ and $\langle P_2(\cos\theta) \rangle_{\theta=90^\circ}$, values of A_2 were calculated over energy intervals corresponding to peaks in the fission cross section of ^{233}U . The groups of channels of the time-of-flight spectrum covering these peaks were chosen in such a way that the resonances were separated as much as possible, but a few of the smaller resonances were hidden almost completely by contributions from neighbouring resonances.

There is a systematic difference between the A_2 -values for sample A and B. The heavy sample A on average has higher A_2 -values. Since the systematic errors in the experiment described above tend to reduce the anisotropy effects, average A_2 -values over sample A and B have been obtained by first normalizing the results for sample B by the ratio of the integral A_2 -values for the total energy regions for sample A to sample B and afterwards calculating the average A_2 -values with statistical weights.

The results for A_2 and the statistical errors ΔA_2 are given in table 4.3 for samples A and B separately, together with the average of both samples obtained in the way described and the energy intervals of the subsequent channel groups. A correlated systematic error over all the resonances is due to the estimated error in the normalization ratio, together with the quoted errors in the f_2 -parameter and averaged P_2 -values. The uncertainty in the background subtraction is also a systematic error, although it is not correlated over the whole energy range. The averaged A_2 -values and the statistical errors together with a summed time-of-flight spectrum for the warm runs are given in fig. 4.1.1 and 4.1.2. These averaged A_2 -values were not renormalized, unlike the values from table 4.3.

Although resonances were resolved effectively only below 60 eV, the time-of-flight spectrum above this energy still showed some structure, but the experimental resolution and counting statistics did not

section 4.2.

enable a useful analysis. The region of unresolved resonances was divided into groups of approximately 100 eV. In table 4.4 values of A_2 are given for both samples over these 100 eV groups from 0 to 2000 eV, together with the average over both samples obtained by renormalizing sample A to sample B.

Table 4.4.

A_2 -values for fission fragments for 100 eV regions from 0 to 2000 eV

Energy Intervals in eV	Sample A		Sample B		Average	
	A_2	ΔA_2	A_2	ΔA_2	A_2	ΔA_2
0 - 100	-1.05	0.03	-0.87	0.02	-1.03	0.02
100 - 200	-1.27	0.11	-1.07	0.08	-1.26	0.07
200 - 300	-1.38	0.16	-0.86	0.11	-1.02	0.09
300 - 400	-1.18	0.21	-0.65	0.14	-0.89	0.12
400 - 500	-1.75	0.29	-1.30	0.20	-1.59	0.16
500 - 600	-1.41	0.30	-0.69	0.19	-0.99	0.16
600 - 700	-1.80	0.28	-1.10	0.19	-1.45	0.16
700 - 800	-1.33	0.34	-0.69	0.23	-0.97	0.19
800 - 900	-1.75	0.35	-1.16	0.24	-1.56	0.20
900 - 1000	-1.34	0.46	-0.64	0.30	-0.93	0.25
1000 - 1100	-0.58	0.41	-0.45	0.29	-0.54	0.24
1100 - 1200	-0.04	0.42	-0.34	0.29	-0.28	0.24
1200 - 1300	-1.07	0.44	-0.91	0.31	-1.07	0.25
1300 - 1400	-0.46	0.49	-0.78	0.35	-0.76	0.30
1400 - 1500	-0.45	0.49	-0.76	0.35	-0.74	0.26
1500 - 1600	-0.51	0.53	-1.18	0.39	-1.08	0.31
1600 - 1700	-0.77	0.54	-0.60	0.38	-0.73	0.31
1700 - 1800	-1.84	0.83	-0.40	0.53	-0.86	0.44
1800 - 1900	-2.29	1.40	-1.51	0.88	-1.92	0.74
1900 - 2000	-1.99	0.90	-1.88	0.61	-2.13	0.51

A crude method for the detection of a relevant structure in the A_2 -values over this energy region is to inspect the value of $\chi^2/(n-1)$ for an average over all 100 eV groups, where n is the number of groups to be averaged, resultingly: $\langle A_2 \rangle = -0.948 \pm 0.016$; $\chi^2/(n-1) = 1.721$; $n = 20$. This result shows that it is not impossible that there is some structure, but that the data are statistically not accurate enough to allow an analysis of structure. In table 4.4 it can be seen that the only indication of structure is a somewhat higher A_2 -value from 1000 to 1200 eV.

The results from table 4.3 have been given in a graphic form in fig. 4.2 as a frequency distribution of A_2 -values covering the main resonances between 0 and 60 eV. The method of constructing a pseudo-histogram was described in chapter II. As mentioned, overlapping of resonances is rather important in the fission cross section of ^{233}U . If there would be a pronounced structure in the frequency distribution, strong overlapping would tend to smooth out sharp peaks and make the distribution as a whole somewhat narrower, because extreme A_2 -values will be drawn towards an average A_2 -value.

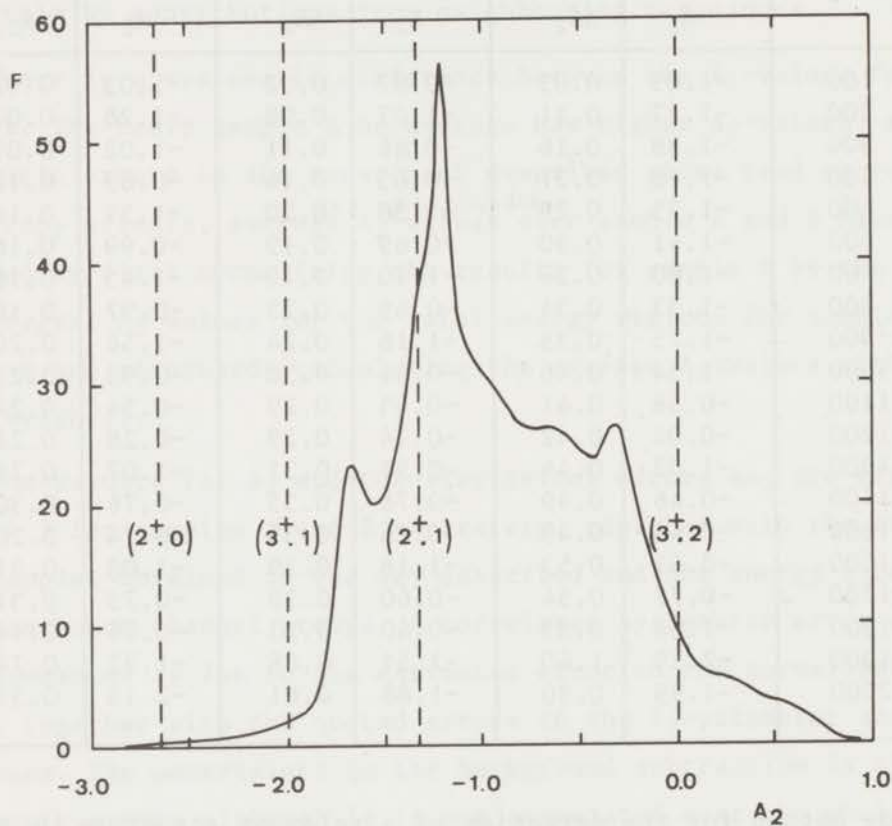


Fig. 4.2.

Frequency distribution of A_2 -values for resonances in the form of a pseudo-histogram; the dashed lines represent the theoretical A_2 -values for the various combinations of (J^π, K) .

section 4.2.

The influence of this effect might be checked in a first-order approximation by taking A_2 -values only over the tops of the resonances where the relative contributions from neighbouring resonances are minimal. However, the statistical errors on these A_2 -values will be considerably larger, since the area has been decreased. To make comparison possible with the original distributions, histograms were calculated from the original A_2 -values and from those for the top regions, with attributive errors in both cases those of the top region. The difference between the two curves shown in fig. 4.3, does not seem to be significant.

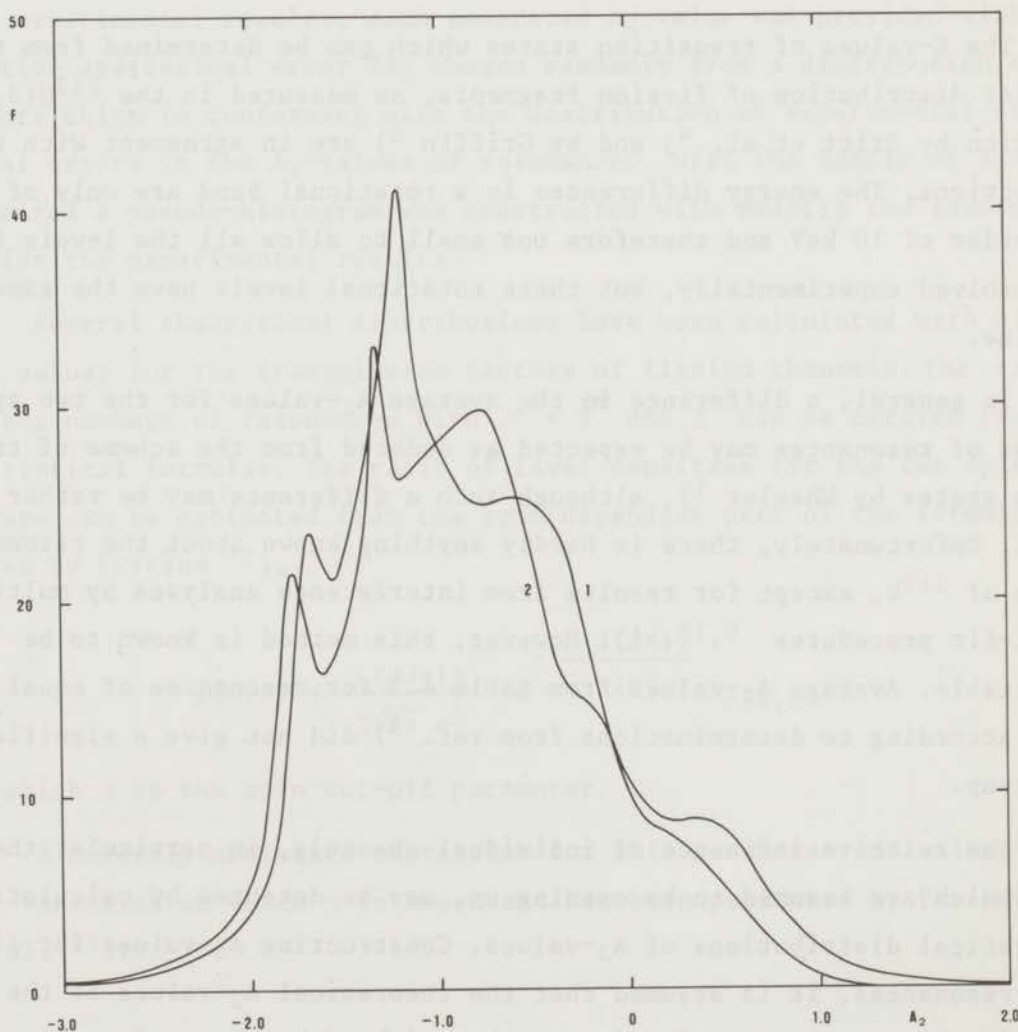


Fig. 4.3

Frequency distribution of A_2 -values for resonances calculated over the full resonance regions (1) and over the tops of the resonances only (2); the statistical errors used in both distributions correspond to the A_2 -values for the top regions.

4.3. Discussions and interpretation

According to Bohr's theory ⁸⁾, the number of fission channels available to fission of ²³³U by low-energy neutrons is small. The transition states at the deformation saddle point, corresponding to these fission channels, have preferably small K-values, which is suggested by the K-dependence of the rotational energies of levels superimposed on vibrational states:

$$E_{\text{rot}} = \frac{\hbar^2}{2I_{\perp}} \{ J(J+1) - K^2 \} + \frac{\hbar^2}{2I_{\parallel}} K^2 \quad (I_{\parallel} \ll I_{\perp}).$$

The K-values of transition states which can be determined from the angular distribution of fission fragments, as measured in the ²³³U(d,pf)-reaction by Britt et al. ⁴⁾ and by Griffin ⁵⁾ are in agreement with these predictions. The energy differences in a rotational band are only of the order of 10 keV and therefore too small to allow all the levels to be resolved experimentally, but these rotational levels have the same K-value.

In general, a difference in the average A₂-values for the two spin groups of resonances may be expected as deduced from the scheme of transition states by Wheeler ¹⁾, although such a difference may be rather small. Unfortunately, there is hardly anything known about the resonance spins of ²³³U, except for results from interference analyses by multi-level-fit procedures ^{9,10,11)}. However, this method is known to be unreliable. Average A₂-values from table 4.3 for resonances of equal spin according to determinations from ref. ⁹⁾ did not give a significant split-up.

The relative influence of individual channels, in particular the ones which are assumed to be opening up, may be detected by calculating theoretical distributions of A₂-values. Constructing A₂-values for fictive resonances, it is assumed that the theoretical A₂-values of the individual channels contributing can be weighted by the product of a partial fission width and a transmission factor representing the degree of opening of the channel; the partial fission width for a particular channel is generated randomly according to a Porter-Thomas distribution.

section 4.3.

The effective A_2 -value for a resonance then can be given by:

$$A_2 = \frac{\sum_f T_f A_{2f} \Gamma_{(F)f}}{\sum_f T_f \Gamma_{(F)f}}$$

in which T_f are the transmission factors, varying from 0 to 1, A_{2f} are the theoretical A_2 -values from table 4.2 and $\Gamma_{(F)f}$ the partial fission widths for the available channels.

To make a comparison possible between theoretical distributions and experimental results, each generated A_2 -value was provided with a fictive statistical error ΔA_2 chosen randomly from a distribution of errors which is conforming with the distribution of experimental statistical errors in the A_2 -values of resonances. With the sample of A_2 -values obtained a pseudo-histogram was constructed with exactly the same procedure as for the experimental results.

Several theoretical distributions have been calculated with different values for the transmission factors of fission channels. The ratio of the numbers of resonances with $J^\pi = 2^+$ and 3^+ can be derived from statistical formulae. The ratio of level densities for the two spin groups can be estimated from the spin-dependent part of the formula as given by Ericson ¹²⁾,

$$\rho(E, J) = \frac{(2J+1)}{2\sqrt{2\pi} \sigma^3} e^{-\frac{J(J+1)}{2\sigma^2}} \rho(E, 0)$$

in which σ is the spin cut-off parameter.

A recently evaluated expression for this parameter and values of the variables on which σ is dependent has been published by Facchini et al. ¹³⁾:

$$\sigma^2 \approx 0.24 A^{\frac{2}{3}} \frac{6}{\pi^2} a t.$$

A is the mass number, a is the single-particle level density and t is the thermodynamic temperature of the nucleus; the following values are

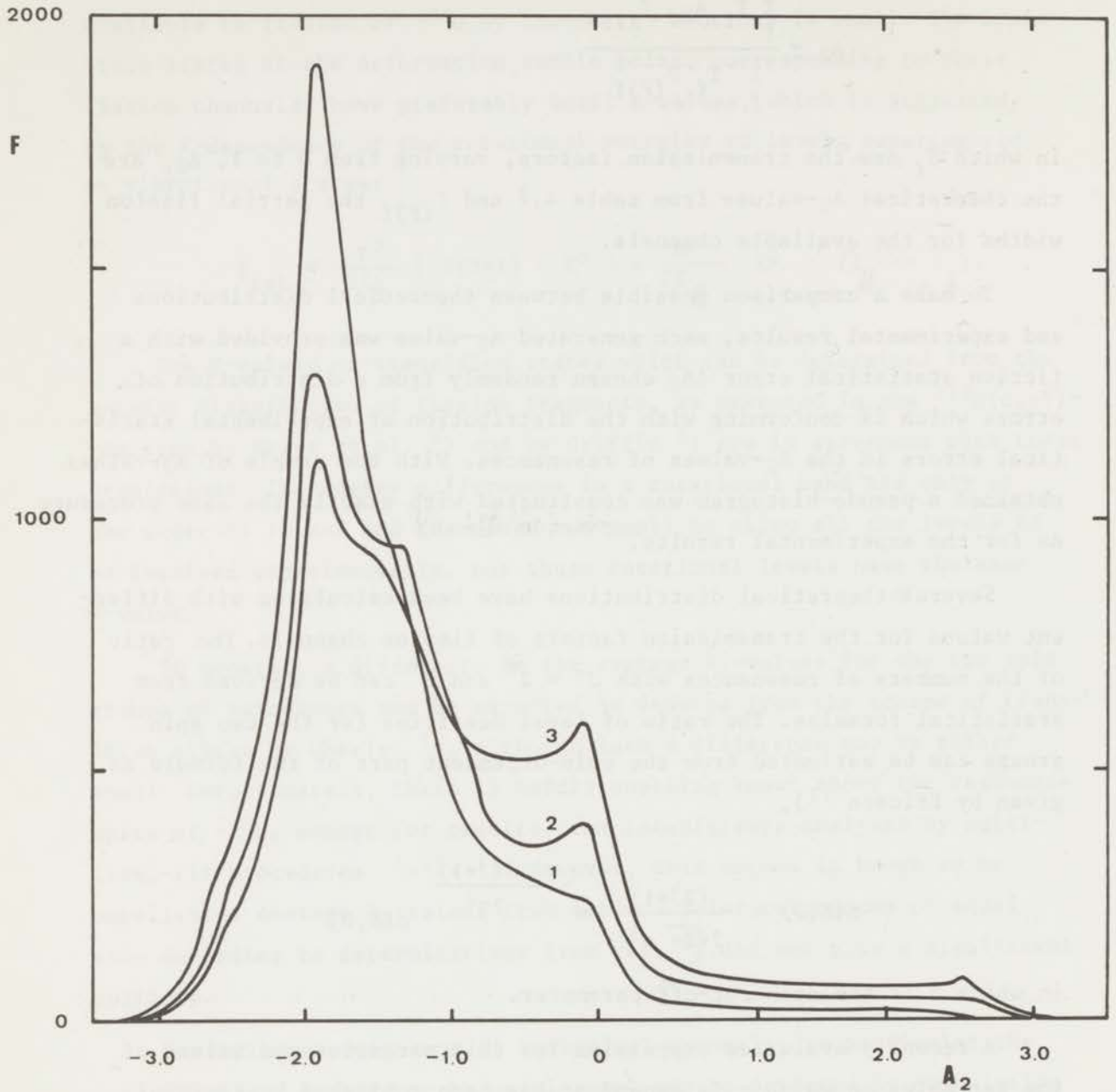


Fig. 4.4

Theoretical frequency distributions with different transmission factors for the channels $(2^+, 2)$ and $(3^+, 2)$. The numbers in the picture refer to the combinations of transmission factors as given in the text.

section 4.3.

specified: $a = 28.70 \text{ MeV}^{-1}$ and $t = 0.39 \text{ MeV}$. The resulting value for σ^2 is 62.1 and the ratio of level densities with spins 2^+ and 3^+ is:

$$\frac{\rho(E, 2^+)}{\rho(E, 3^+)} = 0.75 .$$

The results of these calculations showed that it was possible to construct theoretical distributions that imitated the form of the experimental histogram reasonably well. One general feature was that a split-up in A_2 -values corresponding to different spins could hardly be detected.

Comparison of distributions with increasing contribution from channel $(2^+, 2)$ shows that opening of this channel strongly reduces the shoulder in the histogram at approximately $A_2 = -2.5$. At the same time a low plateau of positive A_2 -values develops. Opening of the channel $(3^+, 2)$ gives a contribution in the region from $A_2 = -1.3$ to 0.

Making a selection of distributions resembling the experimental distribution best, the following situation could be chosen: for resonances with $J^\pi = 2^+$ the channels $(2^+, 0)$ and $(2^+, 1)$ are fully open and the channel $(2^+, 2)$ has a transmission factor ranging from 0.1 to 0.5; for resonances with $J^\pi = 3^+$ the channel $(3^+, 1)$ is fully open and the transmission factor of $(3^+, 2)$ goes from 0.1 to 0.5.

In fig. 4.4 three theoretical distributions are given which together cover the given range of transmission factors. For each histogram a total of 1000 A_2 -values were used of which the numbers of resonances with different spins had the ratio as given above. The three curves represent distributions calculated with the following transmission factors:

- 1) $T(2^+, 2) = 0.1$; $T(3^+, 2) = 0.1$
- 2) $T(2^+, 2) = 0.3$; $T(3^+, 2) = 0.3$
- 3) $T(2^+, 2) = 0.5$; $T(3^+, 2) = 0.5$

In order to get an impression of the possible spread in the distribution of a small sample of resonances, a few histograms were calculated on only 50 resonances for combination 2 of the transmission factors, two of which are given in fig. 4.5. The variations are sizeable, but inconsequential to the general behaviour.

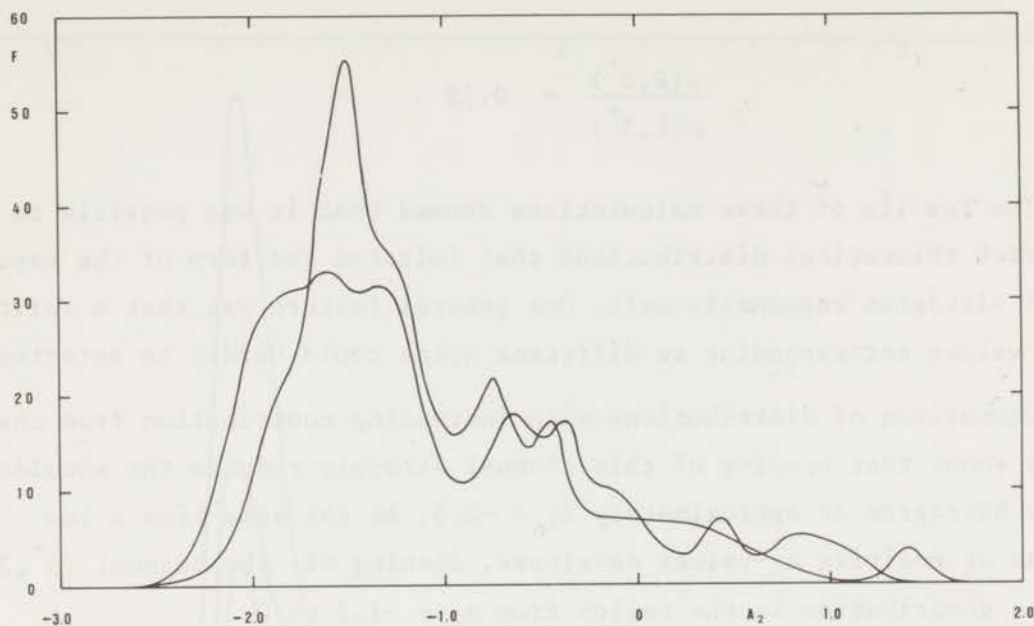


Fig. 4.5

Theoretical frequency distributions on statistical samples of only 50 A_2 -values randomly selected, according to the average combination (2) of transmission factors.

Admixing of neighbouring resonances may cause a narrower distribution of A_2 -values, as mentioned above. The relative importance of this may be seen from fig. 4.6 in which two distributions are given, which have the same set of transmission factors, the first curve is a histogram consisting of pure A_2 -values and the second one has 10% exchange in the A_2 -values of neighbouring resonances.

A comparison of the experimental histogram to the three curves from fig. 4.4, shows a clear difference in the A_2 -value for the peak of the distributions. The theoretically calculated distributions have maximum probabilities between $A_2 = -1.9$ and -2.0 , against a value $A_2 = -1.25$ for the experimental histogram. The reason however, for selecting the transmission factors as specified, is the relative form, in particular the narrowness of the distributions. Theoretical distributions with more admixing of the channels $(2^+, 2)$ and $(3^+, 2)$ are much wider and yield larger fractions of positive A_2 -values.

section 4.3.

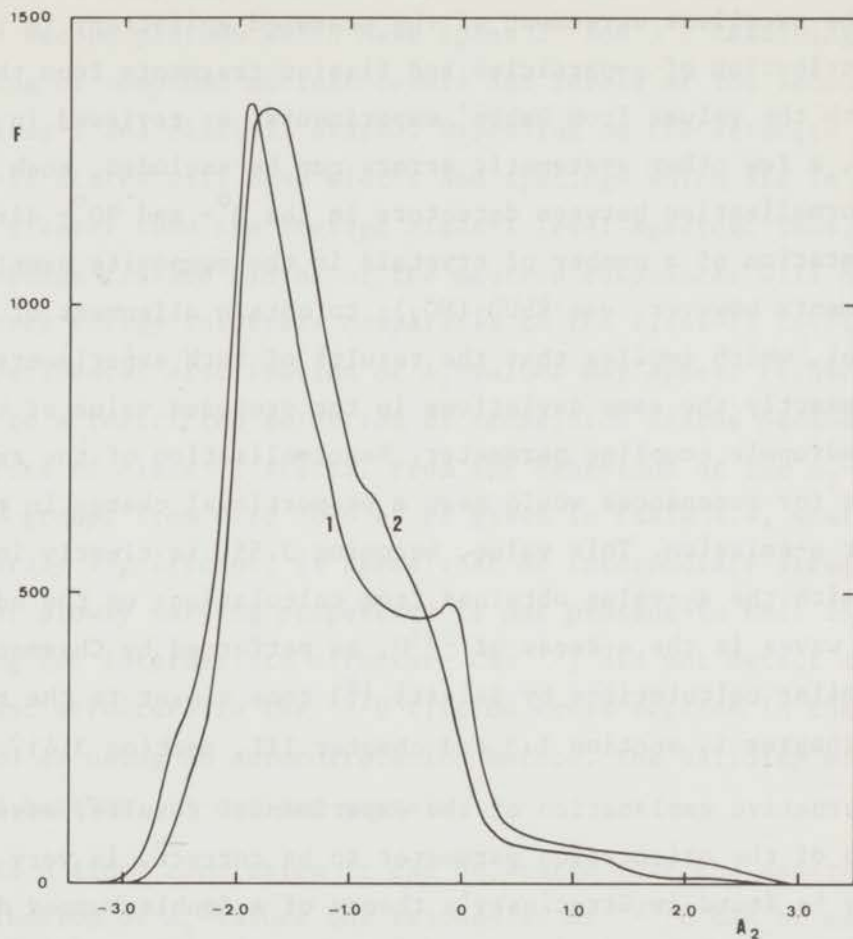


Fig. 4.6

Effect of overlapping of resonances on the frequency distribution; curve 1 corresponds to pure A_2 -values and curve 2 has 10% exchange in the A_2 -values of neighbouring resonances.

The comparison of experimental results and theoretical predictions as based on the simple theory of transition states, therefore implies renormalization of the experimental results giving a histogram which is peaked at $A_2 = -1.95$. Although a combination of systematic errors by no means is impossible, it has been tried to rule out a few. Since the geometrical correction on the Legendre polynomials is relatively accurate and the influence of nuclear scattering on the angular distribution of fission fragments, which would tend to reduce the anisotropy, is not very likely, the explanation of the difference would come down to a correction of

the value of the f_2 -parameter.

From the excellent agreement of the measured anisotropy in the angular distribution of α -particles and fission fragments from thermal fission, with the values from Dabbs' experiments, as reviewed in chapter III, a few other systematic errors can be excluded, such as incorrect normalization between detectors in the 0° - and 90° - direction and misorientation of a number of crystals in the composite samples. Both experiments however, use $\text{RbUO}_2(\text{NO}_3)_3$ to obtain alignment of the target nuclei, which implies that the results of both experiments are subject to exactly the same deviations in the proposed value of the electric-quadrupole coupling parameter. Renormalization of the results on A_2 -values for resonances would mean a proportional change in the A_2 -value for α -emission. This value, becoming 3.55, is clearly in contradiction with the A_2 -value obtained from calculations on the admixing of D- to S- waves in the α -decay of ^{233}U , as performed by Chasman et al. ¹⁴⁾. Similar calculations by Salusti ¹⁵⁾ come closer to the required value (see chapter I, section 1.3 and chapter III, section 3.4).

An alternative explanation of the experimental results, assuming the estimate of the orientation parameter to be correct, is very tentative. It may be found in Strutinsky's theory of a double-humped deformation barrier, which by now is regarded to be uniformly valid for the heavy nuclei, being either fissile or non-fissile by low-energy neutrons ¹⁶⁾. The application of the Strutinsky-potential on the nuclear resonance theory was made by Lynn ¹⁷⁾ and Weigmann ¹⁸⁾.

The exact situation about the relative heights of the two barriers is not known, but in the case of $^{234}\text{U}^*$ it is likely that the second hump at higher deformation ¹⁶⁾ is well below the first at smaller deformation. The fission threshold as measured in the $^{233}\text{U}(d, pf)$ -reaction ^{2,3)} probably represents the barrier at lower deformation. It is generally assumed that the nucleus will deform rapidly towards scission after having passed through a transition state above this barrier.

However, there may be a relatively strong influence due to levels at deformations corresponding to the second minimum between the two barriers. Selection of the transition states will depend now on the

section 4.3.

strength of coupling between compound nuclear levels and those levels in the second minimum which have spins 2^+ and 3^+ . Resulting from this coupling of compound nuclear levels and levels at the second minimum are class-I and class-II states. Depending on the strength of coupling, class-II states will have widths and spacings which are in general many times greater than the average class-I level spacing. Thus, changes in the average fission widths of the neutron resonances will be noticeable only over energy intervals comparable to the class-II level spacing. An experimental distribution of A_2 -values may appear rather narrow, owing to a restricted selection of transition states because of the existence of class-II states. From the behaviour of the A_2 -values over 100 eV groups from 0 to 2000 eV as given in table 4.4, where changes are hardly significant, it seems that an intermediate structure in the form of slowly varying properties is not present in this energy region. Looking for intermediate structure Cao ¹⁹⁾ did not detect any significant structure in the ^{233}U fission cross section in the region up to 1200 eV using an autocorrelation method. The validity of this method however, is not yet certain.

As a final conclusion it can be stated that the experimental distribution of A_2 -values for resonances of ^{233}U can be explained by the theory of Bohr. The difference between theoretical distributions calculated on the basis of this theory and the experimental distribution can largely be covered by systematic errors, of which the most important one is the uncertainty in the value of the electric-quadrupole coupling constant.

References

1. J.A. Wheeler, Fast Neutron Physics (ed. by J.L. Fowler and J.B. Marion; Interscience, New York, 1963) Vol.2, 2051.
2. J.A. Northrop, R.K. Stokes and K. Boyer, Phys. Rev. 115 (1959) 1277.
3. L.N. Usachev, V.A. Pavlinchuk, N.S. Rabotnov, Atomm. Energ. 17 (1965) 479.
4. H.C. Britt, R.H. Stokes, W.R. Gibbs and J.J. Griffin, Phys. Rev. Lett. 11 (1963) 343.
5. J.J. Griffin, Phys. Rev. 132 (1963) 2204.
6. J.R. Huizenga, Proc. of Intern. Physics Conf., Gatlinburg, Tennessee, 1966 (Academic Press, New York, 1967) 721.
7. J.E. Lynn, Theory of Neutron Resonance Reactions (Clarendon, Oxford, 1968).
8. A. Bohr, Proc. 1st Conf. on Peaceful Uses of Atomic Energy (1956) Vol 2, 151.
9. A.R. de L. Musgrove, Austr. Jrn. Phys. 20 (1967) 617.
10. M.S. Moore and G.W. Reich, Phys. Rev. 118 (1960) 718.
11. E. Vogt, Phys. Rev. 118 (1960) 724.
12. T. Ericson, Adv. Phys. 9 (1960) 425.
13. U. Facchini, E. Saetta-Menichella, Energia Nucleare 15 (1968) 54.
14. R.R. Chasman and J.O. Rasmussen, Phys. Rev. 115 (1959) 1257.
15. E. Salusti, Nuovo Cimento 30 (1963) 171.
16. V.M. Strutinsky, Nucl. Phys. A 95 (1967) 420.
17. J.E. Lynn, Physics and Chemistry of Fission, IAEA-Symposium, Vienna (1969) 249.
18. H. Weigmann, Zeitschrift für Physik 214 (1968) 7.
19. M.G. Cao, E. Migneco, J.P. Theobald and M. Merla, private communications, to be published.

Chapter V

ANGULAR DISTRIBUTION OF FISSION FRAGMENTS FROM SUBTHRESHOLD FISSION OF ALIGNED ^{237}Np

5.1. Theoretical considerations

The theory of subthreshold fission and related phenomena originated from the Strutinsky model ¹⁾ of the deformation potential and is a recent development in the field of neutron spectroscopy. A measurement of the angular distribution of fission fragments, produced in subthreshold fission may contribute to the detailed information that is required to test Strutinsky's theory. Fortunately, the interpretation of the experimental results will be more or less independent of the explicit coupling conditions, as defined by Lynn ²⁾ and Weigmann ³⁾, and which have been described in chapter I, section 2.

The assumptions that are necessary for a relatively simple interpretation of the results on the anisotropy in fission-fragment emission are analogous to those made in the explanation of the angular distribution of fission fragments from neutron capture in the fissile nuclei. Also in this type of fission the fragments are supposed to be emitted in the direction of the nuclear symmetry axis which is the axis of prolate deformation. The situation regarding the projection K of the nuclear spin J on the symmetry axis is in principle not different from the case where fission is proceeding through transition states, which are classified as the various intrinsic excitations and collective modes of the deformed nucleus at the deformation barrier and the assumption that K will be conserved from the transition state onwards is equally valid for the interpretation of the angular distribution in subthreshold fission. The process of deformation beyond the fission barrier, in this case after tunneling through the second barrier or after passing a transition state at the second barrier depending on the actual height of this barrier, does not have a different behaviour in comparison with fissile nuclei.

In the theory of transition states by Wheeler ⁴⁾ the β -mode is regarded as the collective motion through which the nucleus can fission

spontaneously from any transition state. The quantum numbers K of the transition states are characteristic of the other collective and intrinsic excitations involved. In fact, K cannot be defined for any stage of the process preceding the occupation of the transition levels at the deformation barrier.

In subthreshold fission the tunneling through either of the barriers is governed by the amplitude of a wave function in the adjacent potential well. The coupling strength between levels in different potential wells is governed by the interaction between the β -vibrational mode and the other collective modes and intrinsic excitations. The K -value which describes the angular distribution of fission fragments, corresponds to the lowest available transition state at the second barrier, which will generally have the strongest interaction with the β -vibrational mode at energies below the threshold for the second barrier. If the energy is comparable to or higher than the second threshold more transition states may be involved and the angular distribution will be determined by the admixing of other K -values.

The ground state of the odd-proton nucleus ^{237}Np has spin and parity $I^\pi = \frac{5}{2}^+$. For s -wave neutron capture the compound nuclear levels which are occupied have $J^\pi = 2^+$ or 3^+ and consequently only intermediate states having the same spin and parity will be able to be excited. In the group structure of the fission cross section of ^{237}Np all the resonances in one group with relatively large fission widths must have the same spin since they are all coupled to a single intermediate level. Different groups are allowed to have different spins. Since the coupling conditions through either barrier might be different for the two possible spin states, depending on the quantum numbers of the transition states above the two barriers, it would be worthwhile to investigate whether there are groups of resonances with 3^+ as well as 2^+ and further to assign a K -value to each of the various groups.

Unfortunately, there have been no theoretical studies on the transition states of odd-odd nuclei, this group of compound nuclei being less fissionable than even-even or odd-mass nuclei. Intrinsic excitations at the deformation saddle point are thought to have spacings in the order of

section 5.1.

100 keV, whereas collective vibrational modes are excited at a much higher energy, that is approximately 500 keV. The rotational band superimposed on a single-particle state has a level spacing in the order of 10 keV.

The structure of quasi-particle states of the uncoupled proton and neutron is very complex and a prediction for the spin of a nuclear ground state from the Nilsson states ^{5,6)} at deformations as far as the second barrier in the deformation potential would hold no significance. However, in the ground state the spins of the unpaired proton j_p and neutron j_n will probably be coupled to the theoretically maximum value. That is to say, the spin of the nuclear ground state is likely to be $J = j_p + j_n$, as the most probable value out of the range of J-values: $J = |j_p - j_n|$, $|j_p - j_n + 1|$, . . . , $j_p + j_n - 1$, $j_p + j_n$. Making a priori no assumption about the values of j_p and j_n , this rule will be valid for any deformation. Furthermore, in the nuclear ground state K will be equal to J, independent of the actual deformation.

It may be concluded from the above that for the lowest transition states of odd-odd nuclei higher K-values will have a preference over lower K-values. Depending on the spin and symmetry of the transition ground state at the second deformation barrier there may exist a considerable difference in the energy of the lowest available transition states 2^+ and 3^+ respectively and which therefore would result in considerably different coupling conditions for the two groups of resonances with different spins.

Although explicit deductions about the K-values of the transition states at the two barriers cannot be made, it can be stated that in the angular distribution of fission fragments large positive anisotropies corresponding to the higher K-values will be observed. It may be remarked, that in the case of class-II states which are below the lowest available transition state, this state will be predominant in the tunneling of the second barrier, as can be seen from the Hill-Wheeler barrier penetration formula and therefore, integral values of K have to be expected, which are equal to the K-value of the lowest available transition state.

It has been the object of the experiment described to measure the anisotropy in the angular distribution of fission fragments from neutron capture in aligned ^{237}Np in the energy range from 0 to 2000 eV. If a certain group can be resolved into individual resonances it has to be checked that all these resonances have the same J-value. For groups of resonances where the resolution is insufficient to distinguish the resonances separately a J-value might be assigned to the whole group.

5.2. Data collection, calculations and results

In an experiment on subthreshold fission undoubtedly the biggest problem is the counting time to acquire sufficient statistical accuracy. The instability of electronic equipment over longer periods, radiation damage to detectors and deterioration of the crystals in the sample are factors which may introduce systematic errors to the measurements. The data collection for ^{237}Np lasted 8 months divided over a period of $1\frac{1}{2}$ year.

The fission cross section of ^{237}Np in the measured energy range from 0 to 3000 eV consists of several groups of resonances. To allow the measurement of as many groups as possible, the delay time which was set at the beginning of the time-of-flight spectrum to cut off the γ -flash and the irrelevant high-energy region, was given a value of only 5 μsec , which is lower than in the experiment on ^{233}U .

The time-of-flight resolution allowed only the first group of resonances from 25 to 50 eV to be resolved into the individual resonances. In a few of the higher groups some structure was perceivable but too weak to be analyzed into its components.

The highest observable peak in the time-of-flight spectra was at 1900 eV. Beyond that energy the only structure discerned was a relatively low region at 2100 eV, which was taken as the highest energy region for background determination. At lower energies there was no clearly defined group between the 1900 eV group and a rather broad group at 1250 eV, except for a slight peak at 1700 eV. Altogether there were 17 well defined groups observed in the region from 0 to 2000 eV plus 4 very weak peaks which may have indicated groups.

section 5.2.

Additionally, in the summed runs of the time-of-flight spectra there appeared to be a number of very low peaks at energies below the 40 eV group. Two of these had energies which corresponded to ^{237}Np resonances ⁷⁾, namely at 3.9 and 5.8 eV. These resonances are also reported by Paya et al. ⁸⁾ to have detectable fission widths.

Other peaks at 8.8, 12.4, 19.3, 32.1, 35.2 and 56.5 eV could be related to ^{235}U . The appearance of these groups is due to the uranium ^{235}U in the base crystals of RUN for which an isotopic mixture was used that, although depleted, still contained 0.43% ^{235}U . Fission fragments originating from fission of ^{235}U may penetrate the coating layer of RNN or escape freely from uncovered spots of the crystals. Since resonances of ^{235}U were observed as weak as the one at 32.1 eV, very slight peaks also due to ^{235}U were certainly present at 39.4 and 51.25 eV, coinciding with ^{237}Np resonances in the 40 eV group, but a correction for these effects was not necessary.

The time-of-flight runs for the data collection on ^{237}Np fission fragments were done with different electron pulse widths of the linear accelerator. Initially runs were taken with $\frac{1}{4}$ μsec pulses only, but since the neutron output of the machine is approximately proportional to the electron pulse width, $\frac{1}{2}$ μsec pulses were used later. Judging by the peak-to-valley ratios for the 39.0 and 40.1 eV resonances, the deterioration in neutron energy resolution was not important.

With the very low count rates the experiment had to deal with, the background became problematic. The total number of counts in the background exceeded the number of counts in the resonances by far. The form of the background however, could be determined rather well, owing to the fact that the energy regions between resonance groups may be regarded as essentially being background. In order to reduce the background as much as possible cadmium was put in the neutron beam, by which nearly all thermal neutrons were removed. It was neither necessary nor advisable to use sodium as a filter at higher neutron energies, because the background form was well determined and it might prevent detection of the higher resonance groups. Separate background runs could be omitted, because of the relatively accurate determination of the background in the actual runs.

The normalization ratio between detectors in the 0° - and 90° -direction was taken to be the ratio of background counts in the cold runs, assuming that the background was independent of the sample temperature and detector location. The validity of this method was verified, as described in chapter III by analyzing the warm runs.

For a value of the orientation parameter f_2 a discussion has been given in chapter III. Although sample A had a considerably heavier coating than sample B, equal f_2 -values could be chosen because of the temperature-independent behaviour of the f_2 -parameter in the region of temperatures obtained with both samples. Since the curves of the α -anisotropy measured as a function of temperature saturated roughly at the temperature $T = 0.2$ K for both samples and also the f_2 -parameter reaches the plateau at approximately the same temperature as can be seen from figs. 3.1 and 3.2 in chapter III, a difference in effective sample surface temperature and measured temperature on the cooling plate can be assumed to be negligible at temperatures above 0.2 K. The evaluated f_2 -parameter for the cold runs is: $f_2 = -0.082 \pm 0.004$. The relatively small value of the quoted error is due to the accuracy of the values for the hyperfine-splitting parameters and to the invariance of f_2 in the subsequent temperature range.

The calculation of A_2 -values is straightforward using the estimated value of f_2 and the values of the Legendre polynomials averaged over the experimental solid angle. A final correction on these Legendre polynomials is the possible misorientation of individual crystals in the sample. The measurements on the α -activity from the composite samples A and B, discussed in chapter III, section 1, were not sufficiently accurate to provide a reasonable indication of this systematic error.

The calculated A_2 -values for both samples had a slight systematic discrepancy. Sample B with a lighter coating appeared to have somewhat higher anisotropy effects. Analogous to the calculations of the results for the experiments with ^{235}U and ^{233}U the results for the sample with averagely lower A_2 -values were renormalized to that with the higher values, according to the argument that systematic errors tend to lower the anisotropy effects. Hence, results for sample A were renormalized by multiplying with the ratio of the total average A_2 -value for sample B to that for sample A.

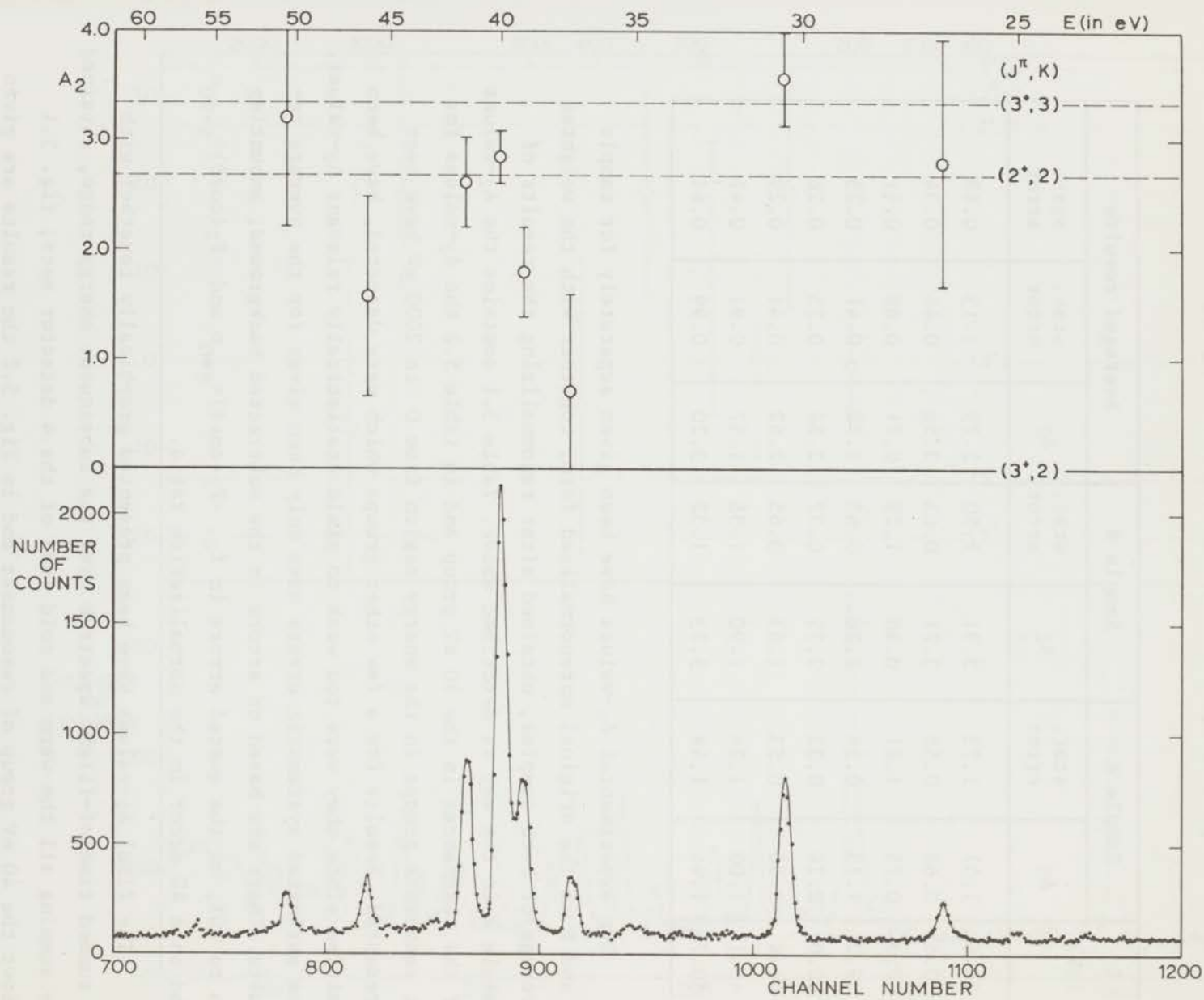


Fig. 5.1.

Fission-fragment spectrum and A_2 -values for the resonances in the 40 eV group.

Table 5.1

A₂-values for resonances in the 40 eV group

E (eV)	Sample A		Sample B		Averaged results		
	A ₂	stat. error	A ₂	stat. error	A ₂	stat. error	syst. error
26.6	1.01	1.73	3.91	1.50	2.79	1.13	0.68
30.5	2.68	0.58	3.71	0.63	3.56	0.44	0.34
37.3	0.75	1.21	0.40	1.29	0.71	0.88	0.41
39.2	1.13	0.54	2.26	0.63	1.79	0.41	0.25
40.0	2.26	0.32	2.75	0.37	2.84	0.25	0.26
41.4	2.55	0.53	1.63	0.65	2.62	0.41	0.29
46.1	1.00	1.24	1.90	1.35	1.57	0.91	0.47
50.7	1.96	1.49	3.73	1.32	3.20	0.99	0.61

The experimental A_2 -values have been given separately for sample A and B in the original unrenormalized form, together with the weighted average of both samples, obtained after renormalizing the results of sample A in the way as described above. Table 5.1 contains the A_2 -values of the resonances in the 40 eV group and in table 5.2 the A_2 -values for 11 resonance groups in the energy region from 0 to 2000 eV have been presented. Results for a few other groups which were detected, have been omitted since they were too weak to yield statistically relevant A_2 -values. The estimated systematic errors have only been given for the average results. These are based on errors in the subtracted background, amounting up to 10%, on the quoted errors in f_2 , $\langle P_2(\cos\theta) \rangle_{\theta=0}^{\circ}$ and $\langle P_2(\cos\theta) \rangle_{\theta=90}^{\circ}$ and on a 4% error in the normalization ratio.

The final A_2 -values have been presented graphically together with a summed time-of-flight spectrum over the subsequent energy range, obtained by summing all the warm and cold runs of the 4 detector sets; fig. 5.1 shows the 40 eV group of resonances and in fig. 5.2 the results are given for the channel region 50 to 550 which approximately corresponds to the energy range 100 to 3000 eV.

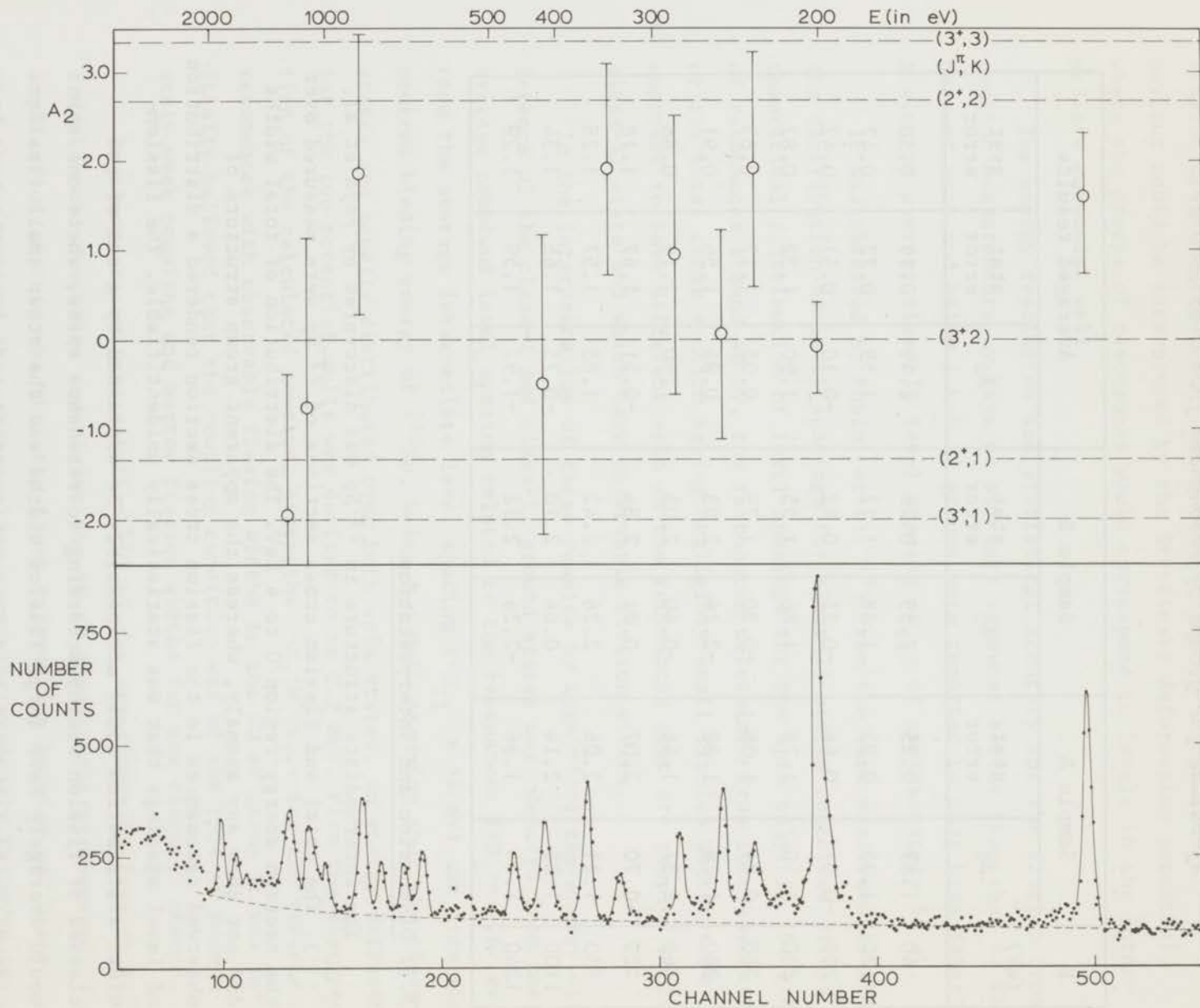


Fig. 5.2.

Fission-fragment spectrum and A_2 -values for the groups of resonances from 100 to 3000 eV.

Table 5.2

A_2 -values for groups of resonances from 0 to 2000 eV

E (eV)	Sample A		Sample B		Averaged results		
	A_2	stat. error	A_2	stat. error	A_2	stat. error	syst. error
40	1.87	0.25	2.59	0.28	2.49	0.19	0.50
120	1.35	0.95	1.38	1.12	1.59	0.72	0.47
200	-0.01	0.66	-0.25	0.82	-0.10	0.51	0.42
230	1.50	1.78	1.86	1.95	1.90	1.32	0.82
250	0.24	1.56	-0.30	1.79	0.05	1.17	0.83
280	1.78	1.88	-2.16	2.83	0.94	1.56	0.91
365	2.37	1.46	-0.40	2.05	1.90	1.19	0.88
420	-0.70	2.07	0.21	2.84	-0.51	1.67	1.18
850	1.21	2.06	2.26	2.42	1.85	1.57	1.28
1100	1.28	2.14	0.64	2.70	-0.75	1.68	1.34
1240	1.44	1.96	-2.26	2.72	-1.97	1.59	1.29

5.3. Discussion and interpretation

The intermediate structure in ^{237}Np was discovered by Paya et al. (8,11). The total and fission cross sections of ^{237}Np were measured over the neutron energy region 0 to 4 keV. The distribution of total widths did not show any anomaly, whereas the apparent group structure of observed resonances in the fission cross section rendered a distribution of level spacings that was statistically unidentifiable. The fission-width distribution could not possibly be explained by a sum of two classes of fission widths according to resonance spins, where one spin would averagely have large fission widths and the other small fission widths, because the ratio of the numbers of resonances in the two classes was in complete disagreement with the ratio of statistical spin factors g_j .

section 5.3.

After the discovery of a similar group structure in the subthreshold fission cross section of ^{240}Pu it was realized that the anomalous behaviour could be interpreted by the Strutinsky deformation potential, where the groups of resonances would correspond to levels in the intermediate potential well.

The energy resolution and statistical accuracy for the fission cross section measurements by Paya et al. were somewhat better than that of the present work and below 1 keV 17 groups were reported to have been detected, giving an average class-II level spacing $\langle D_{\text{II}} \rangle$ of approximately 56 eV.

It was observed by Fubini et al. ¹⁰⁾ from the same measurements that the distribution of level spacings for class-II states conformed with a theoretical distribution of level spacings for one spin only. In the group of resonances around 40 eV, the resonances determined from the measurement of the total cross section having negligibly small fission widths were supposed to have different spin as the resonances that are coupled to the class-II state and which have observable fission widths.

In the interpretation of these results by Lynn ^{2,12)} the energy difference of the class-I and class-II ground states was deduced from the average compound level spacing related to the resonances ($\langle D_{\text{I}} \rangle = 0.67$ eV), from the average intermediate level spacing ($\langle D_{\text{II}} \rangle = 54$ eV) and from the neutron binding energy of ^{238}Np , being 5.4 MeV. Assuming that the class-II states are equally distributed over both spin states, an energy difference for the two potential wells was derived to be 2.2 MeV. From the distribution of the calculated coupling strengths $\langle \chi_{\text{I}} | H^i | \chi_{\text{II}} \rangle$ for the various resonances with observable fission widths in the 40 eV group it was initially believed that the coupling condition was of the type of moderately weak coupling and narrow fission widths for the class-II states.

In a more recent presentation ¹¹⁾ of the experiment by Paya et al. a weak broad resonance underlying the 40 eV group could be observed. The implication of this was that the first deformation barrier was higher than the second and thus the coupling strengths evidently reserved to the situation where the coupling between compound levels and intermediate levels is very weak and the coupling between intermediate levels and the continuum beyond the second barrier relatively strong, resulting in

a sizeable fission width for class-II states. The form of the underlying broad peak in the 40 eV group was such that it was quite possible that there were even two class-II states involved in the 40 eV group. The stronger peak would be centered at approximately 40 eV and the weaker one at 30 eV.

From the resonance parameters for the 40 eV group it was deduced that the effective number of channels for class-II states is 0.87, whereas for class-I states this number becomes 1.25×10^{-3} . The width $\hbar\omega_f$ of the first barrier can be calculated from the Hill-Wheeler barrier penetration formula using a value of 650 keV for the energy of the fission threshold. The value derived is $\hbar\omega_f = 650 \text{ keV}$ ¹¹⁾ and is of the same order as other values found for barrier widths.

The problem of the uncertainty in coupling strengths may be solved in a rather unambiguous way by measuring γ -ray spectra as a function of neutron energy over the group of resonances ¹³⁾. The γ -ray spectrum from the decay of a class-II state should be characterized by strong and widely spaced lines and this spectrum will be cut off at an energy of 3.2 MeV which corresponds to the depth of the intermediate potential well. If the coupling strength between compound and intermediate levels is reasonably strong then the strongest resonance in the fission cross section will contain a sizeable fraction of class-II admixing. For this resonance the radiation width will be reduced owing to a smaller radiation width for a class-II state related with the lower depth of the intermediate well. By comparison of the integral γ -ray intensities and individual lines in the γ -ray spectrum for the various resonances in the group, having differences in class-II admixing, the coupling strength might be determined.

The experimental results obtained by Weigmann et al. ¹³⁾ on the γ -ray spectra of resonances in the 40 eV group revealed no such structure as described above. Individual γ -ray transitions of class-II states were hardly found and the integral intensities were smoothly varying as a function of neutron energy. The coupling condition of narrow class-II states is clearly excluded on the basis of these results. Assuming that the excitation energy is near to the threshold of the second barrier, yielding a transmission factor ~ 0.5 , a tentative estimate was made of

section 5.3.

the fission width of a class-II state from the Bohr-Wheeler formula for the effective number of transition states: $\Gamma_{(F)}^{II} \approx 4.0$ eV.

Recent measurements of the total and scattering cross section of ^{237}Np by Poortmans et al. ¹⁴⁾ in combination with the results of the capture cross-section measurements by Weigmann gave the possibility of determining the resonance parameters, including the spins for 12 resonances. The two classes of resonances have mean capture widths $\langle \Gamma_{\gamma} \rangle_{J=3} = 47$ meV and $\langle \Gamma_{\gamma} \rangle_{J=2} = 57$ meV. Four resonances with detectable fission widths, which belong presumably to the 40 eV group, are all found to have spin 2. These 4 resonances are at 24.5, 26.6, 30.4 and 50.4 eV respectively.

With the above information, part of which is inconsequential to the results of the experiment presently described, an interpretation of the angular distribution of fission fragments appears to be quite straightforward.

From the A_2 -values in table 5.1 for resonances in the 40 eV group, displayed in fig. 5.1, it can be concluded that this group of resonances is consistent with $(J^{\pi}, K) = (2^+, 2)$. The assumption for this conclusion however, is that all resonances have the same spin. For the entire group the statistical and systematic errors quoted on the A_2 -values are sufficiently small to distinguish between the channels $(2^+, 2)$ and $(3^+, 3)$, although the distinction is made with some reserve.

The possibility for the existence of two class-II states in the 40 eV group can only be examined in so far as that these two states would have different spins. Statistical errors of the A_2 -values do not allow such an interpretation. The only indication is that the A_2 -values for the 26.6 and 30.5 eV resonances are slightly higher, than the average value for the other resonances in the group.

The spin assignments by Poortmans et al. ¹⁴⁾ on the 4 resonances in the 40 eV group consistently result to $J = 2$. Of these 4 resonances, the one at 24.5 eV is detected in the experiment presently described, but this resonance is too weak to render a statistically relevant A_2 -value. The other three at 26.6, 30.4 and 50.4 eV correspond to the highest A_2 -values in the 40 eV group. The possibility for a second class-II

state in the 40 eV group that would have $J = 3$ seems herewith to be ruled out. The determination of the combination (J^π, K) from the average A_2 -value for the 40 eV group being $(J^\pi, K) = (2^+, 2)$, is certainly confirmed by Poortmans' results.

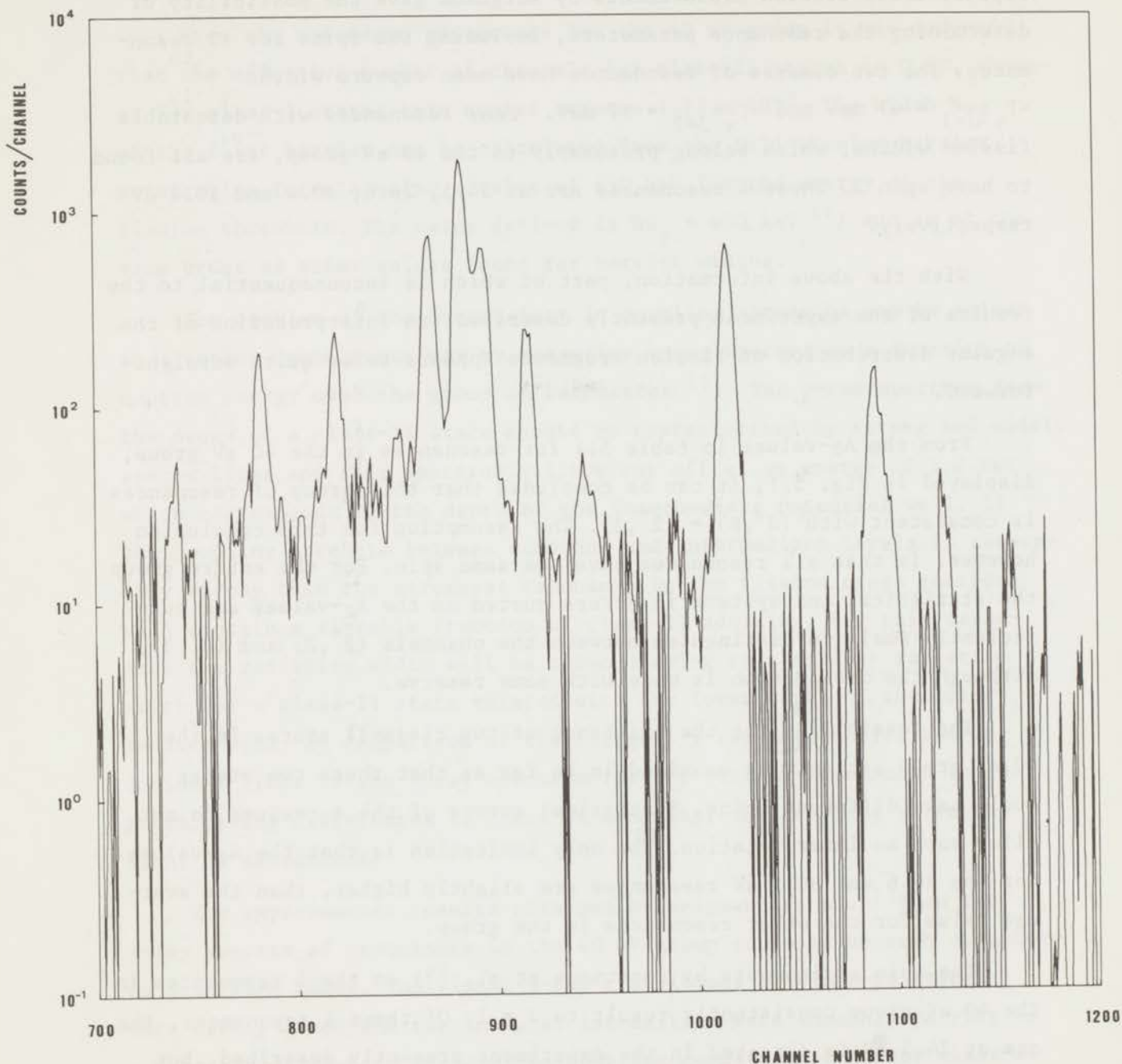


Fig. 5.3.

Logarithmic plot of the background subtracted fission-fragment spectrum of the 40 eV group for the detection of a low broad resonance underlying the group.

section 5.3.

A logarithmic plot of the summed results of cold and warm runs is shown in fig. 5.3. The background was subtracted in order to compare the behaviour of the broad peak underlying the 40 eV group with the results by Paya et al.¹¹). The broad peak is roughly centred at 40 eV and is obviously asymmetric. However, there is no clear evidence for a second peak which would be centred at approximately 30 eV. It is realized that the detection of such a low broad peak strongly depends on the subtraction of background counts from the measured time-of-flight spectra.

For the resonance groups at higher energies the statistical accuracy of the experimental anisotropy is considerably less. Therefore, the results of these groups have to be described as tendencies towards particular K-values rather than explicit assignments. Leaving the A_2 -values with statistical errors greater than 1.7 out of the discussion, the groups generally agree very well with the channels $(2^+, 2)$ and $(3^+, 2)$. In a few cases other channels like $(3^+, 3)$, $(2^+, 1)$ or even $(3^+, 1)$ cannot definitely be excluded, but no A_2 -value forbids either of the two channels with $K = 2$. The distribution over both spins 2^+ and 3^+ seems to be fairly equal. The conversion of experimental A_2 -values to possible fission channels is presented in table 5.3.

Although experimental evidence is not entirely decisive, it can be stated that in the angular distribution of fragments from subthreshold fission of ^{237}Np the channels $(2^+, 2)$ and $(3^+, 2)$ are predominant. The admixing of other fission channels is by no means excluded but is indicated to be of minor importance. From the equal probability in the distribution of A_2 -values of the resonance groups for occupation of the channels $(2^+, 2)$ and $(3^+, 2)$ it follows that there is not a great energy difference between the two transition states at the second deformation barrier. If these transition states are members of the same rotational band, the particle state on which this band is superimposed will have $(J^\pi, K) = (2^+, 2)$. This is not necessarily the transition ground state, since the individual spins of the unpaired proton and neutron in this odd-odd nucleus may couple to a ground state spin higher than 2 or 3. In that case the transition state $(2^+, 2)$ will be a level of intrinsic excitation.

Table 5.3.

(J^π, K) -assignments for groups of resonances from 0 to 2000 eV; x marks the possible channels within one standard deviation and (x) those between one and two standard deviations on the experimental A_2 -values.

J^π, K	$2^+, 0$	$3^+, 1$	$2^+, 1$	$3^+, 2$	$2^+, 2$	$3^+, 3$
(A_2) theor.	-2.68	-2.01	-1.34	0	2.68	3.35
E(eV)						
40					x	
120				(x)	x	
200				x		
230				(x)	x	(x)
250		(x)	(x)	x		
280		(x)	(x)	x	(x)	(x)
365				(x)	x	(x)
420	(x)	(x)	(x)	x	(x)	
850				(x)	x	(x)
1100	(x)	(x)	(x)	x	(x)	
1240	(x)	x	(x)	(x)		

References

References

1. V.M. Strutinsky, Nucl. Phys. A 95 (1967) 420.
2. J.E. Lynn, Structure in Sub-Threshold Fission Modes, report AERE-R 5891 (1968).
3. H. Weigmann, Zeitschr. f. Physik 214 (1958) 7.
4. J.A. Wheeler, Fast Neutron Physics (ed. Fowler and Marion, 1963) Part II, 2051.
5. S.A.E. Johannsson, Nucl. Phys. 12 (1959) 449.
6. S.G. Nilsson, Chin Fu Tsang, A. Sobiczewski, Z. Szymanski, S. Wycech, C. Gustafson, I. L. Lamm, P. Möller and B. Nilsson, Nucl. Phys. A 121 (1969) 1.
7. J.R. Stehn et al., Neutron Cross Sections, BNL-325, Supplement 2, Vol. III (1965).
8. D. Paya, H. Derrien, A. Fubini, A. Michaudon and P. Ribon, Nucl. Data for Reactors, IAEA-Symposium (Paris, 1966) Paper CN-23/69 (only abstract has been published).
9. D. Paya, J. Blons, H. Derrien, A. Fubini, A. Michaudon and P. Ribon, Journal de Physique 29, Suppl. 1 (1968) C1-159.
10. A. Fubini, J. Blons, A. Michaudon and D. Paya, Phys. Rev. Letters 20 (1968) 1373.
11. D. Paya, J. Blons, H. Derrien and A. Michaudon, Physics and Chemistry of Fission, IAEA-Symposium (Vienna, 1969) 307.
12. J.E. Lynn, Physics and Chemistry of Fission, IAEA-Symposium (Vienna, 1969) 249.
13. H. Weigmann, Phys. Letters 30 B (1969) 624.
14. F. Poortmans, H. Ceulemans, J. Theobald and E. Migneco, private communication.

Chapter VI

ANALYSIS OF THE ANISOTROPY IN THE ANGULAR DISTRIBUTION OF FISSION FRAGMENTS FROM ALIGNED ^{233}U USING A MULTILEVEL-FIT PROCEDURE

6.1. Introduction; multilevel-fit formalism

The fission cross section of ^{233}U at low neutron energies exhibits a very complex structure. The total widths of the compound nuclear levels are of the same order as the level spacings. Besides a strong overlapping of resonances there is also an interference between resonances of the same spin and parity. As a result of this the peaks in the fission cross section may become asymmetric and therefore, their shape cannot be described by the usual single-level Breit-Wigner formulae. Consequently, multilevel-fits become necessary for a description of the cross sections of heavy nuclei.

A simple analysis of the angular distribution of fission fragments from aligned ^{233}U was performed in terms of energy regions over observable resonances. It would be worthwhile considering the possibility of an analysis of the data on the basis of a multilevel fit, since the ultimate purpose of such an analysis is to interpret the anisotropy as resulting from the interference between resonances in terms of gradually changing contributions from the various available fission channels.

From the analysis of various fission cross sections the distribution of fission widths often showed a grouping into two classes which were supposed to be correlated with the resonance spin. However, the ratio of the numbers of resonances in the two apparent classes of fission widths did not seem to conform with the statistical ratio of resonance spins. During the earlier stages in the development of the interference theory, the asymmetries in the fission cross section were sometimes assumed to be due to non-detected broad or weak resonances partially hidden by overlapping of stronger resonances. However, experimental evidence for interference was soon available by comparison of the capture with the fission cross sections and from variations in quantities related to fission such as the average number of neutrons per fission event ($\bar{\nu}$) measured as a function of neutron energy. Furthermore, the small number of fission channels, as determined from the fission width distributions, made it theoretically rather probable

section 6.1.

that the fission cross section would feature interference. If a large number of reaction channels is available, interference will become less important owing to a statistical cancellation for a situation where the signs of the partial amplitudes are randomly distributed. For instance, the radiative capture cross section is characterized by many exit channels and a single-level approach for the cross-section analysis will generally be satisfactory.

In the R-matrix formalism by Wigner and Eisenbud ¹⁾ the relation between the derivative matrix (R) and the collision matrix (S) leads to the following expression for the cross sections:

$$\sigma_{ij} = \pi \lambda_i^2 \sum_J g_J |\delta_{ij} - S_{ij}|^2,$$

in which δ_{ij} is the Kronecker symbol; the indices i and j denote the neutron channel and an arbitrary exit channel respectively and the summation J is over the various spin states. In the single-level formulation the expression for the collision matrix S_{ij} reduces to the usual reaction amplitude in the Breit-Wigner formulation:

$$S_{ij} \sim \frac{y_{\lambda i} y_{\lambda j}}{E_\lambda - E - \frac{1}{2}i\Gamma_\lambda},$$

where $y_{\lambda i}$ and $y_{\lambda j}$ are the reduced width amplitudes.

An approximation for a multilevel-fit formula was obtained by Feshbach et al. ²⁾ by making the assumption that the collision matrix elements can be summed first over all compound states λ :

$$\sigma_{ij} = \pi \lambda_i^2 \sum_J g_J \left| \sum_\lambda \frac{y_{\lambda i} y_{\lambda j}}{E_\lambda - E - \frac{1}{2}i\Gamma_\lambda} \right|^2.$$

For cross sections with level spacings in the order of the level widths this formula will become inaccurate and therefore this approximation is generally not suitable for the fission cross sections.

Extensive applications of R-matrix theory by Reich and Moore ³⁾ and by Vogt ⁴⁾ on resonance interference, yielded a theoretically correct analytical method with which the cross sections could be described by expressions having the R-matrix characteristics E_λ and $\Gamma_{\lambda j}$ as variables. However, in order to be able to make a practical use of this method in the cross-section analyses, the final expressions for the reaction cross sections had to be obtained by making assumptions on the number of reaction channels in the considered cross section and on the character of the interference. In many cases this is an impractical approach. It was evident that the results for resonance parameters obtained with this method, in particular the resonance spins, were far from unambiguous.

For reasons of computational limitations on the R-matrix methods in which inversions are involved of $N \times N$ -matrices where N is the number of levels which is required to be large, a more suitable method had to be developed for a purely analytical description of the cross sections.

Adler and Adler ⁵⁾ derived a very simple formulation that would describe the experimental cross section adequately. The reaction cross section in this approach is a linear sum of symmetric and antisymmetric terms:

$$\sigma_{nj} = \frac{1}{\sqrt{E}} \sum_{\kappa} \frac{G_{\kappa}^{(j)} v_{\kappa} + H_{\kappa}^{(j)} (\mu_{\kappa} - E)}{(\mu_{\kappa} - E)^2 + v_{\kappa}^2}$$

where $G_{\kappa}^{(j)}$, $H_{\kappa}^{(j)}$, μ_{κ} and v_{κ} are resonance parameters. Least-squares fitting routines were constructed by Adler and Adler ⁶⁾ for this method of multilevel analysis of the cross sections.

The relation between the Adler-Adler resonance parameters and the original R-matrix resonance parameters E_λ and $\Gamma_{\lambda j}$ can only be calculated under the additional assumption that the number of interfering levels is small. This clearly points out the disadvantage of the method against its mathematical simplicity. Explicit reference to the reaction channels by means of the partial reaction widths cannot be found in

section 6.2.

this formula for the reaction cross section. Therefore, the Adler-Adler formulation will yield an excellent analytical fit to the various cross sections, but it is doubtful as to whether the anisotropy in fission-fragment emission, which is directly related to the quantum numbers K of the fission channels, will be described unambiguously by this formula.

6.2. The fission cross section of ^{233}U

The fission cross section of ^{233}U was fitted with the single-level formula by Nifenecker and Perrin ^{7,8)}. According to the results of this fit it was claimed that the reasonably accurate description by the Breit-Wigner formula indicated that interference effects should form a minor contribution to the fission cross section. However, the agreement with the experimental total cross section was rather poor when using the resonance parameters obtained from this fit on the fission cross section. Furthermore, the single-level resonance parameters for ^{233}U evaluated by Stehn et al. ⁹⁾ did not even yield a qualitative agreement with either the total or the fission cross section.

The earlier multilevel fits based on the extensive R-matrix formulation gave correct fits to the fission and other cross sections, but the resulting sets of multilevel-fit resonance parameters apparently were relatively inconsequential to the correctness of the obtained fit; a rather wide range of different resonance parameter sets would give almost equivalent cross section patterns.

A very detailed analysis by Vogt ¹⁰⁾ in the neutron-energy region from 0 to 5 eV on the total, the fission, the scattering cross section and on the quantity $1 + \alpha$, where α is defined by $\frac{\sigma_c}{\sigma_f}$, indicated that approximately three fission channels would be open for each of the two resonance spin states.

Reich and Moore ¹¹⁾ calculated resonance parameters from fits to the total and fission cross section up to 11 eV according to the R-matrix formalism previously derived ³⁾. The conclusion from the results was that only a few fission channels were available for resonances of

one spin state, for which sharp peaks and distinct interference effects would be noticed, whereas the other spin state could be characterized by wide overlapping resonances, corresponding to many available fission channels and thus, a statistical cancellation of interference. A consequence of this interpretation is that there would exist a considerable difference in the fission threshold for the two spin states.

The measurements on the total cross section by Pattenden and Harvey ¹²⁾ did not give sufficient information to allow a very detailed multilevel fit.

In the multilevel-fit analyses mentioned above spin assignments were attempted by classifying the reduced width amplitudes. However, the ratio of resonances in the two spin groups was contradictory to the expectation from the ratio of statistical spin factors in the formulae for level densities.

Calculations by Musgrove ^{13,14)} indicated that up to 25% of the resonances in ²³³U might have been unobserved, because of their relative weakness and overlapping. The total and the fission cross section up to 11 eV were fitted simultaneously by multilevel analysis, using the Feshbach approximation ²⁾ for multilevel formulae with the additional assumption that for a particular resonance, fission would proceed through one fission channel only. The spins were assigned to 14 resonances assuming spin 3 for the spin of the 10.4 eV level. These results showed that 2⁺ resonances corresponded to large fission widths, indicative of several open fission channels, and that the 3⁺ resonances would have a much narrower widths. A similar method was used by Bergen and Silbert ^{15,16)} on the fission cross section and the ratio of capture to fission cross section (α) from 20 to 64 eV. Applying the Reich-Moore formalism with the additional assumption that for a particular resonance only one spin state would be available the analytical fit obtained was rather accurate in comparison with the single-level fit. The same method was also used by Sauter and Bowman ¹⁷⁾ in the region up to 30 eV by simultaneously performing a multilevel fit on their measured scattering cross section and on the fission cross section by Nifenecker ⁷⁾. The obtained fits were too inaccurate to

section 6.2.

allow spin assignments, indicating that the assumption of one fission channel per resonance was incorrect.

The results of this group of multilevel procedures were satisfactory considering the analytical description of the cross sections experimentally observed, but the physical significance of the methods was doubtful as may be seen from the ultimate spin assignments and tentative predictions concerning the number of fission channels available to the two spin groups of resonances.

The Adler-Adler approach was numerically much easier to be performed but the physical meaning of the resonance parameters was even less relevant than the Vogt or Reich-Moore formalisms. The first attempts by Adler, Adler and Goodwin ¹⁸⁾ gave exact fits to the total cross section from 0 to 30 eV; it may be remarked that the choice of the resonance energies was somewhat arbitrary.

In more recent experiments the various cross sections were measured over extended energy ranges with an improved experimental accuracy. At the linear accelerator at Rensselaer Polytechnic Institute (USA) the fission and the capture cross section of ²³³U were measured simultaneously from 0 to 2000 eV [ref.^{19,20)}]. The resonances were well resolved for neutron energies up to 65 eV. A simultaneous fit on σ_f and σ_c ²¹⁾ using the Adler-Adler multilevel formalism, provided an analytical description that was sufficiently accurate considering the requirements for nuclear reactor calculations. Fission cross section measurements at the linear accelerator of CBNM, Euratom at Geel, together with a multilevel fit performed for resonances up to 65 eV ²²⁾ gave the results in the form of the Adler-Adler resonance parameters with an accuracy similar to the ORNL results.

The Adler-Adler parameters of the two latter analyses have been given in table 6.1, since these results have been used for further calculations on the present data.

Table 6.1.

Resonance parameters of ^{233}U

$\mu(\text{eV})$		$\nu(\text{eV})$		$G_f(\text{b.eV}^{\frac{3}{2}})$		$H_f(\text{b.eV}^{\frac{3}{2}})$	
ORNL	CBNM	ORNL	CBNM	ORNL	CBNM	ORNL	CBNM
-2.79	-2.790	0.37	0.370	-1511.99	-1514.986	-513.24	-521.078
0.18	0.180	0.07	0.070	-0.190	-0.190	-0.830	-0.830
1.43	1.598	0.35	0.495	66.91	147.741	-31.81	-26.875
1.78	1.800	0.12	0.092	111.08	79.521	-1.78	-1.024
2.29	2.307	0.05	0.041	42.47	34.867	17.64	12.311
3.29	3.040	0.51	0.420	36.93	-14.624	-42.08	-34.259
3.63	3.657	0.08	0.103	20.91	23.992	7.23	8.730
4.53	4.750	0.39	0.390	44.29	56.798	-51.91	-23.455
5.74	5.810	0.18	0.210	11.04	16.120	-24.25	-26.671
6.80	6.856	0.09	0.091	168.68	1.283	35.89	0.240
7.5	7.450	0.11	0.251	5.93	13.155	2.23	1.221
8.67	8.860	0.26	0.412	15.01	45.952	4.05	20.862
9.15	9.180	0.15	0.200	17.63	13.691	-15.41	-36.038
10.35	10.420	0.16	0.162	276.95	263.003	7.65	-8.185
11.2	11.210	0.27	0.300	41.21	42.445	-4.76	-19.462
12.76	12.860	0.16	0.166	226.13	221.875	44.65	37.340
13.51		0.14		-12.21		4.42	
13.63	13.760	0.24	0.200	101.85	70.416	3.03	4.577
15.28	15.400	0.12	0.094	118.4	99.618	-33.36	-29.328
16.15	16.460	0.22	0.220	106.78	210.856	7.14	142.435
16.51	16.540	0.13	0.080	97.21	13.088	17.74	-83.245
17.92	18.110	0.10	0.100	37.37	35.860	4.27	13.040
18.46	18.580	0.25	0.260	78.36	138.367	20.69	17.923
18.86	19.000	0.15	0.150	213.21	173.698	-61.33	-94.971
20.53	20.620	0.21	0.205	116.58	125.0	6.91	-20.31
21.85	21.950	0.13	0.114	131.87	123.2	95.43	49.97
22.23	22.380	0.24	0.220	545.37	492.40	-90.62	-33.67
22.94	23.040	0.38	0.380	96.53	170.95	-6.68	1.234
23.54	23.640	0.33	0.315	61.03	48.730	-95.86	-125.0
25.13	25.270	0.19	0.190	85.0	84.040	-44.81	-48.650
26.57	26.700	0.28	0.230	58.7	60.270	19.73	22.44
28.42	28.480	0.28	0.260	29.85	43.420	86.46	54.37
28.91	29.080	0.31	0.310	233.67	225.30	-62.48	-32.29
29.68	29.750	0.11	0.110	-0.16	0.679	13.34	16.606
30.15	30.200	0.10	0.105	2.27	-0.068	-0.61	1.632
30.76	30.810	0.15	0.140	52.79	57.09	51.39	41.620
31.20	31.270	0.47	0.470	149.57	123.0	-72.18	-85.67
31.97	32.030	0.15	0.150	113.99	102.30	6.79	6.781
32.74	32.800	0.43	0.430	42.61	17.95	-96.58	-98.84
34.03	34.100	0.66	0.660	112.79	40.85	26.7	73.87
34.53	34.590	0.42	0.420	168.73	209.1	21.71	65.79
35.19	35.200	0.12	0.155	27.07	42.17	-8.85	-12.068
35.49	35.550	0.16	0.190	10.72	25.095	-24.48	-33.81
36.52	36.500	0.09	0.085	59.13	75.57	11.5	-10.46
37.46	37.470	0.19	0.218	64.0	88.93	14.4	19.42
39.48	39.480	0.22	0.300	67.55	90.164	76.24	116.940
39.71	39.710	0.11	0.160	34.07	47.736	-27.73	-26.458
40.15	40.150	0.45	0.460	97.39	156.800	-80.0	-101.442
41.08	41.080	0.10	0.100	19.88	33.903	13.37	15.608
	41.900		0.400		16.117		7.380
42.62	42.600	0.11	0.160	62.23	99.103	15.86	0.629
43.47	43.450	0.13	0.146	32.49	45.692	6.16	-10.375
44.70	44.480	0.56	0.339	93.00	38.679	36.62	-13.902
45.21	45.300	0.25	0.050	1.91	-0.806	-23.98	0.875
45.99	46.070	0.12	0.070	33.33	32.437	-26.17	-8.864
47.17	47.270	0.23	0.230	75.74	90.760	-9.08	30.471
48.64	48.670	0.13	0.130	167.38	200.033	-21.20	-12.940
49.12	49.000	0.09	0.300	9.68	19.330	-6.64	-0.949
50.21	50.300	0.45	0.400	55.75	51.313	-31.14	4.922
50.99	51.150	0.38	0.200	16.84	4.937	-4.13	18.371
51.95	51.905	0.62	0.620	12.00	53.557	-41.84	34.837
52.93	53.000	0.22	0.230	53.45	91.480	-62.43	-36.482
53.97	54.000	0.14	0.150	61.95	90.750	-25.09	-14.953
54.77	54.770	0.09	0.090	61.08	80.866	6.13	7.288
56.09	56.090	0.27	0.270	69.62	106.698	128.22	146.752
56.35	56.440	0.30	0.270	211.98	225.687	-60.39	-31.019
57.48	57.500	0.49	0.460	282.72	345.336	20.92	8.529
58.51	58.510	0.23	0.250	91.51	117.092	26.41	2.895
61.30	61.350	0.40	0.375	185.51	233.236	47.48	53.202
62.50	62.520	0.20	0.098	107.86	96.786	-14.96	-14.487
	64.080		0.500		282.465		57.830
64.30	64.300	0.40	0.257	228.02	58.479	-22.05	-126.008
	64.770		0.106		-20.249		-33.864

section 6.3.

6.3. Calculations and results

The experimental time-of-flight spectra obtained in the warm runs for the measurement of the fission-fragment angular distribution should, in principle, be suitable for a multilevel-fit analysis. By means of the resonance parameters obtained from this fit the anisotropies as a function of neutron energy can then be resolved into the contributions of the individual resonances. An estimate of the effects of overlapping on the distribution of anisotropies for the resonances was already made in chapter IV by comparing the effects in the top part of resonances to those calculated from the extended resonance region (see fig. 4.3).

It has been tried to separate contributions to the angular distribution from neighbouring resonances by adjusting a set of multilevel parameters obtained from accurate experiments to the summed results of warm runs in which no anisotropies are present. The next step then is to use the calculated forms of individual resonances for the analysis of the resonance anisotropies by means of the least-squares fitting procedures. In this method the A_2 -values are assigned to individual resonances, where a resonance is defined by the Adler-Adler parameters, μ , ν , G and H . It would have been a more detailed approach to analyze the anisotropies in the resonances by assigning separate A_2 -values to the symmetric and anti-symmetric parts of the resonances. However, the statistical accuracy of the experimental data does not allow such an analysis.

The two sets of multilevel-fit parameters (ORNL and CBNM) reviewed in the previous section were the only ones over the energy region of resolved resonances from 0 to approximately 60 eV with sufficient accuracy. An analytical description of the time-of-flight spectra by the sets of multilevel-fit parameter involves detailed adjustment of experimental properties which also characterizes the reduction of time-of-flight spectra to cross section, but now performed in the reverse order. The resolution and Doppler broadening, the background in the fission fragment spectra and the neutron spectrum all have to be calculated and fitted to the fission fragment time-of-flight spectrum

from the warm runs.

The broadening parameters and time shifts due to resolution and Doppler broadening were calculated as functions of neutron energy as described in chapter II, section 5. The contribution of the Doppler effect to the broadening is practically negligible, owing to the low temperatures at which the experiments were performed. The resulting values for the broadening parameter generally agreed very well, whereas a constant correction over the whole energy region had to be applied to the total time shift. The latter implies simply a more precise calculation of the zero time-of-flight. The broadening function was folded in on the fission cross section by a division of this function into 16 equal time intervals. The small deviation of the form of the broadening function from a symmetric gaussian curve was taken into account by using a standard set of areas for these 16 intervals, according to the asymmetry in the resolution function.

The calculations were performed on a background subtracted run, which means that the broadened cross section should be fitted simply by multiplication with the neutron spectrum. However, systematic deviations between calculated and experimental spectra made it necessary to include a small correction to the background which could be negative as well as positive. It may be remarked at this point, that these deviations may be due to systematic errors in the background subtraction and neutron spectrum of the present experiment as well as of the experiment from which the multilevel parameters were taken.

A correction had to be made for the absorption and scattering of neutrons by ^{238}U . A number of sharp dips were visible in the fission fragment spectrum for the sample not facing the neutron beam, which received neutrons after transmission through the crystal slabs of both samples. The calculated transmission factor for the ^{238}U resonances at 6.67, 20.5 and 32.1 eV corresponded very well to these dips in the time-of-flight spectrum.

The neutron spectrum was fitted by a smooth curve of the type:

section 6.3.

$$N(E)dE = C E^P (1 - e^{-\frac{a}{\sqrt{E}}}) dE,$$

in which the exponential term accounts for neutron absorption by the cadmium. Deviations from this form could mainly be ascribed to background counts for which a smooth numerical function was evaluated. The experimental points for the neutron spectrum and background correction were obtained simultaneously by a least-squares fitting routine. The background correction generally was rather small and a distinct energy correlation over the whole energy region could not be detected. For the individual channels the background did not exceed the statistical errors. For further calculations the background correction was taken equal to the deviations between experimental data and fitted curve. A smooth curve for the background correction was obtained by integration over energy intervals in the order of 2 eV. Such a numerical procedure can be carried out assuming that the background is a slowly varying function of neutron energy. In a few cases deviations were apparently due to inappropriate fitting of one of the resonances, in which cases a slight adjustment of the multilevel-fit parameters for the particular resonance yielded a correct fit.

From the fact that an additional background had to be included to obtain a satisfactory fit of the time-of-flight spectrum by a set of multilevel parameters, it is doubtful as to whether the neutron spectrum and background correction function acquired from the warm runs would also accurately correspond to the cold runs. Although the background from these runs was subtracted using exactly the same procedure, the statistical errors on the experimental points for the background determination gave rise to systematic errors in the background subtraction of similar size as these statistical errors and hence, the subtraction of the background for cold and warm runs is expected to have differences in the order of these systematic errors. The neutron spectrum and background correction derived from the warm runs were normalized to the cold runs by the ratio of total counts in the energy region from 0.4 to 60 eV of cold and warm runs, where the counts in the cold runs were corrected for the average anisotropy

effect. The A_2 -values for individual resonances were calculated by performing a simultaneous fit on the time-of-flight spectra in the 0° - and 90° -directions, over an energy range which could be regarded to be relevant for one particular resonance. The A_2 -values for the neighbouring resonances were fitted in the same procedure. By taking all the resonances subsequently as the central resonance in the appropriate energy ranges the A_2 -values for the individual resonances were obtained. A second and a third iteration were performed by taking the resulting A_2 -values from the previous step as starting values in the fitting procedures for the next iteration. After 3 iterations there was no significant difference between the initial and the final A_2 -values. The results of the calculations, averaged for sample A and B are given in the form of a pseudo-histogram in fig. 6.1.

6.4. Discussion of the results and the method

A comparison of the experimental histogram (fig. 4.2) from chapter IV with the histogram in fig. 6.1 obtained from the multilevel-fit procedure, shows that the correction on the A_2 -values for overlapping of resonances did not result in a very pronounced structure in the histogram. A grouping of A_2 -values into a few classes according to fission channels is not observed. From the calculations of theoretical distributions of A_2 -values it can on the contrary be concluded that such a definite group structure cannot be expected as soon as a few fission channels with different K-values are available to the neutron resonances of either spin. Furthermore, statistical fluctuations in the distributions of small numbers of resonances are relatively large as shown before, and the appearance of a group structure in histograms constructed from only 50 to 60 A_2 -values is by no means unambiguous. The accuracy of the experimental data, regarding counting statistics and determination of systematic errors, was such that a form analysis on the time-of-flight spectra was feasible only by employing the Adler-Adler formulation which numerically is the most simple approach. However, this method does not allow a very detailed channel analysis. The individual contributions from the various fission channels are

section 6.4.

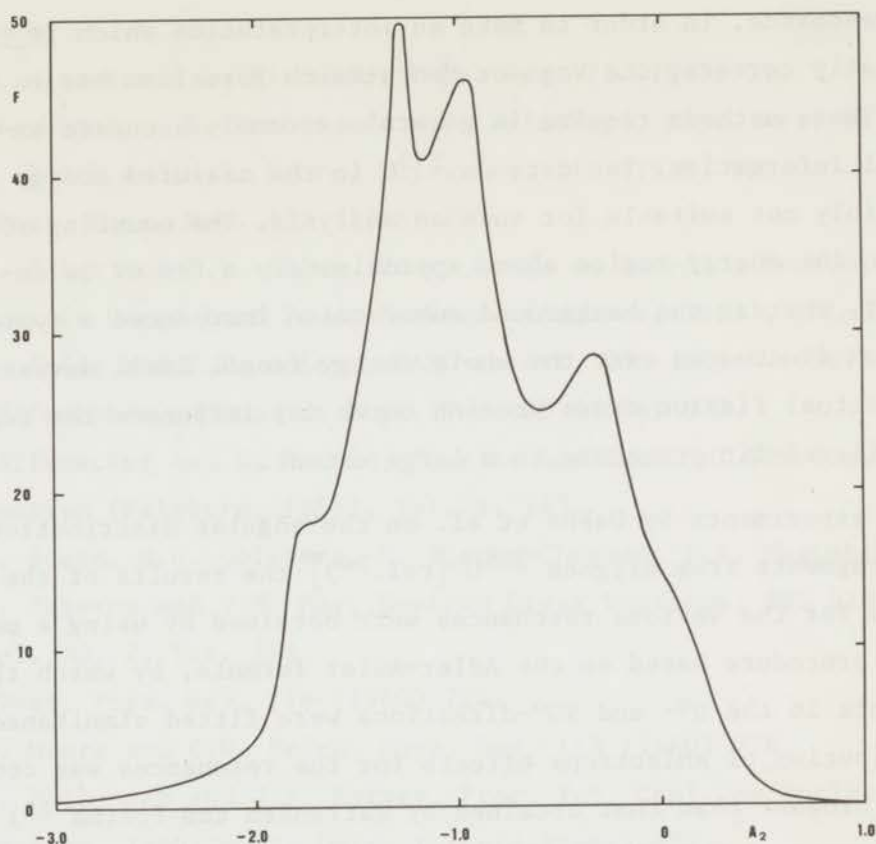


Fig. 6.1.

Histogram of A_2 -values for resonances with a correction for contributions from overlapping resonances obtained by a multilevel-fit analysis on the fission-fragment time-of-flight spectrum.

not reflected in the Adler-Adler formulae. A first approach in accounting for the effects of interference between resonances would be a separation of the symmetric and asymmetric parts in the fission cross section for a particular resonance and calculate independent A_2 -values for both parts. This might be a suitable method of describing the variations observed in the anisotropy of fission-fragment emission over the peak of the resonance at 0.28 eV in the fission cross section of ^{235}U in the energy range below 1 eV [ref.²³]. However, the resulting A_2 -values do not yet allow to draw a definite conclusion about the relative contributions from the various channels

in this resonance. In order to make an interpretation which is theoretically correct, the Vogt or Moore-Reich formalism has to be applied. These methods require in general extremely accurate experimental information. The data on ^{233}U in the measured energy range are certainly not suitable for such an analysis. The counting statistics in the energy region above approximately a few eV is insufficient, whereas the background subtraction introduced a systematic error which fluctuates over the whole energy range. Small deviations from the actual fission cross section curve may influence the results of a multilevel-fit procedure to a large extent.

In the experiments by Dabbs et al. on the angular distribution of fission fragments from aligned ^{235}U [ref.²⁴] the results of the anisotropies for the various resonances were obtained by using a multilevel fit procedure based on the Adler-Adler formula, by which the measurements in the 0° - and 90° -directions were fitted simultaneously. The distribution of anisotropy effects for the resonances was considerably broader than that obtained by Pattenden and Postma²³) in the experiments at Harwell in which the A_2 -values for resonances were calculated by a simple analysis. The discrepancy in the width of the distribution of A_2 -values may be due to the fitting technique as well as to experimental systematic errors. From the results of the multilevel fit on the present data of ^{233}U it can be concluded that extremely accurate data are required to analyze the anisotropy in fission-fragment emission into the several components of the available fission channels.

References

References

1. E.P. Wigner and L. Eisenbud, Phys. Rev. 72 (1947) 29.
2. H. Feshbach, C.E. Porter and V.F. Weisskopf, Phys. Rev. 96 (1954) 448.
3. C.W. Reich and M.S. Moore, Phys. Rev. 111 (1958) 929.
4. E. Vogt, Phys. Rev. 112 (1958) 203.
5. D.B. Adler and F.T. Adler, Proc. Conf. on Breeding Economics and Safety in Large Fast Power Reactors (Argonne, 1963), ANL-6792, 695.
6. D.B. Adler and F.T. Adler, USAEC-report, COO-1546-4 (1967).
7. H. Nifenecker, Journ. de Phys. Tome 25 (1964) 877.
8. H. Nifenecker and G. Perrin, Physics and Chem. of Fission, IAEA-Symposium (Salzburg, 1965), Vol. I, 245.
9. J.R. Stehn, M.D. Goldberg, R. Wiener-Chasman, S.F. Mughabghab, B.A. Magurna and V.M. May, Neutron Cross Sections, BNL 325 (1965) Suppl. No. 2, Vol. III.
10. E. Vogt, Phys. Rev. 118 (1960) 724.
11. M.S. Moore and C.W. Reich, Phys. Rev. 118 (1960) 718.
12. N.J. Pattenden and J.A. Harvey, Proc. Int. Conf. on Nuclear Structure (Kingston, 1960; publ. Univ. Toronto Press) 882.
13. A.R. de L. Musgrove, Austr. Jrn. Phys. 20 (1967) 73.
14. A.R. de L. Musgrove, Austr. Jrn. Phys. 20 (1967) 617.
15. D.W. Bergen, report LA-3676-MS (1967).
16. D.W. Bergen and M.G. Silbert, Phys. Rev. 166 (1968) 1178.
17. G.D. Sauter and C.D. Bowman, Phys. Rev. 174 (1968) 1413.
18. F.T. Adler, D.B. Adler and W.A. Goodwin, Transactions ANS 7 (1964) 86.
19. L.W. Weston, R. Gwib, G. de Saussure, R.R. Fullwood and R.W. Hockenbury, report ORNL-TM-2140 (1968).
20. L.W. Weston, R. Gwin, G. de Saussure, R.W. Jagle, J.H. Todd, C.W. Craven, R.W. Hockenbury and R.C. Block, report ORNL-TM-2353 (1968).
21. G. de Saussure, report ORNL-TM-2745 (1968).
22. M.G. Cao, E. Migneco, J.P. Theobald, M. Merla, to be published.
23. N.J. Pattenden and H. Postma, submitted to Nucl. Phys.
24. J.W.T. Dabbs, C. Eggerman, B. Cauvin, A. Michaudon and M. Sanche, Proc. of 2nd Symposium on Physics and Chemistry of Fission, IAEA, Vienna (1969) 321.

SUMMARY

Anisotropies in the angular distributions of fission fragments and α -particles from oriented heavy nuclei have been measured with the target nuclei ^{235}U , ^{233}U and ^{237}Np . Nuclear orientation has been obtained with the method of hyperfine interaction, by cooling crystals of the chemical compound $\text{RbUO}_2(\text{NO}_3)_3$ abbreviated as RUN, to temperatures in the order of 0.1 K. Measurements are reported of the fission-fragment anisotropy for the neutron-induced fission of the target nuclei ^{233}U and ^{237}Np as a function of neutron energy from 0 to 2000 eV. These experiments have been done at the electron linear accelerator at AERE, Harwell with samples consisting of many RUN-crystals. The anisotropy in the α -emission from ^{233}U and ^{237}Np and the fission-fragment emission from capture of thermal neutrons in the target nuclei ^{235}U and ^{233}U have been measured with individual RUN-crystals at the High Flux Reactor at RCN, Petten.

In the fission process of heavy nuclei induced by low-energy neutrons the transition states at the deformation barrier can be described by the spin J of the compound nucleus, the projection K of J on the symmetry axis and parity π . The angular distribution of fission fragments is governed by the K -values of the energetically available transition states. A. Bohr predicted that in the fission of even-even compound nuclei, transition states will be predominant that are characterized by lower K -values. This has been verified in the case of $^{234}\text{U}^*$ by measuring the anisotropy in the angular distribution of fission fragments from neutron-induced fission of aligned ^{233}U for individual resonances in the neutron energy range from 0 to 60 eV. From the ground state spin and parity $\frac{5^+}{2}$ for ^{233}U , it follows that s-wave resonances are 2^+ and 3^+ states.

The experimental distribution of anisotropy values for the resonances is rather narrow. It can be explained by theoretical distributions only if the results are renormalized to a somewhat higher average anisotropy by a change in the orientation parameter of the target nuclei. The difference may be due to inefficient cooling or to magnetic-dipole coupling in the hyperfine interaction. Independent experiments are required to resolve the uncertainty in the orientation parameter.

The rather narrow distribution of the anisotropy values implies a strong mixing of the available transition states. The results can be fitted by a theoretical distribution of anisotropies based on a situation where 2 to 3 fission channels are open for 2^+ resonances and 1 to 2 for 3^+ resonances. The invariant behaviour of the anisotropy in the energy region up to 2000 eV indicates that there is no intermediate structure present in this energy region, which is in agreement with a strong mixing of the available transition states.

The recently discovered resonance group structure in the sub-threshold fission cross section of ^{237}Np can be explained by the double-humped deformation barrier as proposed by Strutinsky. The implication of this theory is that all the resonances in one group have the same spin. The transition-state spectrum of the odd-odd nucleus $^{238}\text{Np}^*$ is probably characterized by rotational bands superimposed on excitations of the unpaired nucleons. From the ground-state spin $\frac{5^+}{2}$ for ^{237}Np , the available transition states must have $J^\pi = 2^+$ and 3^+ . Since the spins of the unpaired nucleons are coupled preferably to the highest possible spin and since the K-value for the lowest member of a rotational band is equal to J, the fission fragments will be emitted predominantly in the direction of the nuclear spin, which corresponds to higher K-values.

For the first group of resonances in the fission cross section at 40 eV the anisotropy in the fission fragment emission has been measured for all the individual resonances. The resulting anisotropy values consistently agree with the fission channel $(J^\pi, K) = (2^+, 2)$. The resonance groups at higher neutron energies up to 2000 eV have anisotropies that correspond mainly to the channels $(2^+, 2)$ and $(3^+, 2)$.

SAMENVATTING

Anisotropieën in de hoekverdelingen van splijtingsfragmenten en α -deeltjes van georiënteerde zware kernen zijn gemeten aan de kernen ^{235}U , ^{233}U en ^{237}Np . Kernoriëntatie is verkregen met behulp van de methode van hyperfijninteractie door kristallen van het dubbelnitraat $\text{RbUO}_2(\text{NO}_3)_3$, afgekort als RUN, af te koelen tot temperaturen in de orde van 0.1 K. Een verslag is gegeven van metingen betreffende de anisotropie van splijtingsfragmenten van de zware kernen als functie van de neutronenergie van 0 tot 2000 eV. Deze experimenten zijn verricht bij de lineaire elektronenversneller bij het AERE te Harwell aan preparaten die uit vele RUN-kristallen bestaan. De anisotropie in de α -emissie van ^{233}U en ^{237}Np en de emissie van splijtingsfragmenten verkregen door vangst van thermische neutronen in de kernen ^{235}U en ^{233}U zijn gemeten aan afzonderlijke RUN-kristallen bij de Hoge Flux Reactor bij het RCN te Petten.

In de door laagenergetische neutronen geïnduceerde splijting van zware kernen kunnen de overgangstoestanden ter plaatse van de deformatiebarrière worden beschreven door de spin J van de samengestelde kern, de projectie K van J op de symmetrieas en de pariteit π . De hoekverdeling van splijtingsfragmenten wordt bepaald door de K -waarden van de energetisch beschikbare overgangstoestanden. A. Bohr voorspelde dat in de splijting van even-even kernen de door lagere K -waarden gekarakteriseerde overgangstoestanden zullen overheersen. Dit is geverifieerd in het geval van $^{234}\text{U}^*$ door meting van anisotropieën in de hoekverdeling van splijtingsfragmenten van de door neutronen geïnduceerde splijting van gealigneerde ^{233}U kernen voor individuele resonanties in het neutronenergie gebied van 0 tot 60 eV. Uitgaande van spin en pariteit $\frac{5^+}{2}$ voor de grondtoestand van ^{233}U zijn s-golf resonanties 2^+ en 3^+ toestanden.

De experimentele verdeling van de anisotropiewaarden voor de resonanties vertoont een geringe spreiding. De waarnemingen kunnen slechts worden verklaard door theoretische verdelingen, indien de resultaten worden genormeerd tot een iets hogere gemiddelde anisotropie door een wijziging van de oriëntatieparameter voor de trefkernen. Het verschil is waarschijnlijk te wijten aan een niet-effektieve koeling of

aan magnetische-dipool koppeling in de hyperfijninteractie. Onafhankelijke experimenten zijn vereist om de onzekerheid in de oriëntatieparameter op te lossen.

De tamelijk nauwe verdeling van de anisotropiewaarden voor de resonanties impliceert een sterke menging van de beschikbare overgangstoestanden. De resultaten kunnen worden aangepast door een theoretische verdeling van anisotropieën die gebaseerd is op een situatie met 2 of 3 open kanalen voor 2^+ resonanties en 1 tot 2 voor 3^+ resonanties. Het vlakke verloop van de anisotropie in het energiegebied tot 2000 eV wijst uit dat er in dit energiegebied geen intermediaire structuur aanwezig is, wat in overeenstemming is met een sterke menging van de beschikbare splijtingskanalen.

De onlangs ontdekte groep-structuur van resonanties, die optreedt in de werkzame doorsnede voor splijting van ^{237}Np bij neutronenenergieën beneden de splijtingsdrempel, kan worden verklaard met behulp van de dubbele splijtingsbarrière van Strutinsky. Deze theorie impliceert dat alle resonanties in één groep dezelfde spin hebben. Het spectrum van overgangstoestanden van de oneven-oneven kern $^{238}\text{Np}^*$ wordt waarschijnlijk gekarakteriseerd door rotatiebanden gesuperponeerd op excitaties van de ongepaarde nukleonen. Uitgaande van een spin en pariteit $\frac{5^+}{2}$ voor de grondtoestand van ^{237}Np , moeten de beschikbare overgangstoestanden 2^+ en 3^+ hebben. Aangezien de spin van de ongepaarde nukleonen bij voorkeur gekoppeld zijn tot de grootst mogelijke spin en de K-waarden voor het laagste niveau van een rotatieband gelijk is aan J, zullen de splijtingsfragmenten hoofdzakelijk worden uitgezonden in de richting van de kernspin, wat overeenkomt met hogere K-waarden.

Van de eerste groep resonanties in de werkzame doorsnede voor splijting bij 40 eV is de anisotropie in de emissie van splijtingsfragmenten gemeten voor alle resonanties afzonderlijk. De resulterende anisotropiewaarden stemmen op consistente wijze overeen met het splijtingskanaal $(J^\pi, K) = (2^+, 2)$. De groepen resonanties bij hogere neutronenergieën tot aan 2000 eV hebben anisotropieën die hoofdzakelijk met de kanalen $(2^+, 2)$ en $(3^+, 2)$ overeenkomen.

CURRICULUM VITAE

Op verzoek van de Faculteit der Wiskunde en Natuurwetenschappen volgt hier een overzicht van mijn studie.

Na het behalen van het diploma HBS-B aan de Christelijke Hogere Burgerschool te Emmeloord begon ik in 1963 met de studie Natuurkunde aan de Rijksuniversiteit te Leiden. Het kandidaats-examen D' in de vakken natuurkunde, wiskunde en scheikunde werd afgelegd in 1966 en in mei van datzelfde jaar trad ik toe tot de werkgroep adiabatiscche demagnetisatie en kernfysika van het Kamerlingh Onnes Laboratorium die onder de dagelijkse leiding van dr. W.J. Huiskamp staat en waarvan prof. dr. C.J. Gorter de supervisie heeft. Gedurende een jaar assisteerde ik drs. J.N. Haasbroek en dr. R.F. Wielinga by calorische en magnetische onderzoeken bij lage temperaturen.

In 1967 verleende de Stichting Fundamenteel Onderzoek der Materie, F.O.M., mij een kandidaats-assistentschap in de werkgroep K IV gestationeerd bij het Reactor Centrum Nederland te Petten. De dagelijkse leiding van deze afdeling berustte bij dr. H. Postma. Van juni 1967 tot januari 1969 assisteerde ik dr. E.R. Reddingius met de onderzoeken by de Hoge Flux Reactor betreffende anisotropieën in de door vangst van thermische neutronen geïnduceerde gamma-emissie van gerichte kernen.

In februari 1969 legde ik het doktoraal examen experimentele natuurkunde af met de bijvakken klassieke mechanika en reaktorfysika. In het kader van het laatstgenoemde vak werd enig evaluatiewerk verricht aangaande de werkzame doorsneden van splijtbare kernen. De vereiste tentamina werden afgelegd bij de hoogleraren dr. P. Mazur, dr. P.W. Kasteleijn, dr. J.A.M. Cox en dr. J.A. Goedkoop.

Hierna trad ik als wetenschappelijk medewerker in dienst van de Stichting F.O.M. In het kader van de Nederlands-Britse samenwerking tussen de Stichting en de United Kingdom Atomic Energy Authority nam ik samen met dr. H. Postma en de heer N.J. Pattenden deel aan de experimenten betreffende de hoekverdeling van splijtingsfragmenten geëmitteerd na vangst van laag-energetische neutronen in gerichte zware kernen. Dit onderzoek werd voor een groot gedeelte uitgevoerd bij de lineaire elektronenversneller van het Atomic Energy Research Establishment te Harwell in Engeland, waartoe ik daar geruime tijd ben gestationeerd geweest. Een ander deel van de in dit proefschrift beschreven experimenten werd gedaan bij de Hoge Flux Reactor te Petten.

NAWOORD

Bij het totstandkomen van dit proefschrift wil ik gaarne mijn dank betuigen aan allen die hiertoe hebben bijgedragen.

De direktie van het Reactor Centrum Nederland ben ik erkentelijk voor de mogelijkheid om, in het kader van de samenwerking tussen de Stichting Fundamenteel Onderzoek der Materie en het RCN, de tekst tegelijkertijd als proefschrift en als officieel RCN-rapport te laten verschijnen.

De stimulerende leiding van dr. H. Postma, zowel bij de experimenten als bij het bewerken van het manuscript, is voor mij van grote betekenis geweest.

Veel waardering heb ik voor de vaardige technische assistentie van de heer J.J. Smit bij het experimentele werk. De heer K. Ravensberg dank ik voor het nauwkeurige werk aan de kryostaten en voor het verzorgen van de tekeningen in dit proefschrift.

I gratefully acknowledge the hospitality of the Atomic Energy Research Establishment, in particular the Nuclear Physics Division at the linac under the supervision of Dr. E.R. Rae. I thank Mr. N.J. Pattenden for the friendly co-operation in the experiments and for his valuable comments on the draft of this thesis. I am much indebted to Mr. J.E. Jolly for his constant attention to the experiments and for his assistance with the many calculations; the keen interest in the work was highly appreciated. Thank is due to Dr. J.E. Lynn for the discussions on the interpretation of the experimental results. I wish to express my gratitude to Mr. J.C. Waldron for the careful preparation of the alignment samples.

Ik ben mevr. E.A.M. Endel-Kramer veel dank verschuldigd voor de akkurate wijze waarop zij het vele tijpwerk verzorgde. De reprografische dienst ben ik erkentelijk voor de druktechnische uitvoering van het proefschrift. Tenslotte dank ik mej. Bernadette Robertson voor het korri-geren van de engelse tekst.

STATE OF TEXAS
COUNTY OF [illegible]

[The following text is extremely faint and largely illegible due to the quality of the scan. It appears to be a legal document, possibly a deed or contract, containing names, dates, and descriptive clauses. The text is oriented upside down relative to the page's header.]

STELLINGEN

I

De experimentele methoden voor spinbepaling van neutronresonanties van splijtbare kernen, die gebruik maken van het splijtingsproces, geven slechts ondubbelzinnige resultaten indien per spintoestand niet meer dan één splijtingskanaal beschikbaar is.

II

Bij de splijting van ^{237}Np door vangst van laagenergetische neutronen is er slechts een gering energieverval tussen de laagste beschikbare overgangstoestanden voor de twee spintoestanden ter plaatse van de tweede splijtingsbarrière.

III

In de moleculaire theorie van kernsplijting is het bij relatief geringe elongatie doelmatig de invloed van schilstructuren in de aanstaande fragmenten te beschrijven met afzonderlijke parameters voor de nekformatie.

W. Nörenberg, Second IAEA Symposium on Physics and Chemistry of Fission, Vienna, 1969, p. 51.

IV

"Brute-force" polarisatie van ^3He , gekoeld met behulp van adiabatische kompressie geeft de mogelijkheid om op effectieve wijze neutronen te polariseren in het energiegebied 0 tot 100 eV.

V

De grote spreiding in de experimentele resultaten van Dabbs et al. voor de hoekverdeling van splijtingsfragmenten ontstaan door neutronvangst in georiënteerd ^{235}U , als functie van de neutronenergie, kan te wijten zijn aan de wijze van berekening van de anisotropiewaarden voor de neutronresonanties door middel van multilevel-fit procedures.

J.W.T. Dabbs, C. Eggerman, B. Cauvin, A. Michaudon and M. Sanche, Second IAEA Symposium on Physics and Chemistry of Fission, Vienna, 1969, p. 321.

VI

De onzekerheid in de parameters voor de hyperfijn interactie van uraniumisotopen in $\text{RbUO}_2(\text{NO}_3)_3$ dient te worden opgelost met behulp van resonantietechnieken en door bepaling van eventuele asymmetrie in het β -verval van ^{237}U , dat georiënteerd is in deze stof.

VII

De methode van "P- and η -search" als optimalisatieprocedure bij de aanpassing van veel-parameter functies is in het bijzonder geschikt voor het geval dat het χ^2 -hypervlak veel relatieve minima heeft en de kans op divergentie groot is.

D.W. Marquardt, Journal of the Society for Industrial and Applied Mathematics, Vol. 11, 1963, p. 431.

VIII

De economische isolatie van het zuiver-wetenschappelijk onderzoek na de tweede wereldoorlog is bepalend voor een schaalvergroting van toekomstige investeringen in technische ontwikkelingen.

IX

Een intellectuele benadering bij de vertolking van "Lieder" brengt het gevaar met zich mee dat de muzikale inhoud kunstmatig wordt beperkt.

Dietrich Fischer Dieskau; Die Kindertotenlieder, Gustav Mahler; His Masters Voice 1970.

X

Het sekularisatieproces kan worden verstaan vanuit een hernieuwde christelijke opdracht tot integratie van wetenschap en godsdienst.

Angelica Krogmann, Simone Weil; Lemniscaat, Rotterdam, 1970.

The picture on the front cover represents a liquid-drop model for the fission process of a rotating heavy nucleus. The nuclear surface is described by the formula: $\rho^2 = az^2 + bz^2 + c$, where ρ is the distance of the surface to the nuclear symmetry axis, z . With the condition of volume preservation only two free parameters describe the fission process (ref. J.N.P. Lawrence, report LA-3774).

The rotation axis is the direction of the nuclear spin which also is the direction of nuclear orientation. The situation where this axis is perpendicular to the nuclear symmetry axis is predominant in the fission process of even-even compound nuclei.

